Investigations of Townsend discharges in neon by mass spectrometry

INVESTIGATIONS OF TOWNSEND DISCHARGES IN NEON BY MASS SPECTROMETRY

J.W.H.Dielis

INVESTIGATIONS OF TOWNSEND DISCHARGES IN NEON BY MASS SPECTROMETRY

PROEFSCHRIFT

ter verkrijging van de graad van doctor in de technische wetenschappen aan de Technische Hogeschool Eindhoven, op gezag van de rector magnificus, prof.dr. P. van der Leeden, voor een commissie aangewezen door het college van dekanen in het openbaar te verdedigen op dinsdag 4 september 1979 te 16.00 uur.

door

JOSEPHUS WILHELMUS HUBERTUS DIELIS

geboren te Eindhoven

DIT PROEFSCHRIFT IS GOEDGEKEURD
DOOR DE PROMOTOREN

PROF.DR. A.A. KRUITHOF
EN
PROF.DR.IR. D.C. SCHRAM

CONTENTS

I	INTRODUCTION	1
II	EXPERIMENT	3
II.1	Introduction	3
II.2	Townsend discharge and quadrupole system	3
II.3	Townsend discharge at 77 K	7
II.4	Measuring technique	9
II.5	Sampling hole	12
II.5.1	Introduction	12
II.5.2	Ion sampling from low pressure gas discharges	13
II.5.3	Experiments	16
II.5.4	Results	17
II.5.5	Discussion	22
III	FORMATION AND DESTRUCTION OF MOLECULAR IONS IN A TOWNSEND DISCHARGE IN NEON	29
III.1	General introduction	29
III.2.1	Model of the Townsend discharge	33
III.2.2	General properties of Townsend discharge quantities	38
III.2.3	Method	39
III.3	Elementary processes	41
III.3.1	Associative ionization	41
III.3.1.1	Introduction	41
III.3.1.2	Analysis	44
III.3.1.3	Experiment	45
III.3.1.4	Results	46
III.3.1.5	Discussion	47
III.3.1.6	Conclusion	52
III.3.2	Termolecular association	53
III.3.2.1	Introduction	53
III.3.2.2	Analysis	55
III.3.2.3	Experiment	56
III.3.2.4	Results	56
III.3.2.5	Discussion	59
III.3.2.6	Conclusion	59

III.3.3 Dissociation 6
III.3.3.1 Introduction 6
III.3.3.2 Analysis 6
III.3.3.3 Experiment 6
III.3.3.4 Results 6
III.3.3.5 Discussion 6
III.3.3.6 Conclusion 6

IV DECAY OF METASTABLE NEON ATOMS 6
IV.1 Introduction 6
IV.1.1 Recent developments 6
IV.1.2 Present experiment 7
IV.2 Analysis of the experiments 7
IV.3 Penning ionization as a tracer reaction 8
IV.4 Experiments 8
IV.5 Results 8
IV.6 Discussion 8
IV.6.1 Diffusion coefficient 8
OV.6.2 De-excitation rate 8
IV.6.3 Excimer formation rate 9
IV.6.4 General conclusion 9

V MOBILITIES OF POSITIVE IONS IN NEON 9
V.1 Introduction 9
V.2 Experimental method 10
V.3 Calculation of the intermolecular potential 10
V.4 Results 10
V.4.1 Mobility of Ne^+ in Ne 10
V.4.2 Mobility of N_2^+ in Ne 10
V.4.3 Molecular ion-atom potential energy curve 10
V.5 Conclusions 11
V.6 Concluding remarks 11

APPENDIX: ASSOCIATIVE IONIZATION 11

LIST OF REFERENCES 12

SUMMARY 12

SAMENVATTING 129

NAWOORD 131

PERSOONLIJKE GEGEVENS 132

CHAPTER I

INTRODUCTION

The purpose of this work is to use the properties of the Townsend discharge for the study of elementary processes in ionized gases. We are mainly interested in the formation, destruction and transport of ions at various temperatures below 300 K. Ions are detected with mass spectrometry. Also the decay processes of metastable atoms have our interest. Other experiments in which mass spectrometers have been used in combination with gas discharges are: flowing afterglows (ion-molecule reactions) (Sch75, Sch70, Bol70), drift tubes (mobilities of ions in gases, ion-molecule reactions) (McD72, Bea68), positive columns (Hin70) and afterglows (Smi73, Sau66, Arm74).

Because of its simplicity the Townsend discharge is very suitable for the study of elementary processes. The current and consequently the densities of electrons and ions are so low that no space charge distortion of the electric field occurs. Cumulative effects can be ruled out because of the densities of excited and ionized particles. Until now the physical quantity studied mostly in a Townsend discharge is Townsends first ionization coefficient (Kru37, Cha63, Hoo69). Current-voltage charateristics and Paschen curves were measured (Mon71). The transition from Townsend discharge to glow discharge was investigated (Hol64). Also the onset of the development of streamers has been investigated in Townsend discharges (Kir69).

In this work we couple a Townsend discharge with a quadrupole mass spectrometer. The combination of the Townsend discharge and the mass spectrometric determination of sampled positive ions, is a mighty weapon in the investigation of reaction kinetics and transport properties of positive ions.

To get the right conditions for experiments in this field, an ultra-high vacuum system and the use of cataphoretically purified gas are necessary. This system is described in chapter II. Here also the dependence of the

transmission of the sampling hole on the various discharge conditions for positive ions is discussed.

Two processes resulting in the formation of molecular ions in neon are associative ionization (Hornbeck-Molnar reaction) and termolecular association. In chapter III we describe the experiment in which the reaction rates of both processes are measured. A comparison with theoretical and othe experimental results is given. The collisional dissociation of the molecular ion by a neon ground-state atom appears to be an important loss process at higher reduced electric field strength. The reaction rate for dissociation as a function of mean ion kinetic energy is determined as well as the dissociation energy of the Ne_2^+-molecular ion.

In chapter IV we describe an experiment for determining the decay frequency of $^3P_2$-metastable neon atoms as a function of gas density and temperature by mass spectrometry. A comparison of the measured diffusion coefficient, the excitation rate and the excimer formation rate with theory and previous experimental results is made.

Mobilities of positive ions in a gas under the influence of an electric field are determined up to values of the reduced electric field strength (electric field strength divided by the gas particle density) of 850 Td. Her 1 Td = 10^{-21} Vm^2. The experimental technique is a time of flight method. Mobilities of Ne^+ in neon and N_2^+ in neon as functions of E/N at two temperatures (77 K and 300 K) are measured. From these results the interaction potential between N_2^+ and Ne is determined and compared with theory in chapter V.

CHAPTER II

EXPERIMENT

II.1 Introduction

In this chapter the experimental set up for studying the elementary processes, as mentioned in chapter I, is described. In general it consists of a Townsend discharge (T.D.) coupled with a quadrupole mass filter by means of a small sampling hole for ion extraction. For the experiments at 77 K a similar set up has been built and placed in a cryostat. Section II.2 gives a general description of the T.D. and the quadrupole system. Also attention is payed to the gas handling system. The T.D. experiment at 77 K will be described in short in section II.3. The stationary and time sampling measuring system is described in section II.4. Part II.5 deals with the features (transmission etc.) of the sampling hole for various discharge conditions.

II.2 Townsend discharge and quadrupole system

The two electrodes of the T.D., see figure 2.1, are placed in a stainless steel vacuum chamber. The anode is a fused silica electrode, connected with a stainless steel cylinder by means of a graded seal. The fused silica electrode is covered with a thin layer of tin-oxyde, burned in at a temperature of 475° C. This layer has a transmission for the 253,7 nm line of mercury of approximate 50%, so that the T.D. can run in the non-selfsustaining mode by primary photo-electrons released from the cathode. The electrical conductivity of the anode layer is such that no measurable voltage drop is present over the anode.

The cathode is a stainless steel electrode, covered with a thin gold layer. This coating prevents the growth of oxides on the metal surface (see part II.4). The sampling hole in the cathode was prepared as follows. In the centre, at the back of the 5 mm thick cathode, a conical hole is turned up nearly to the opposite surface. The vertical angle is 110°. By grinding

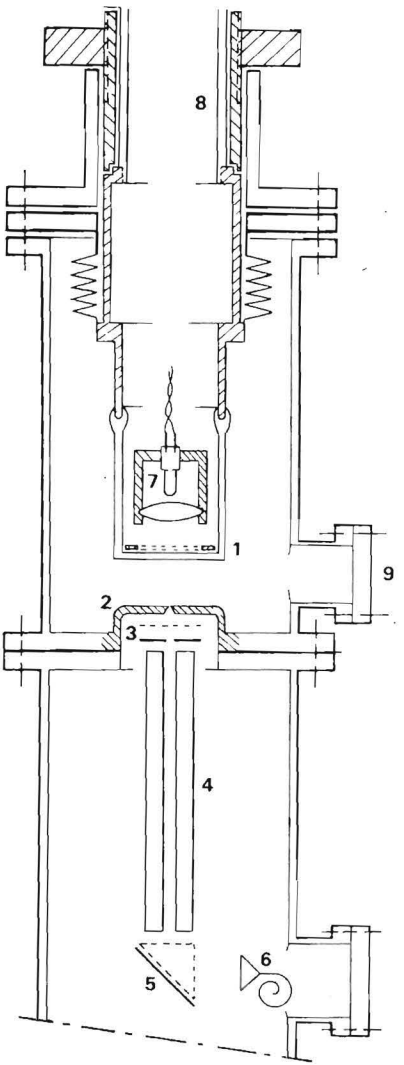

Figure 2.1

Discharge chamber and mass spectrometer
1 fused silica electrode
2 stainless steel electrode with conical hole
3 ion optical system
4 quadrupole mass filter
5 electrostatic mirror
6 channel electron multiplier
7 U.V. light source
8 electrode distance adjustment
9 viewing port.

and polisning the surface of the cathode a sharp edged, circular sampling hole of any particular size can be obtained. In the different experiments hole diameters of 30 μm and 100 μm are used. The diameters of both electro are 6×10^{-2} m. The distance between anode and cathode can be varied from to 3×10^{-2} m by moving the anode in vertical way.

Within the fused silica/pyrex anode construction an U.V. light source (low pressure mercury lamp; penray; C-13-63 ORIEL) is placed in combinati

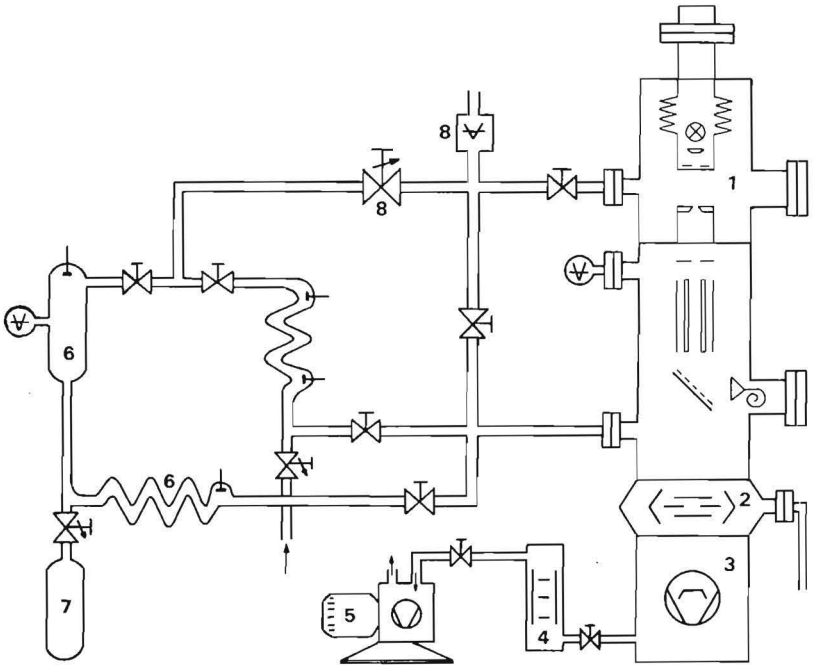

Figure 2.2 Experimental set up

1	*discharge chamber*	*5*	*rotary pump*
2	*freon cooled baffle*	*6*	*cataphoretic tube*
3	*oil diffusion pump*	*7*	*neon gas cylinder*
4	*molecular sieve*	*8*	*automatic pressure controller*

with a lense system and an adjustable aperture to obtain a homogeneously illuminated spot of any particular size on the cathode. In this way the T.D. can run in the non-selfsustaining mode. Behind the cathode a quadrupole mass filter (QMF) is placed in a vacuum chamber. The QMF has a length of 20 cm and rod diameters of 1 cm. The resolution $M/\Delta M$ is 100. The QMF is bakeable up to 400^{o} C. Between the extraction hole and the QMF a grid and aperture lense are placed to obtain optimum entrance conditions for the ions in the QMF. The ions leaving the mass filter are deflected by an electrostatic mirror and collected by a channel electron multiplier. Because of this deflection no U.V. light from the discharge nor from the external light source can hit the surface of the channeltron. The discharge and quadrupole chambers are ultra high vacuum pumped by a 1 m^3s^{-1} oil diffusion pump (Leybold Heraeus) and a rotary pump (Balzers). A freon cooled baffle between vacuum chamber and diffusion pump prevents oil from reaching the vacuum

system. Backflow of contaminations from the rotary pump is prevented by a molecular sieve. This is to be seen in figure 2.2.

In gas discharge physics clean gas is of enormous importance. For thi reason much attention is payed to the gas handling system. The neon gas is standard research grade (Ne "He 40" from l'Air Liquide) contained in a 15 kPa.m^3 metal cylinder. The stated composition of the gas is 99.99% Ne and 0.01% He. The nitrogen concentration is less than 5 ppm, whereas other impurity concentrations are less than 1 ppm. In order to lower further the nitrogen impurity degree, the gas is cataphoretically cleaned and impuriti are adsorbed at the cathode of the cataphoretic discharge and at the walls of the cathode chamber. Cataphoresis (Hir78, Fre66) is the partial segregation of gas components taking place when a gas mixture is subjected to an electric discharge. Measurements of Tombers *et al.* (Tom71) on Ne-N_2 mixtures show not only the normal cataphoretic pumping if nitrogen to the cathode, but also clean-up of the gas at the molybdenum as well as the aluminium cathode.The latter removal process occurs through gas burial, resulting from sputtering effects. This cleaning effect of the gas is orde of magnitude greater than the normal cataphoresis, and therefore very desirable for gas purification systems. Especially when a flowing gas syst has to be used, this latter volume removal process of nitrogen is the major purifying effect. Our gas handling system consists of a ± 100 cm long positive column, with a titanium cathode placed in a pyrex balloon. The walls of this cathode chamber are covered with a titanium layer, sputtered from the cathode. Therefore the impurity density at the positive side of the cataphoretic tube decreases not only by the cataphoretic effec but also by gettering in the cathode section. The anode section of the cataphoretic system is a 5 l pyrex balloon. This large supply of pure neor is sufficient for most experiments and no flow of gas from the metal cylinder into the cataphoretic tube has to be applied, in order to compens for the loss of gas pumped away through the sampling hole in the T.D.

From the ratio N_2^+/Ne^+, with a Penning ionization cross section of 10.4×10^{-20} m^2 (Wes75), we can calculate the maximum value of the nitrog impurity concentration. Mass spectrometric measurements show an impurity nitrogen of less than 1 ppm, while impurities such as water and carbon hydrates are an order of magnitude smaller. This low degree of impurity i

confirmed by the measurements of the decay frequency of neon metastables. These decay rates are, because of the large Penning ionization cross section, very sensitive for impurities. A mass scan of the neon gas is shown in figure 2.3.

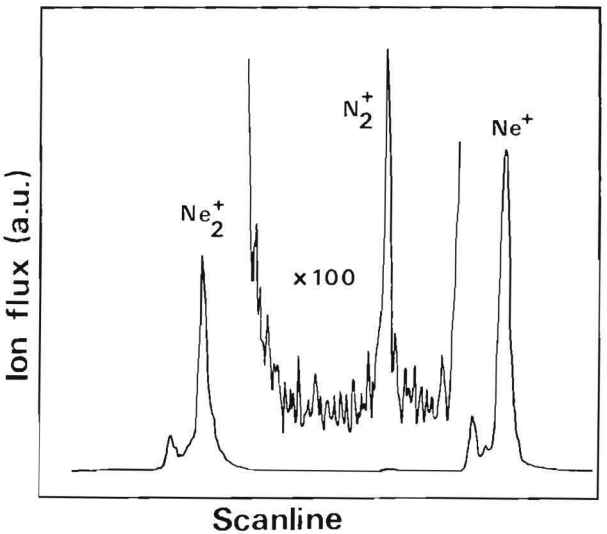

Figure 2.3
Mass scan of the neon gas after cataphoresis.

The entire vacuum system including the gas handling system can be baked out up to 380° C. After a bake out of several days the ultimate pressure in the QMF-chamber is 5×10^{-7} Pa, while in the cataphoretic section this pressure is a few times 10^{-6} Pa. The neon gas used for the T.D. experiment is obtained from the anode section of the cataphoretic system. A differential capacitance manometer combined with an automatic pressure controller keeps the gas pressure in the T.D. constant in time (within a few hundredths of a torr). The pressure is equal to a reference pressure accurately adjusted by means of an oil manometer.

III.3 Townsend discharge at 77 K

Experiments have been carried out to obtain the decay frequency of $^3P_2$ metastable neon atoms and to determine the mobilities of positive ions in neon, both at 77 K. For these experiments a set up was used, originally built for the investigation of ion clustering (Hol77) in discharges at low

temperatures and high densities. The general construction is the same as described in section II.2, only the T.D. is placed in a cryostat. Filling this cryostat with liquid nitrogen gives a homogeneous temperature of 77 K for the whole T.D. for several hours. There is also a possibility of a Rootes pump to be connected to the cryostat, as can be seen in figure 2.4. Then by pumping the nitrogen vapour a temperature between 77 K and 42 K can be achieved. A facility for laser and optical absorption experiments is provided for. Figure 2.4 gives a vertical section of the cryostat, with the T.D., mass filter and channel electron multiplier.

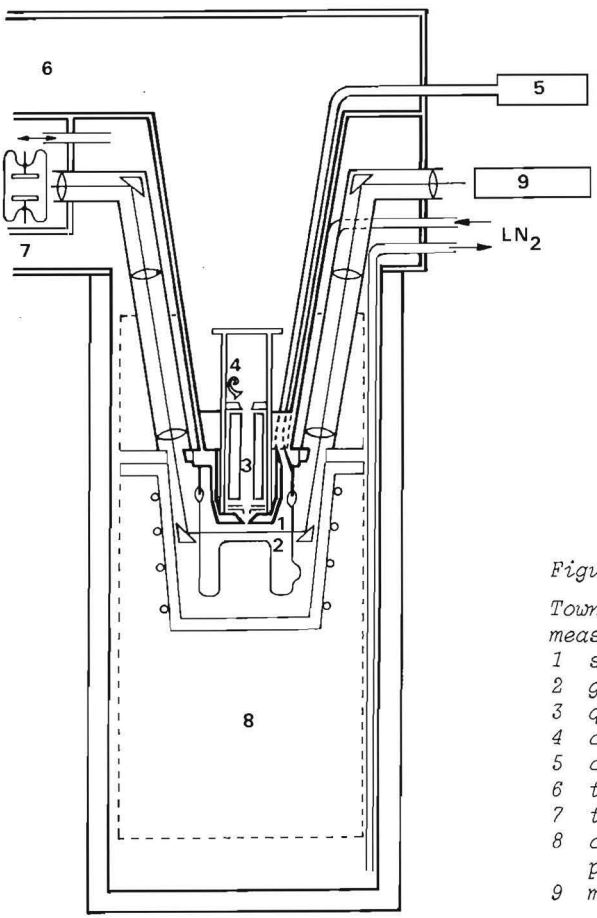

Figure 2.4

Townsend discharge set up for measurements at 77 K.
1 stainless steel cathode
2 gold covered anode
3 quadrupole mass filter
4 channel electron multiplier
5 cryostat
6 to diffusion pump
7 to Rootes pump
8 cataphoretic system for gas purification
9 monochromator and multiplier

II.4 Measuring technique

Dependent on the elementary process to be studied two ways of operating the T.D. were chosen.

Type of discharge	Elementary process
Stationary discharge	- Associative ionization - Termolecular association - Collisional dissociation of molecular ions
Townsend afterglow	- Decay frequencies of metastable states - Mobility of positive ions in neon

The stationary discharge is here defined as a non-selfsustaining discharge constant in time. The current density is less than 10^{-4} Am^{-2}. Under these conditions we measure the flux of the various ions at the cathode as a function of several discharge parameters. The afterglow is the situation after a selfsustaining or non-selfsustaining discharge has been terminated and a small reversed electric field, below breakdown field strength, is applied between the electrodes. Here we are interested in the number and type of ions as a function of the lapse of time since initiating the afterglow under various experimental conditions. The measuring system developed for the latter experiments is a time sampling system, controlled by a micro processor (Motorola M 6800). In figure 2.5 the time sampling system is shown in a block diagram. Positive ions, formed by several reactions in the T.D., drift under the influence of the homogeneous electric field to the cathode. A small number of the ions passes the orifice and arrives, via an ion optical system and the mass filter at the channel electron multiplier where the ions are detected. The other ions impinge on the cathode and are neutralized. Pulses from the channeltron are amplified by a charge-sensitive pre-amplifier (808 Canberra) and an amplifier (816 Canberra). The pulses are further shaped by a timing-scaler (835 Canberra). The typical pulse amplitude is 8 V, whereas the pulse width is 1.0 μs. The measurement of ion fluxes at the cathode is always carried out by pulse counting. For afterglow measurements the pulses are processed by a micro processor system. The micro processor operates as a 1024-channel analyser. The arrival times after initiation of

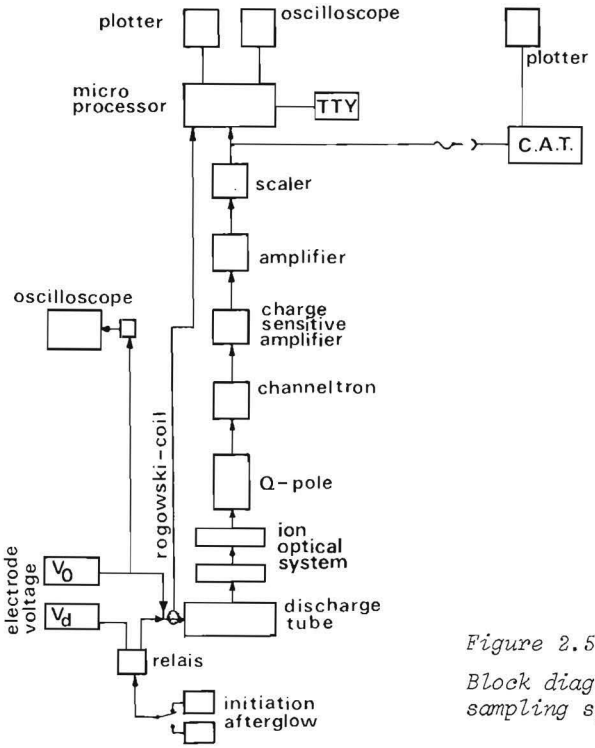

Figure 2.5

Block diagram of time sampling system.

the afterglow of the specific ions are measured. Each time corresponds with an address channel in the memory of the micro processor. When an ion arrives within a specific time slice, the content of the corresponding address is increased by 1. Repeated pulsing of the discharge and the afterglow gives a histogram of arrival times of the particular kind of ion studied. The actual state of the histogram is constantly visible on an oscilloscope. The timing sequence is explained in figure 2.6.

At time t = 0 the voltage on the fused silica electrode, called the anode in section II.2, is reversed from a positive voltage in the afterglow to a negative voltage, by means of a mercury wetted relay. After a time period of a few milliseconds the T.D. ignites and runs at a constant burning voltage. The exponential decrease in voltage occurs because of the large RC time, caused by the 100 MΩ series resistance used for current limiting of the T.D.. Therefore the repetition frequency of the pulsed discharge is limited to a maximum value. The burning voltage at the fused silica

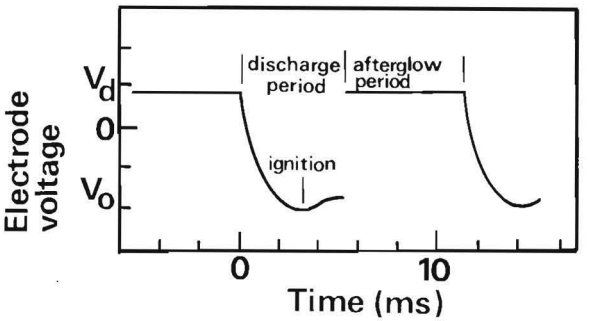

Figure 2.6
Time sequence of afterglow measurements.

electrode is negative compared to the grounded stainless steel electrode, so the positive ions drift away from the extraction hole and are not detected. After an adjustable time interval the stationary discharge is stopped and the afterglow is initiated by reversing the voltage on the fused silica electrode, by means of the relay , to an adjustable positive voltage. Because this drift voltage is always much smaller than the burning voltage of the discharge, a current limiting series resistance is not necessary. The risetime from the negative discharge voltage to the positive drift voltage in the afterglow appears to be 0.2 μs. The repetition frequency of the sequence of discharge and afterglow is adjustable to a maximum value of 100 Hz. The current pulse, due to the reversing of the voltage, marks the beginning of the afterglow. This pulse is detected with a Rogowski coil around the lead of the fused silica electrode. The pulse picked up by this coil starts a clock in the micro processor. The minimum and maximum time intervals to be measured in the afterglow are programmed in the micro processor and amount to 100 μs and 128 ms, respectively. This corresponds to a time resolution of 0.1 μs and 128 μs, respectively. Via a software program on the M 6800 simple operations with the data, as rearranging and scaling of the histogram, are possible. With a 1024-channel analyser (C.A.T. computer of average transients) a mass scan of the positive ions in the discharge is made before starting a measurement. In this way we can assess whether the densities of impurities in the gas are low enough for the typical kind of measurement to be made.

II.5 Sampling hole

II.5.1 Introduction

For mass spectrometrical investigations in gas discharge physics, ions have to be extracted from the discharge region. The transport of ions from the bulk of the discharge plasma to the extraction hole depends on the specific experimental conditions. In positive columns and afterglows the ambipolar diffusion of electrons and ions takes care of the transport to the wall, in which the sampling hole usually is situated. In flowing afterglows convective flow carries the ions to the sampling hole, whereas in drift tubes, where the ion densities are so low that the ions move independently in the external electric fields, these fields govern the transport of the ions to the extraction place.

As long as parameters like the flow velocity, the gas pressure and the electric field are constant, ion sampling as a function of discharge parameters not related to the extraction process, is sound. Examples are the time dependent monitoring of ions from a discharge afterglow and the change in ion currents detected when a known influx of foreign atoms is introduced in a flowing afterglow system.

A more difficult problem arises when absolute numbers of sampled ions are required. The total transmission is composed of the transmission of the sampling hole, the transmissions of the ion optical system and the quadrupol mass filter, and the efficiency of the detector. Firstly, the transmission characteristics of the sampling hole for ions should be known. Collisions of the ions with the inner wall of the orifice lead to a smaller ion flux at the detector than the one entering the orifice. Electric fields, caused by oxides on the surface near or within the extraction hole, or produced by sharp edges at the entrance and exit of the sampling hole, might diminish the detected ion flux. We should realize that in going from the discharge to the evacuated environment behind the hole, the gas density decreases many orders of magnitude. For gas pressures so high that ions make collisions with gas atoms in and behind the sampling hole, ion-molecule reactions might take place. Secondly, elastic scattering of ions with neutral gas atoms behind the hole can cause the trajectories of those ions

to change considerably so that they no longer fulfil the entrance conditions of the quadrupole mass filter. These conditions are mainly determined by the angle of injection and the diameter of the input aperture. Therefore the transmission of the mass filter for ions might decrease enormously. The absolute calibration of the transmission of the ion optical system, the quadrupole mass filter, and the quantum efficiency of the detector are hard to determine. In the present chapter the detector efficiency is taken constant at the different discharge conditions. In the following sections the total transmission, *viz.* the transmission of the sampling orifice, the transmission of the ion optical system and the transmission of the QMF is briefly called the transmission of the hole. It is possible to get very good knowledge of the relative behaviour of the total transmission of the hole as a function of neutral gas density, by making use of the similarity properties of the T.D.. In section II.5.2 we will elaborate on what is known about transmission characteristics of holes as they are used in low pressure gas discharge experiments and give some experimental results of data on the problems.

II.5.2 Ion sampling from low pressure gas discharges

This section deals with experiments on ion sampling from low pressure gas discharges, by several authors with the aim to study the transmission characteristics of an extraction orifice.

For the molecular flow region Arijs (Ary74) made a theoretical and experimental study of the ion effusion through small holes with cylindrical geometry. He took into account the loss of charged particles by collisions with the wall of the hole, under the assumption that each ion striking the wall of the hole is neutralized. The velocity distribution of the ions is shifted by the drift velocity of the ions in the direction of the hole. A calculation was made of the ion flow rate as a function of the drift kinetic energy of the ions, with the length/radius ratio of the hole as a parameter. For this molecular flow region and the ratio of length vs. radius of the hole $h/R \ll 1$, as is the case in our situation, the flow rate is proportional to the mean ionic velocity in the direction of the sampling hole. For drift kinetic energies less than 10 times the thermal energy kT, the ion flow rate

decreases about three orders of magnitude when h/R increases from 0.01 to 50. Moreover, the ion flow rate is no longer proportional to the mean ionic velocity for drift kinetic energies higher than the thermal energies. These calculations agree with the experimental results of the author.

Hintzpeter (Hin70) investigated experimentally the ambipolar flow of Ne^+ out of a positive column of a low pressure glow discharge. He used an infinitesimally thin aperture, electronically kept at the potential of the plasma at the wall. For hole diameters between 10 μm and 100 μm the flux density of Ne^+ ions, in the molecular flow regime, appears to be constant. No dragging along with the gas flow was observed. For holes with the radius R larger than one-half of the mean free path, a decrease in the ion flux density by a factor of 2 was measured, and was ascribed to a distortion of the wall boundary layer ("wandschicht"). The resulting lense action bends the ions to the wall.

From these experiments one can see the advantage of using a Townsend discharge for ion sampling rather than a plasma, *e.g.* a glow discharge. The distortion of the Debye sheath at the place of the orifice influences the sampling of ions from a plasma, whereas in a T.D. no such Debye sheath effects are present.

For the convective flow regime Parkes (Par71) investigated theoretically and experimentally the flow of negative oxygen ions through a sampling hole of 250 μm at the end of a drift tube. He calculated the effective sampled area in the drift tube as a function of gas pressure and atomic mass, using a simple model. Measurements at pressures between 0.1 kPa and 0.4 kPa show that for reduced electric field strengths larger than 90 Td the sampled area in the drift tube is a hemisphere with a radius equal to the hole radius. Lowering the reduced electric field strength to 10 Td causes an increase in effective hole area approximately inversely proportional to the drift velocity of the ions. Qualitative agreement of the experimental results with the results of the simple model, in which diffusion is not taken into account, is obtained.

Milloy and Elford (Mil75) studied the characteristics of the sampling system by comparing the ion current transmitted by the sampling hole in the exit plate of a drift tube with that predicted from a known distribution of ion current over the exit plate. Transmission characteristics of Li^+, K^+ and Cs^+ in Ar as functions of gas density for the convective flow regime show a decrease in the Li^+-flux as well as an increase in the Cs^+-flux with increasing gas density. The dependence of the transmission of the extraction hole on the gas density for various exit hole diameters between 0.2 mm and 1.0 mm gives for the smallest diameters an increasing transmission at increasing gas density. Here a transition region from molecular flow to convective flow can be supposed. A decrease in the transmission at increasing gas density for the larger diameters, is observed in the convective flow region. Also the dependence of the transmission on the mass ratio of the ions and the gas atoms was investigated. The agreement with theory improves when the mass ratio increases.

The conclusion of all these investigations is that experiments should be carried out at low gas pressures and small sampling apertures, *i.e.* in the case of molecular flow. Sometimes, however, high pressure or large holes must be used in order to obtain sufficient signal strength. When pressure dependent studies in the higher pressure region are done, these higher pressures are inevitable. In that situation the dependence of the transmission of the aperture on pressure, hole diameter, reduced field strength *etc.* must be known. The physical quantities which must be known to obtain an absolute calibration for the transmission of a hole for ion sampling of a discharge are the flux of ions at the point of extraction in case no sampling hole is present and the transmission of the hole itself, the ion optical system, the mass filter and the sensitivity of the detector. In most experiments only the relative transmission of the hole as a function of discharge parameters, *e.g.* the gas pressure, has to be known. As mentioned earlier, in the relative transmission are included the transmissions of the hole itself, the ion optical system and the mass filter. As will be seen the transmission of the quadrupole filter depends on the ion trajectories behind the hole. If these trajectories satisfy the entrance conditions of the quadrupole, a 100% transmission of the mass filter is achieved. Collisions of an ion with gas atoms before entering the quadrupole, might cause the

trajectory of the ion to miss the acceptance conditions, and the transmiss of the mass filter decreases.

In most discharges *e.g.* flowing afterglows and positive columns, the ion flux density at the point of extraction as a function of discharge parameters, is not known. A determination of the relative transmission of the sampling and detection system is then not possible. In a T.D., however the ion flux density at the extraction place can be calculated rather simp

II.5.3 Experiments

In this section experiments are described for the determination of th relative transmission of the sampling hole as a function of gas density an other parameters. If one electron departs from the cathode, $e^{\alpha d}$ electrons reach the anode, with α the total ionization coefficient. So $e^{\alpha d}-1$ ions ar formed through ionization. The particle current density of Ne^+ ions at the cathode, $j^+(0)$, and the particle current density of the electrons at the anode of the T.D., $j^-(d)$, can be written as

$$j^+(0) = j^-(0)\cdot(e^{\alpha d} - 1) \qquad (2.$$

and

$$j^-(d) = j^-(0)\cdot e^{\alpha d} \qquad (2.$$

where d is the distance between anode and cathode and $j^-(0)$ the electron current density at the cathode. For the non-selfsustaining T.D. by far the major part of the electron current density at the cathode $j^-(0)$ is caused an external source of ultra-violet radiation. The small influence of electrons liberated by the positive ions is neglected. Also it can easily seen that $j^-(d)$ is related to the total current I by

$$j^-(d) = \frac{I}{eA} \quad , \qquad (2.$$

where e is the positive elementary charge and A is the geometrical area of the cathode. In our experiment we vary at constant E/N both the reduced ga pressure p_o and the electrode distance d in such a way that $p_o d$ is constan Because of the similarity of the discharges the quantity α/p_o is only a function of the reduced electric field strength E/N. From equations (2.1),

(2.2) and (2.3) it can be seen that in that case the ion current density at the cathode as well as the discharge current should be constant as functions of gas pressure.

For several stainless steel cathodes, with and without gold layer, and with 30 μm and 100 μm diameter sampling holes the ion flux at the detector and the discharge current have been measured as functions of pressure under the similarity conditions mentioned. These measurements have been carried out for E/N = 71 Td and 141 Td with $p_o d$ = 1.33, 2.67, 4.0 and 5.2 Pa.m for the 30 μm hole. For the 100 μm hole low pressure measurements have been done for E/N = 93 Td and 170 Td with $p_o d$ = 1.20 Pa.m, whereas high pressure measurements have been carried out for E/N = 71 Td with $p_o d$ = 4.0 and 5.3 Pa.m and E/N = 141 Td with $p_o d$ = 4.0 Pa.m.

II.5.4 Results

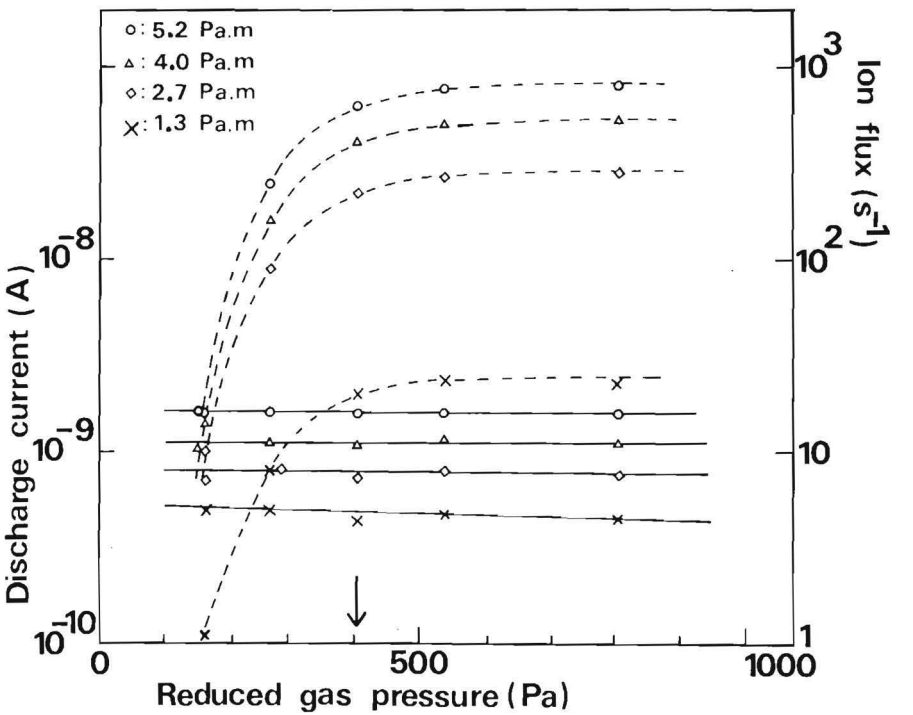

Figure 2.7 Discharge current (——) and ion flux (---) vs. reduced gas pressure for a stainless steel electrode with 30 μm hole at an E/N of 71 Td. Parameter is $p_o d$.

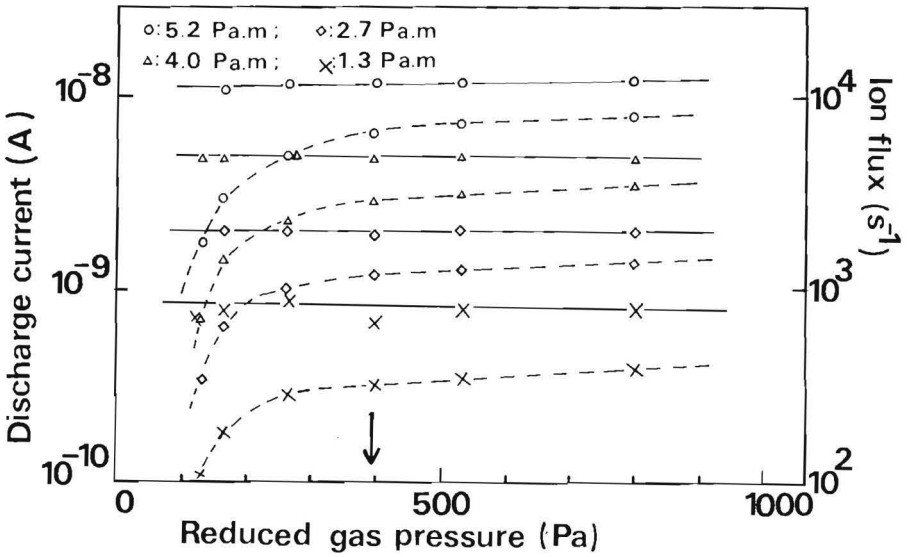

Figure 2.8 Discharge current (——) and ion flux (---) vs. reduced gas pressure for a stainless steel electrode with 30 μm hole at an E/N of 141 Td. Parameter is $p_o d$.

The results of the measurements carried out are shown in the figures 2.7 to 2.12. The first thing we notice is that in all cases the discharge current is constant with gas pressure. This is an experimental proof for t similarity of the discharge for the conditions imposed. This implies that the atomic ion current density at the cathode also should be constant. So the variation in the sampled ion flux as a function of reduced gas pressur can only be caused by changes in the transmission characteristics of the sampling hole. This is of course only correct after a correction for ion-molecule reactions, leading to the extra formation or destruction of atomi ions, has been made. For the measurements carried out in this chapter, the influence of these reactions can be neglected. The destruction of atomic ions is caused by termolecular association, a three-body process, and therefore occurring at higher gas densities. The influence of this process can be neglected, as will be explained in II.5.5. The formation of atomic ions by dissociation of molecular ions can only be of importance at those small values of *E/N*, for which associative ionization causes the initial molecular ion density to be about as large as the atomic ion density. In this *E/N* region, however, the dissociative reaction rate is so small (*c.f.*

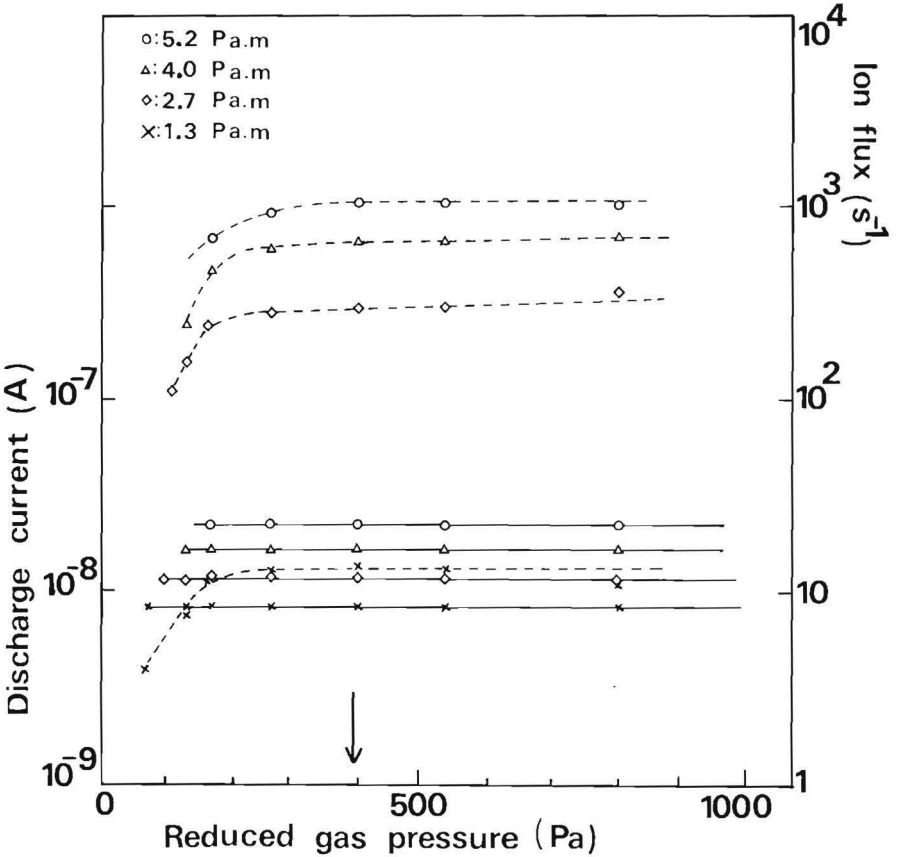

Figure 2.9 Discharge current (——) and ion flux (---) vs. reduced gas pressure for a gold covered electrode with 30 μm hole at an E/N of 71 Td. Parameter is $p_o d$.

II.3.3) that the extra formation of atomic ions can be neglected. As for he detected ion flux, it can be seen that a distinction should be made etween reduced pressures larger than 400 Pa and reduced pressures smaller han 400 Pa.

ow pressure region

As can be seen from the figures 2.7 and 2.8 for the stainless steel athode and the 30 μm hole, the Ne^+-ion flux decreases more than one order f magnitude when the pressure is changed from 400 to 130 Pa at E/N = 71 Td or all $p_o d$ values concerned. At an E/N of 141 Td this decrease of the ion

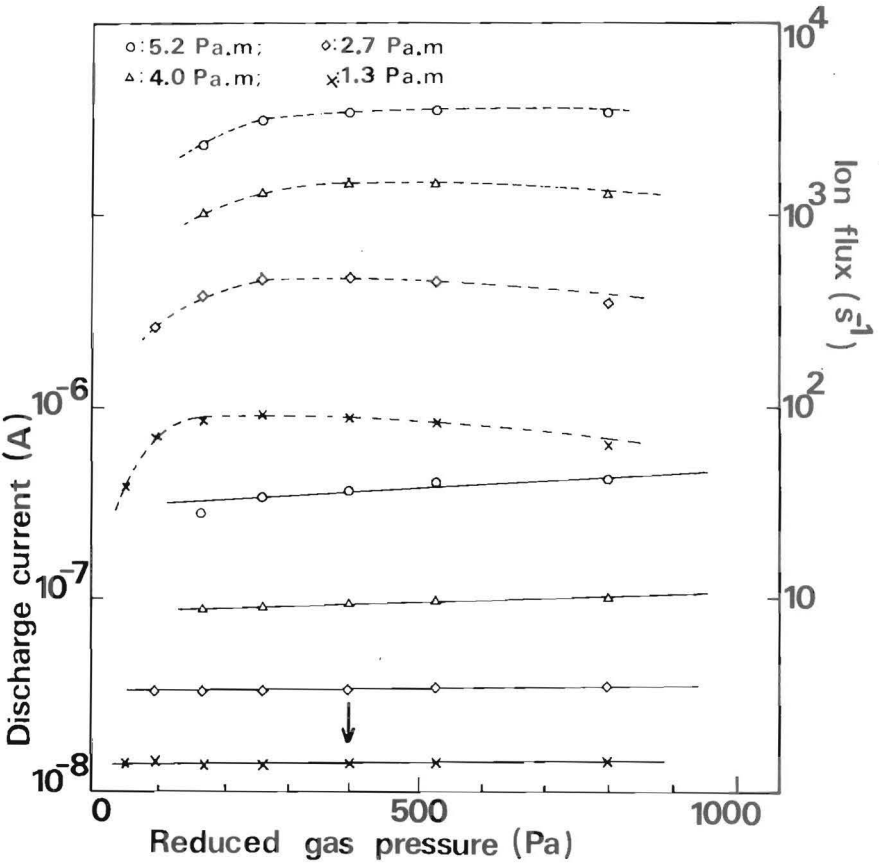

Figure 2.10 Discharge current (——) and ion flux (---) vs. reduced gas pressure for a gold covered electrode with 30 μm hole at an E/N of 141 Td. Parameter is $p_o d$.

flux starts at a pressure of about 250 Pa. As can be seen in the figures 2.9 and 2.10, covering of this cathode with a thin gold layer gives a much smaller drop in the detected ion flux under the same conditions. At an *E/N* of 71 Td this slight decrease starts at a pressure of 200 Pa, whereas for *E/N* = 141 this point is at a pressure of 130 Pa.

When the stainless steel, gold covered cathode has a hole diameter of 100 μm, there is only a small decrease in the detected Ne^+-flux at the low pressure side, as can be seen in figure 2.11. The reduced pressure at which the Ne^+-flux decreases, for both *E/N* of 93 Td and 170 Td, is at a reduced pressure of about 50 Pa.

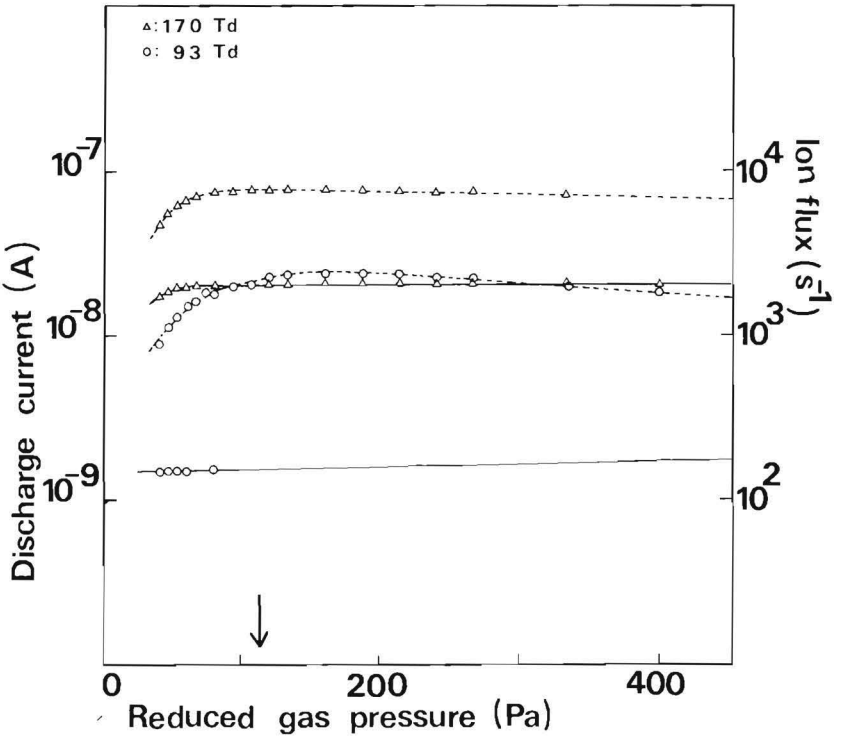

Figure 2.11 Discharge current (——) and Ne^+-flux (---) for a gold covered cathode with 100 μm hole diameter at a $p_o d$ of 1.20 Pa.m. Parameter is E/N.

High pressure region

For pressures up to 800 Pa, for both the stainless steel and gold covered cathode with 30 μm sampling holes, the measured ion flux is constant as a function of reduced gas pressure for all E/N and $p_o d$ concerned. This can be seen in the figures 2.7 to 2.10. In figure 2.12 one can see that for the cathode with a gold layer and a 100 μm hole, the measured ion flux decreases over at least one order of magnitude when the pressure is raised from 500 Pa to 3500 Pa for the E/N and $p_o d$ concerned.

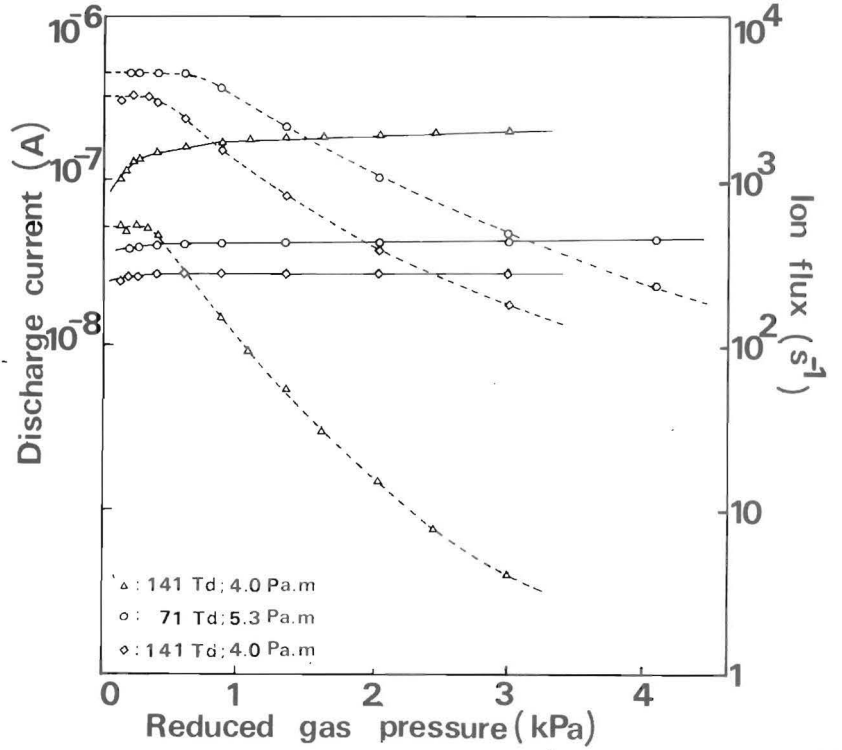

Figure 2.12 Discharge current (——) and Ne^+-flux (---) for a gold covered cathode with 100 μm hole diameter. Parameter is E/N (Td) and $p_0 d$ (Pa.m).

II.5.5 Discussion

The results of the measurements carried out to determine the transmission of the sampling hole as a function of gas density in the T.D. and given in the previous section, are important for those measurements that have to be done as a function of gas density. Especially the determination of the reaction rate for associative ionization, carried out in chapter III, is a measurement in which the gas density has to be varied over as wide as possible a range in the low pressure region, *i.e.* below 400 Pa. In this situation one must be certain of a measured flux of ions through the sampling hole proportional to the ion current density at the cathode.

For the two sampling holes of 30 μm and 100 μm in diameter one can calculate the pressure for which the mean free path λ for elastic scattering of the neon atoms equals two times the radius R of the hole (Die62). These pressures are 400 Pa for the 30 μm aperture and 120 Pa for the 100 μm aperture, indicated in the figures 2.7 to 2.11. Below these pressures a free molecular flow of the gas through the hole takes place. As in the previous section a distinction is made for the two pressure regions.

Low pressure region

For both cathodes with the 30 μm aperture the flow of gas is a free molecular one for pressures below 400 Pa. One would expect, as mentioned in section II.5.2, the ion transmission of the sampling hole to be constant as a function of gas density. On the contrary, the experiments show a drop in the measured ion flux below 330 Pa for the stainless steel cathode and below 135 Pa for the cathode with a gold layer. This physical phenomenon may be ascribed to the influence of fringing electric fields around the hole. These stray fields deflect a fraction of the ions from their collisionless track through the hole towards the edge of the aperture, and these ions are not detected. Obviously the trajectories of these scattered ions behind the hole do not fulfil the entrance conditions of the quadrupole. As mentioned earlier the acceptance for the operation of a quadrupole mass filter at 100% transmission, is determined by the injection angle and the input aperture diameter. According to Dawson and Whetten (Daw69) for 100% transmission the diameter of the input aperture at the plane of entry of the mass filter, must be smaller than $r_o/\sqrt{M/\Delta M}$, where r_o is the distance from the axis of the quadrupole to the nearest point of the electrodes of the quadrupole. The tangent of the angle of injection for 100% transmission, has to be smaller than $3.5\ r_o/l$, where l is the length of the quadrupole electrodes. When the input diameter and the angle of injection are larger than those maximum values, the transmission of the mass filter decreases. For the mass filter we have used, the values for the maximum diameter of the input aperture and the maximum angle of injection are 0.5 mm and 4.8^o, respectively, at a resolution of 100. Dawson (Daw74) calculated the transmission as a function of the resolution for various values of the ratio D/r_o of the input diameter D and r_o. As can be seen

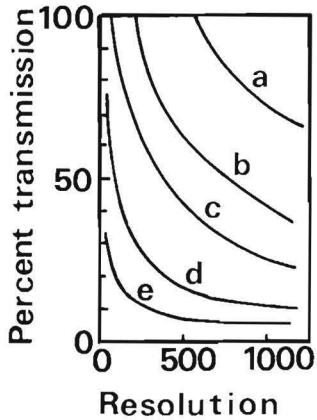

Figure 2.13

Transmission of a quadrupole mass filter for various values of the ratio of input diameter D and r_o.
a 0.04
b 0.06
c 0.10
d 0.20
e 0.40
(after Dawson (Daw74)).

from figure 2.13, at a resolution of 100, an increase of this ratio from 0.10 to 0.40 gives a decrease in the transmission from 100% to 20%, respectively.

Brubaker (Bru60) measured the transmission of K^+ ions through a quadrupole mass filter for various angles of injection, with the ions entering on axis, as is to be seen in figure 2.14. The maximum angle of injection for 100% transmission, as calculated from the expression mentioned earlier, appeared to be 16^o. The strong dependence of the transmission on the angle of ion entry is obvious.

For the stainless steel cathode without a gold layer, the effects of the fringing fields will be amplified by the presence of oxydes on the surface of the cathode and around the hole. This is confirmed by the fact that the decrease in the measured ion flux starts at higher density than in the case of the gold covered cathode.

As can be seen from figure 2.11, only a slight decrease in the ion flu occurs, for the cathode with the 100 μm aperture, at a reduced pressure of 50 Pa. The explanation is that the ratio of the area in which the fringing fields have no influence on the motion of the ions through the hole to the geometrical area of the hole is much larger for the 100 μm than for the 30 μm aperture.

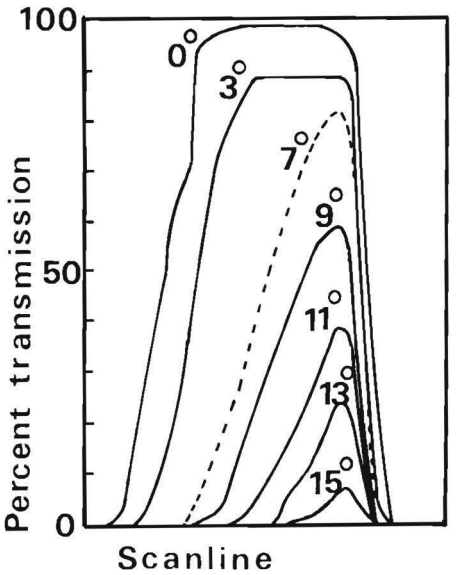

Figure 2.14

Transmission of a quadrupole mass filter for various values of angles of injection (after Brubaker (Bru60)).

At higher gas densities, in which the mean free path becomes smaller than the diameter of the aperture, collisions between ions and gas atoms take place in the sampling hole, so that the fringing electric field plays a relatively minor role.

For the 100 μm aperture the slight decrease in the measured Ne^+-flux at low pressures can also be explained by the lateral diffusion of electrons in the discharge. Because of this low pressure and the constancy of $p_o d$, the electrode distance is rather large. A distance of 25 mm to 30 mm is no longer small as compared to the 45 mm area on the cathode, from which the photo-electrons are released. Electrons on the way to the anode will diffuse laterally. The effect of this diffusion on the total electric current through the T.D. is negligeable because primary electrons are released by photo emission only in an area with a diameter of 45 mm on the 60 mm diameter cathode. All electrons, despite their diffusion, will reach the anode. But as a result of this lateral diffusion, the electron current density along the axis of the T.D. will grow less than by the factor of $\exp(\alpha d)$, as formula (2.2) predicts. For the measured sampled Ne^+-flux as a function of gas density, as shown in figure 2.11, the influence of the diffusion of the electrons is calculated. The quantity used in this

calculation is the ratio D^-/K^- of the diffusion coefficient D^- and the mobility K^- for electrons. The lateral diffusion of ions can be neglected because the value D^+/K^+, the ratio of diffusion coefficient and mobility for ions, is much smaller than this ratio for electrons in the experimental conditions used.

At an E/N of 93 Td the decrease in ion flux can be accounted for by electron diffusion, by taking a value of 8.5 V for D^-/K^-, whereas for E/N is 170 Td a value of 10.0 V has to be taken. With these values for D^-/K^- the transmission of the sampling hole as a function of low gas density becomes constant. Comparing the D^-/K^- values found for both E/N with those calculated by Hughes (Hug70), which were 10.0 V and 14 V for an E/N of 93 and 170 Td, respectively, shows a satisfactory agreement.

High pressure region

The effects in the transmission of the ions for increasing pressure cannot be ascribed to the same physical mechanism which plays a role for the low pressure side. For increasing pressure and the used aperture sizes the molecular flow changes into viscous flow. We do not know how long the transition area will be. The most probable explanation for the decrease in the transmission of the hole at increasing gas pressure, are collisions of the ions with neutral gas atoms within and behind the extraction orifice As a consequence of these scattering collisions, an increasing part of the ions entering the hole will not fulfil the entrance conditions required for 100% transmission of the quadrupole mass filter. This effect with the 100 µm hole is confirmed by the measurements on the 30 µm hole, as can be seen in the figures 2.7 to 2.10. In the 30 µm hole no effects up to 800 Pa have been observed. For this extraction hole the transition region between molecular and viscous flow is shifted towards higher pressures.

Another effect which should be considered is the ion-molecule reaction of neon ions with two ground state neon atoms, $Ne^+ + 2Ne \rightarrow Ne_2^+ + Ne$. It is certain that this reaction cannot play a role in interpreting the strong decrease in the transmission at the high pressure side. The value of the reaction rate necessary for explaining the decrease in figure 2.12 would be 2 orders of magnitude greater than the one generally accepted. This is

confirmed experimentally by the observation that the loss of Ne^+-flux is not balanced by an increase in measured Ne_2^+ molecular ion flux.

A general conclusion which can be drawn from the foregoing measurements is, that for pressure dependent measurements, like the ones on associative ionization as treated in chapter III, only restricted pressure intervals can be used. In the case of the gold covered electrode this interval goes from 200 Pa to at least 800 Pa for a 30 μm hole, whereas this pressure region stretches from 65 to 400 Pa for the 100 μm hole.

In all other pressure regions one should take care to make a relative calibration of the transmission characteristics of the hole. Because of the applicability of the similarity rules in the T.D. and the possibility to calculate the ion flux density at the cathode as a function of discharge parameters in a rather simple way, this discharge is well suited for investigations of ion transmission characteristics of sampling holes.

CHAPTER III

FORMATION AND DESTRUCTION OF MOLECULAR IONS IN A TOWNSEND DISCHARGE IN NEON

In this chapter three elementary processes leading to the formation and destruction of molecular ions are studied in a Townsend discharge in neon. Section 1 gives a general introduction of these processes. The model of the T.D. and the experimental method are given in section 2. In sections 3.1, 3.2 and 3.3 a study is made of the associative ionization process, the termolecular association reaction and the collisional dissociation of Ne_2^+-ions, respectively.

III.1 General introduction

In this chapter we limit ourselves to those elementary reactions in Townsend discharges which lead to the formation and destruction of atomic and molecular ions in gas discharges. The way these elementary processes used to be investigated was to study macroscopic physical quantities in gas discharges and ionization chambers, and from these to derive microscopic features of the processes studied. Later beam experiments were developed in which *e.g.* ion-molecule reactions took place under much better defined conditions. The great advantage of beam experiments is that collision parameters *e.g.* the relative energy between the interacting particles, can be chosen "monochromatically". Also state selection of atoms, *e.g.* between the several metastable states, is possible in beams of particles. Gas discharges are media experiments, in which not only the particles under investigation are present but a lot of other species in various atomic states are created, which can interfere with the reaction to be studied. Collision parameters often cover a whole spectrum. A broad distribution over relative energies of reacting particles may exist of which only the mean value can be changed. This takes place by changing the temperature of the gas in the case of neutral molecules and by varying the electric field in the case of charged particles. Some reactions, however, one of which is mentioned below, cannot be studied in beam experiments. A reaction in which one of the reactants is a very short-living excited particle, so that this

particular particle is already de-excited by emission of radiation even before entering the reaction region, cannot be studied in a beam experiment. The study of this kind of reactions is only possible in an experiment where collisions happen so often that a considerable fraction of these particles may indeed react before being de-excited. Also three-body collisions can only be studied in gas discharges. The reactions we are interested in will now be specified in more detail.

Two reactions frequently occurring in discharges from which molecular ions arise, are the associative ionization reaction (Dah62, Hor51c, Pah59)

$$Ne^{**} + Ne \rightarrow Ne_2^+ + e^- , \tag{3.1}$$

where Ne** is a highly excited state, and the termolecular association reaction (Bea68, Ori73)

$$Ne^+ + 2Ne \rightarrow Ne_2^+ + Ne . \tag{3.2}$$

Because of the large amount of energy which the molecular ions may gain in the electric field of a discharge in comparison to their dissociation energy, a third reaction in which the molecular ions are destroyed, will be taken into account as well. The molecular ions are supposed to be dissociated in a collision with a ground state atom, according to

$$Ne_2^+ + Ne \rightarrow Ne^+ + 2Ne , \tag{3.3}$$

which is the reverse of reaction (3.2). In this introduction only the general features of these reactions and the way of measuring the reaction rates will be discussed; a detailed description is given in the sections III.1, III.2 and III.3.

The purpose of the present experiment is the determination of the reaction rates for the processes (3.2) and (3.3) as functions of the average relative energy of the particles in the swarm. For the associative ionizatio reaction only the product of reaction rate and lifetime of the highly excite neon atom can be found as a function of reduced electric field strength. It is not possible to determine the two factors of the product separately.

Associative ionization in inert gases, also called Hornbeck-Molnar ionization, after the first authors who proposed this reaction, is a two-body reaction responsible for the formation of molecular ions at low gas densities. The lifetimes of the highly excited reactants are so long that even at reduced pressures of a few pascals molecular ions are formed in this way (Hor51d). Three experiments are known in which the product $k_r\tau$ of the associative ionization rate k_r and lifetime τ of excited reactants were determined. Hornbeck made rough measurements on the probability of the formation of molecular ions in noble gases by studying a pulsed T.D. (Hor51c). Von Pahl measured mass spectrometrically the flux of atomic and molecular ions effusing through an orifice in the wall of a low pressure positive column and determined $k_r\tau$ (Pah59). Dahler *et al.* measured the current ratio of atomic and molecular ions, generated in an ionization chamber coupled with a high pressure mass spectrometer, as a function of gas density and also obtained values for $k_r\tau$ (Dah62). The results on $k_r\tau$ of the experiments mentioned above mutually differ by more than 3 orders of magnitude.

No fundamental theoretical treatment of this reaction mechanism exists. As will be described in the appendix a theory developed by Demkov and Komarov for the ionization reaction $A^* + B \rightarrow A + B^+ + e^-$, where A and A^* are atoms in the ground and highly excited states, respectively, B and B^+ are atoms in the ground and ionized states, respectively, and e^- is the outcoming electron, can be used in treating the associative ionization reaction (Dem67). In the present experiment the product of associative ionization rate and mean lifetime of Ne** is determined by measuring the ratio of atomic ion flux and molecular ion flux at the cathode of a T.D. as a function of gas density for low gas pressures.

The termolecular association reaction, often named conversion, is a three-body process and therefore occurring at higher gas densities. Two main experimental methods can be distinguished by the range of ion energy for which the reaction rate is determined. The first class of experiments are drift-tube experiments (Ori73, Bea68), in which the reaction rates of ion-molecule reactions can be determined as a function of mean ion energy by varying the reduced electric field strength. Effective ion temperatures up to 10,000 K can be achieved. In these experiments the ion transport

equations, including a diffusion term and a term for the reaction to be studied, are solved and fitted to the measured arrival time spectrum of the ions. The second class of experiments are afterglow experiments (Vit72, Sau66, Smi68, Che68), in which the ion-molecule reaction rate can only be determined for the temperature of the gas. These temperatures usually range from liquid nitrogen temperature up to room temperature. From the decay spectra of the density of the ions of interest, the reaction rate can be calculated. For neon, the results of these conversion experiments show reaction rates scattered by a factor of 5. The results of theoretical calculations, carried out for ion temperatures equal to the gas temperature, disagree mutually by almost an order of magnitude (Smir67, Mah65, Nil65, Dic72).

No experiments are known in which the dissociation rate of superthermal molecular inert gas ions in collisions with parent ground state atoms is measured. Only the dissociation energy has been previously measured. The experimental techniques used are ion-scattering experiments (Mas58), spectral line shape studies (Con65) and experiments in which the appearance potential of the molecular ions is determined by electron impact (Mun63). Ab initio calculations of potential energy curves of Ne_2^+ from which the dissociation energy can be calculated (Coh74) and semi-empirical calculations (Mul70) are the only theoretical sources for the evaluation of the dissociation energy. Data on the dissociation energy show a spread of a factor of 4.

The large scatter in the experimental data on the above mentioned reactions obtained by previous authors, the limited range of ion energies used in studying the termolecular association and missing data on the dissociation rate of the molecular neon ion over a large range of energies, lead us to investigate the processes discussed in a well controlled Townsend discharge in neon in which the electrode distance d, the gas density N and the reduced electric field strength E/N can be chosen mutually independently. This implies a free choice of mean ionic energy and the possibility to distinguish between two- and three-body collision processes. The sampling of ions from a T.D. between plane parallel electrodes for current densities lower than 10^{-4} Am^{-2} has the advantage that the discharge can be described with the aid of a simple model. Cumulative processes, space

charge effects and space charge shielding around the sampling hole are insignificant. From this model we are able to calculate the dependence of the atomic and molecular ion current densities at the cathode on the discharge parameters reduced electric field strength, electrode distance and reduced gas pressure.

The product of the reaction rate for associative ionization and the mean lifetime of the excited reactant, is determined by fitting the expression for the ratio of atomic and molecular ion fluxes at the cathode to the experimental data. These data are known as a function of gas density, the reduced electric field strength being constant. The termolecular association rate for the Ne^+-ion and the dissociation rate for the Ne_2^+-ion are determined by fitting the expressions for the current densities at the cathode for the atomic ion and molecular ion, respectively. These data are obtained as functions of electrode distance, the reduced electric field strength and the gas density being constants.

III.2.1 Model of the Townsend discharge

As mentioned in the introduction in the present experiment use has been made of a T.D. between two plane parallel electrodes. The cathode contains the small orifice for ion sampling. In the model these electrodes are supposed to be infinitely large. This is allowed because in our experiments the ratio of electrode diameter to electrode distance is larger than 3. So the discharge is homogeneous in directions perpendicular to the axis of x. The cathode is situated at $x = 0$ and the anode at $x = d$, as indicated in figure 3.1.

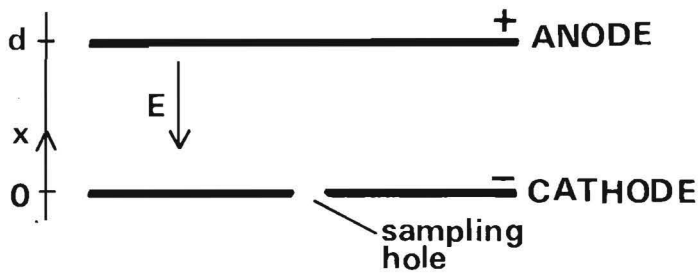

Figure 3.1 Electrode configuration of T.D.

In the present experiment the T.D. is used in the non-selfsustaining mode. The discharge is maintained by means of electron emission from the cathode by irradiation with U.V. light. In that case, as described in the introduction, an independent choice of the electrode distance d, the gas density N and the reduced electric field strength E/N is possible, yielding a free selection of *e.g.* the ion swarm energy. The current density is lower than 10^{-4} Am^{-2} in order to provide a homogeneous electric field with no space charge distortion. Moreover, space charge shielding around the orifice is absent. No cumulative processes *e.g.* stepwise excitation and ionization or dissociative recombination, occur. The Debye length of a plasma with densities comparable to those in the T.D. is larger than the geometrical dimension of the discharge tube, so no ambipolar diffusion of ions and electrons takes place. Table 3.1 gives typical values of characteristic quantities of the T.D. under the present experimental conditions.

Table 3.1 Characteristics of T.D.

current density	$e.j^{-}(d)$	$< 10^{-4}$	Am^{-2}
anode voltage	V	100-500	V
reduced gas pressure	p	0.01-15	kPa
electrode distance	d	$(0-3) \times 10^{-2}$	m
reduced electric field strength	E/N	10-300	Td

Before giving expressions for the atomic and molecular ion fluxes at the cathode as functions of the discharge parameters, the various processes which govern the electron density will be mentioned. A detailed treatment of these processes will be carried out in the sections III.3.1, III.3.2 and III.3.3. Atomic ions and electrons are mainly formed by direct ionization of ground state atoms according to

$$Ne + e^{-} \xrightarrow{k_i} Ne^{+} + 2e^{-} , \tag{3.4}$$

where k_i is the ionization rate. Direct excitation of ground state atoms to highly excited electronic states Ne_j^{**} according to

$$Ne + e^{-} \xrightarrow{k_{ej}} Ne_j^{**} + e^{-} , \tag{3.5}$$

where k_{ej} is the excitation rate, makes two compatative reactions become possible. The associative ionization reaction

$$Ne_j^{**} + Ne \xrightarrow{k_{rj}} Ne_2^+ + e^- , \tag{3.6}$$

where k_{rj} is the reaction rate for molecular ion formation, is one possibility. The other one is the unproductive decay of these highly excited states according to

$$Ne_j^{**} \xrightarrow{\tau_j} Ne + \ldots , \tag{3.7}$$

where τ_j is the decay time. At higher gas densities molecular ions arise mainly by termolecular association, with reaction rate k_c, of an atomic ion with two ground state atoms according to

$$Ne^+ + 2Ne \xrightarrow{k_c} Ne_2^+ + Ne . \tag{3.8}$$

The dissociation reaction

$$Ne^+ + Ne \xrightarrow{k_d} Ne^+ + 2Ne , \tag{3.9}$$

where k_d is the dissociation rate, is the reverse of reaction (3.8) and accounts for the loss of molecular ions in the discharge volume. Another process is the transport of electrons and ions to the anode and the cathode, respectively, under the influence of the applied electric field, and hence their disappearance from the discharge. This transport is described by the drift velocity of the particle which is defined as the mean velocity of those particles in the direction of the electrodes. The drift velocities of the atomic and molecular ions are v^+ and v_2^+, respectively. The drift velocity of the electrons is v^-. In the present work values for v^+ and v_2^+ were taken from Beaty and Patterson (Bea68) and from Hornbeck and Molnar (Hor51d), while data on v^- were taken from Hughes (Hug70).

Note that in the model the diffusion of the ions and the electrons is neglected with respect to their drift. The inverse proportion of the diffusion coefficient to the neutral gas density, and the small values of the gradients in the electron and ion densities, justify this simplification in nearly all experiments. Only in the associative ionization experiments the

gas density becomes so small that the diffusion of electrons cannot be neglected anymore. The influence of the diffusion of ions is negligeable in comparison to the influence of electron diffusion (*c.f.* II.5.5). In the associative ionization experiments, however, only the ratio of the atomic and the molecular ion fluxes is used. The influence of diffusion is assumed to be small enough to use the simplificated model. The above mentioned processes of formation and destruction of electrons, highly excited atoms and ions are given diagrammatically in figure 3.2.

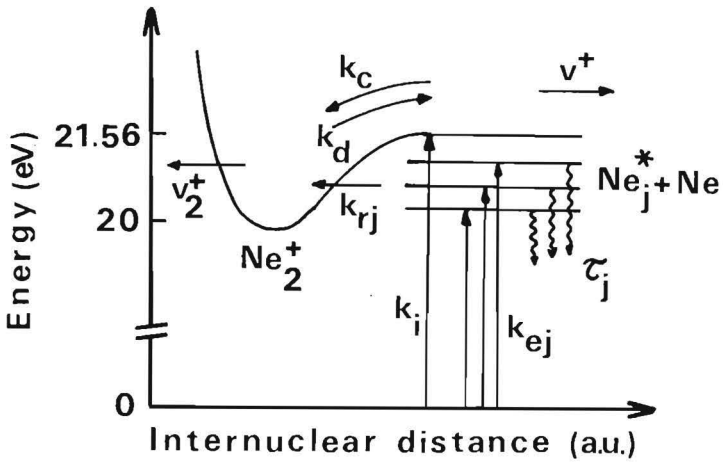

Figure 3.2 Processes in a T.D.

For every kind of particle j, *viz.* electrons, atomic ions and molecular ions, the continuity equation can be written as

$$\frac{\partial n_j(x,t)}{\partial t} + v_j \frac{\partial n_j(x,t)}{\partial x} = S(x,t) \tag{3.10}$$

where n_j is the particle density, v_j the drift velocity, t the time and S the source function, describing the processes of formation and destruction. For a stationary discharge the first term is zero, whereas the second term, describing the drift of the particle under the influence of the electric field, and the source function are time independent. One can replace the direct ionization rate of (3.4) by the direct ionization coefficient α_1, defined as the number of electrons which is formed through direct ionization by one electron per unit length in the direction of the electric field. This

leads up to

$$\alpha_1 = \frac{N.k_i}{\bar{v}} \quad , \tag{3.11}$$

where N is the neutral gas density. In the same way the rates for the reactions (3.5), (3.6) and (3.7) can be brought together in one quantity α_2, defined in a similar way as α_1 but describing the associative ionization and called the indirect ionization coefficient. The total ionization coefficient α can be written as

$$\alpha = \alpha_1 + \alpha_2 \tag{3.12}$$

For calculations in this work use has been made of data on the total ionization coefficient of de Hoog (Hoo69). When we apply equation (3.10) to electrons, atomic ions and molecular ions, three coupled differential equations arise which can be written as

$$\bar{v} \frac{dn^-}{dx} - \alpha \bar{v} n^-(x) = 0 \tag{3.13}$$

$$v^+ \frac{dn^+}{dx} + \alpha_1 \bar{v} n^-(x) + k_d.N.n_2^+(x) - k_c.N^2.n^+(x) = 0 \tag{3.14}$$

and

$$v_2^+ \frac{dn_2^+}{dx} + \alpha_2 \bar{v} n^-(x) - k_d.N.n_2^+(x) + k_c.N^2.n^+(x) = 0 \quad , \tag{3.15}$$

respectively. Here $n^-(x)$, $n^+(x)$ and $n_2^+(x)$ are the densities of electrons, atomic and molecular ions, respectively, as functions of x in the T.D..

Assuming the following boundary conditions for the atomic and molecular ion densities at the anode

$$n^+(d) = 0 \tag{3.16}$$

and

$$n_2^+(d) = 0 \quad , \tag{3.17}$$

respectively, together with the discharge current density $j^-(d)$ of the T.D.

$$j^-(d) = \bar{v} n^-(0).e^{\alpha d} \tag{3.18}$$

and the reciprocal free paths G and B for dissociation of Ne_2^+ and the conversion of Ne^+

$$G = \frac{k_d . N}{v_2^+} \tag{3.19}$$

and

$$B = \frac{k_c . N^2}{v^+} \quad , \tag{3.20}$$

respectively, the solutions of the continuity equations (3.13) to (3.15) can be found in closed form. For atomic ions the reduced ion current density, *i.e.* the ion current density at the cathode $j^+(0)$ divided by the discharge current density $j^-(d)$, can be written as

$$\frac{j^+(0)}{j^-(d)} = \frac{(G-\alpha_1)}{(\alpha-B-G)} e^{-\alpha d} + \frac{G}{(B+G)} + \frac{(\alpha_1 B-\alpha_2 G)}{(B+G)(\alpha-B-G)} e^{-(B+G)d} \tag{3.21}$$

and the reduced molecular ion current density can be written as

$$\frac{j_2^+(0)}{j^-(d)} = \frac{(B-\alpha_2)}{(\alpha-B-G)} e^{-\alpha d} + \frac{B}{(B+G)} - \frac{(\alpha_1 B-\alpha_2 G)}{(B+G)(\alpha-B-G)} e^{-(B+G)d} \quad . \tag{3.22}$$

As can be seen these equations give the fundamental dependencies of the reduced ion current density on the discharge parameters, namely the gas density N, the electrode distance d and the reduced electric field strength E/N. The dependence on the last mentioned quantity will be shown in III.2.3. At this point the advantage of the free choice of these parameters in a non-selfsustaining T.D. becomes clear.

III.2.2 General properties of T.D. quantities

The root mean square velocity $\sqrt{\overline{v_i^2}}$, which charged particles acquire in a gas of density N under the influence of a homogeneous electric field E is a function of the quantity E/N (McD72). The mean energy or swarm energy $\frac{1}{2} m_i \overline{v_i^2}$, which an ion with mass m_i obtains in a gas with temperature T, consisting of molecules with mass M, can be written, according to Wannier (Wan51), as

$$\frac{1}{2} m_i \overline{v_i^2} = \frac{1}{2} m_i v^{+2} + \frac{1}{2} M . v^{+2} + \frac{3}{2} k . T \quad , \tag{3.23}$$

where v^+ is the drift velocity of the ion. The first term on the right side stands for the drift energy of the ions. The second term represents the energy the ions acquire in consequence of the randomizing of the drift movement by ion-neutral collisions. The last term is the energy of the ions as a result of the temperature movement of the gas molecules. Calculations of the ion swarm energies in this work are always carried out using Wanniers expression.

The ratio of the direct ionization coefficient α_1 and the gas density N, α_1/N, depends on E/N alone and not on N, as can be seen from (3.11). The reduced indirect ionization coefficient α_2/N depends, as will be explained in III.3.1, on E/N as well as on N. The total reduced ionization coefficient α/N therefore depends on E/N and N, especially for small values of E/N where α_2 becomes comparable with α_1. At decreasing gas density and constant E/N, $\alpha_1/N + \alpha_2/N$ approaches α_1/N, so α/N must show a density dependence, which never has been studied systematically (Kru37, Loe60, Hoo69, Cha63).

III.2.3 Method

The purpose of the present work is to determine, from processes (3.4) to (3.9), the ratio of ionization rate and excitation rate k_i/k_e, the product of associative ionization rate and mean lifetime of highly excited neon atoms $k_r\tau$, the termolecular association rate k_c and the rate for collisional dissociation of Ne_2^+ k_d as functions of E/N, and hence as functions of the mean energy of the colliding particles (*c.f.* sections III.3.1 to III.3.3).

A short preview of the experimental method and mathematical analysis is given here. In order to obtain the reaction rate for each single process from the set of three processes, to be studied *viz.* associative ionization, termolecular association and collisional dissociation, the reduced ion fluxes are measured as functions of <u>one</u> discharge quantity of the three mentioned, namely the gas density N, the electrode distance d or the reduced electric field strength E/N. The other two quantities are kept constant. For each elementary process these measurements can be carried out in that specific region of discharge parameters where the influence of the process to be studied has an optimum, while at the same time the influence of the other elementary processes is small. The meaning of "small" can be twofold.

In the first place other processes may be not much in evidence under those specific discharge conditions. It may also occur that these processes do indeed take place but do not interfere in the analysis of the process to be studied. *E.g.* when studying the associative ionization process, the ratio of reduced atomic and molecular ion densities is measured as a function of the reciprocal gas density, with E/N and Nd as parameters. The gas densities chosen are so small that the conversion process, which is a three-body process, gives a negligible contribution to the formation of molecular ions.

The mathematical analysis of most experimental data was carried out by iteration. In the first round the reaction rates for the processes which

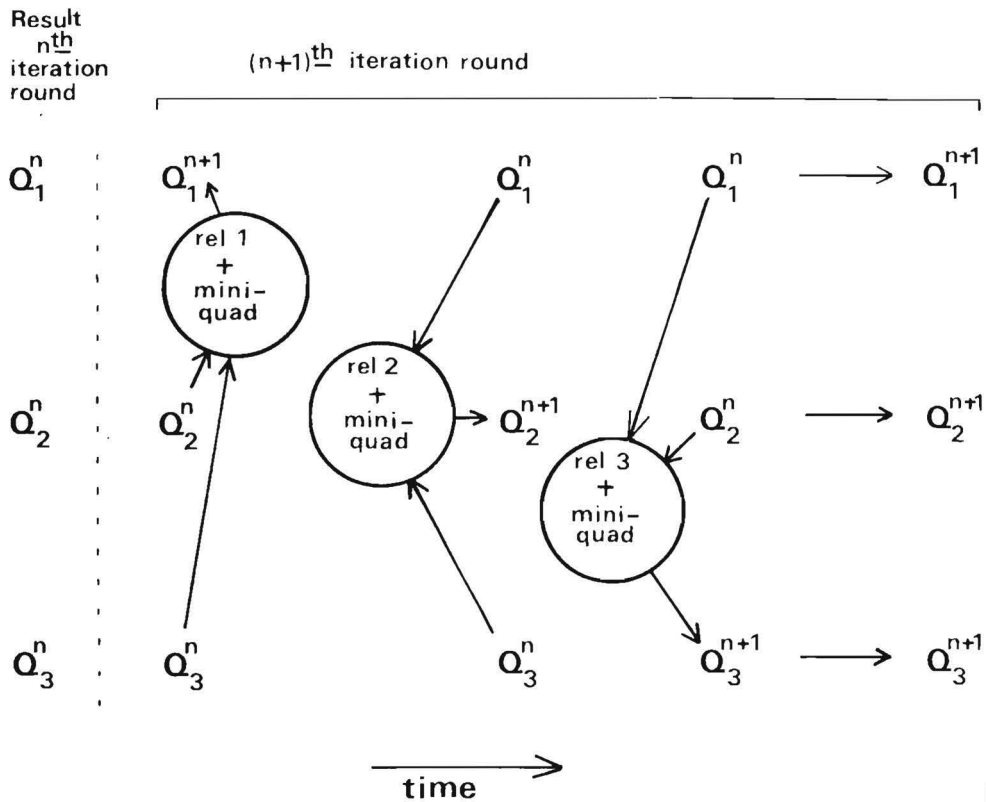

Figure 3.3 Generalized diagram of the iterative process. Q_1, Q_2 and Q_3 are rate coefficients of specific elementary processes, appearing as constants in relation i (i = 1, 2 or 3). Each relation gives the functional dependency of a specific physical quantity, e.g. the molecular ion flux, on a discharge quantity, e.g. the electrode distance.

have only a small effect on the reduced ion currents, compared to that specific elementary process, are taken to be zero. In this way (3.21) and (3.22) reduce to simpler expressions. By means of a non-linear least square procedure ("MINIQUAD" on the Burroughs 7700, THE Eindhoven), equation (3.21) and/or (3.22) are fitted to the experimental points, giving a value for the reaction rate of the process to be studied. This procedure is carried out for all the three elementary processes mentioned earlier. In the second round the complete expressions (3.21) and (3.22) are used. For the two less important processes, that accompany the process to be studied, the values for the reaction rates found in the first round, are used as constants in equation (3.21) and/or (3.22). These expressions are fitted to the experimental points by means of the least mean square procedure, and a new value for the reaction rate of the process studied is obtained. This procedure is carried out for all the three elementary processes again. A next round, identical to the second round, will be carried out until the rest terms are so small that sufficient accurate values are obtained for the reaction rates we are interested in. A flow diagram of this iterative process is given in figure 3.3.

III.3 Elementary processes

III.3.1 Associative ionization (A.I.)

III.3.1.1 Introduction

Diatomic rare gas atoms of helium, neon and argon were first identified by Tüxen (Tux36) in an experiment using a mass spectrometer. In experiments by Arnot and M'Ewen (Arn39) the appearance of He_2^+ was investigated and they assumed that the formation process of He_2^+ contains two steps. First the excitation by electron impact of a ground state helium atom takes place and then a collision of that excited atom with another ground state atom occurs, resulting in the formation of a molecular ion. Hornbeck and Molnar investigated mass spectrometrically the formation of molecular ions from helium through xenon following electron impact at gas pressures from 0.01 to 1 Pa (Hor51d). One result of these measurements was that the appearance potentials for molecular ions were about 1 eV smaller than the ionization

potential of the corresponding atom. Also it was concluded by these authors that only highly excited states contribute to the molecular ion formation process mentioned by Arnot and M'Ewen. It might seem somewhat surprising that in the experiments of Hornbeck and Molnar as in the present experiments molecular ions are observed at such low gas densities that the free flight time for an excited atom is larger than a microsecond. This, however, is consistent with the assumption that only highly excited states are involved in the associative ionization reaction. These atomic states have long radiative lifetimes and cascade radiation causes them to stay even longer in the reaction band of about 1 eV below the ionization limit.

As mentioned in the introduction, three experiments on associative ionization in neon, are known. In the analysis of all these experiments as well as the present experiment, the associative ionization is supposed to arise from only one highly excited state. Hornbeck (Hor51c) measured the transient current following the release of a short pulse of photo-electrons from the cathode of a T.D.. In the current pattern two breaks could be seen, one of them ascribed by Hornbeck to the formation of atomic ions and the other one to molecular ions. From the observed slopes of the breaks he concluded the latter ion to be formed within 1 μs and A.I. to be the process responsible. Mathematical expressions on the formation processes were fitted to the data, giving rough values for the ratio of the ionization rate to the excitation rate, as well as for the product of the rate for A.I. and the excited lifetime for helium, neon and argon for constant values of E/N. No mass spectrometer for ion identification was used in this experiment.

Studies of Von Pahl on the formation of molecular noble gas ions in a stationary low pressure positive column, were carried out by measuring mass spectrometrically the fluxes of atomic and molecular ions on the wall (Pah59). The ions formed in the discharge move in the ambipolar field to the wall of the discharge tube where they were sampled through a small orifice. From the measured ratio of atomic and molecular ion fluxes as functions of gas density the value of $k_r\tau$ was obtained. According to the author the results are affected by uncertainties in the value of the ratio of the ionization rate and the excitation rate, and by uncertainties about the influence of the process of dissociative recombination. The most extensive measurements known were done by Dahler *et al.*(Dah62). Their

measurements were carried out in a mass spectrometer coupled to an ionization chamber. The mass spectrometer is differentially pumped with a capacity sufficiently large to permit operation at ionization chamber pressures up to 70 Pa. The gas is ionized and excited by an electron beam. Electrons could be accelerated to energies from 15 eV up to 70 eV. The ions formed were pushed out of the ionization chamber by an ion-repeller at field strengths of 1.2 to 5 kVm^{-1} and mass analysed. In Dahlers work current ratios of Ne^+ and Ne_2^+-ions were measured as functions of ionization chamber pressures (up to 35 Pa) for electron energies of 20 and 70 eV. From these measurements data were obtained for the product $k_r\tau$ of the reacting highly excited atoms, and the termolecular association rate k_c for helium, neon and argon. With respect to the data on helium, the value of $k_r\tau$ found by Dahler *et al.* is at least an order of magnitude larger than more recent results for helium by Robben (Rob72), and Wellenstein and Robertson (Wel72). Dahlers results for $k_r\tau$ in argon agree reasonably well with experiments of Becker and Lampe (Bec65) using the same experimental technique, but are a factor 4 to 60 larger than previous experimental results (Huf66, Kau60, Hor51c, Pah63, Fit73, Pah58). One should discuss Dahlers results keeping in mind that his result on the conversion rate k_c in neon is two orders of magnitude larger than previous, well established experimental and theoretical results, mentioned in III.3.2.

A fundamental theory which can be used to calculate the cross section for associative ionization is that of Demkov and Komarov (Dem66). They found an expression for the transition probability of the process

$$A^* + B \rightarrow A + B^+ + e^- , \qquad (3.24)$$

which has a similar mathematical form as the Landau-Zener expression. The elegance of Demkovs expression is that it contains only one parameter.

As can be seen the data on $k_r\tau$ obtained in the experiments described earlier differ by more than three orders of magnitude. In view of this mutual disagreement, in the present work mass spectrometrical studies of the A.I. process in a T.D., in which cumulative processes *e.g.* dissociative recombination do not take place, have been carried out.

III.3.1.2 Analysis

In section III.2.1 expressions have been derived giving the dependence of the reduced ion current densities at the cathode of the T.D. on discharge parameters. These expressions contain too many parameters to make a direct fit of these relations to measured current densities.

The A.I. is studied at gas densities less than 400 Pa, where the contribution of termolecular association on the formation of Ne_2^+ is small. In the present experiment the influence of dissociation is negligibly small, as will appear below. In the first iteration round, as can be seen from figure 3.3, we put k_c and k_d zero and (3.21) and (3.22) reduce to

$$\frac{j^+(0)}{j^-(d)} = \frac{\alpha_1}{\alpha}\,(1 - e^{-\alpha d}) \tag{3.25}$$

and

$$\frac{j_2^+(0)}{j^-(d)} = \frac{\alpha_2}{\alpha}\,(1 - e^{-\alpha d}) \tag{3.26}$$

The ratio of reduced atomic to molecular ion current densities can be written written as

$$\frac{j^+(0)}{j_2^+(0)} = \frac{\alpha_1}{\alpha_2}\ . \tag{3.27}$$

From the equations (3.15) and (3.16) we deduce

$$\alpha_2 . v^- . n^-(x) = \sum_j k_{rj} . N . n_j^{**}(x)\ . \tag{3.28}$$

At this point the simplification is made that A.I. takes place through only one highly excited state *i.e.* the different close-lying levels j are treated as a single state with excitation rate k_e, decay time τ and A.I. rate k_r. In a stationary discharge the density of the excited state n^{**}, using equations (3.5) to (3.7) can be written as

$$n^{**}(x) = \frac{k_e . N . n^-(x)}{1/\tau + k_r . N}\ . \tag{3.29}$$

Substitution of equations (3.28), (3.29) and (3.11) into equation (3.27) gives

$$\frac{j^+(0)}{j_2^+(0)} = \frac{k_i}{k_e}\left(1 + \frac{1}{k_r\tau}\frac{1}{N}\right) . \qquad (3.30)$$

Relation (3.30) represents, in first approximation, a linear relationship between the ratio of the ion current densities and the reciprocal gas density. The cut-off of the graphical representation at the axis of ordination divided by its inclination gives the reciprocal $k_r\tau$-value, whereas k_i/k_e is given by the cut-off. In the experiments the measured ion flux through the orifice in the cathode in counts per second, is proportional to the ion current density $j^+(0)$, while the measured total current I through the T.D. is proportional to the discharge current density $j^-(d)$. In the A.I. experiment atomic and molecular ion fluxes are measured as functions of the reciprocal gas density, for a constant value of E/N and at constant Nd. For such a series of measurements k_i/k_e has a fixed value. The constancy of Nd implies the dissociation reaction (3.9) to have a negligible influence on the value of $k_r\tau$ determined. The mean free path of Ne_2^+-ions for dissociation is inversely proportional to N. Because the similarity rules are obeyed, the probability of a dissociative collision before arriving at the cathode is the same for molecular ions generated at similar positions in the discharge, and this probability is proportional to Nd. From equation (3.30) one sees that the dissociation reaction does not influence the determined value of $k_r\tau$. In the second round of the iterative analysis, the first round results for the dissociation rate and the termolecular association rate are put into equations (3.21) and (3.22). These complete expressions are fitted to the experimental points to obtain better values for k_i/k_e and $k_r\tau$, etc. The effect of including the conversion and dissociation processes in the analysis of the A.I. measurements, as is done in the iteration process, show $k_r\tau$ to decrease by at most 10%, whereas k_i/k_e decreases from about 25% at low E/N up to a factor of 2 at high reduced electric field strength.

III.3.1.3 Experiment

The A.I. experiments have been carried out in the T.D. in neon with variable electrode distance at 295 K. In the non-selfsustaining discharge

the atomic and molecular ion fluxes and the discharge currents have been measured at constant E/N and constant pd, as functions of gas pressure p from 65 to 330 Pa. As can be seen from II.5.4 the transmission of the sampling orifice for ions is constant in this pressure range. The parameter E/N varies from 46 to 245 Td, whereas pd is 1.2 and 2.0 Pa.m.

III.3.1.4 Results

Typical plots of the measured ion fluxes ratios as functions of the reciprocal gas pressure for reduced electric field strengths of 92 and 214 Td are shown in the figures 3.4 and 3.5. The results of these experiments on $k_r\tau$ and k_i/k_e, as functions of E/N are shown in the figures 3.6 and 3.7. As can be seen from these figures the product of the A.I. rate and the mean decay time of highly excited neon atoms contributing to the A.I. reaction, shows a systematic increase by a factor 3 from 0.6×10^{-23} m^3 at an E/N of 45 Td to about 2.0×10^{-23} m^3 at an E/N of 245 Td. The ratio k_i/k_e of the ionization rate and the excitation rate, the latter representing the excitation by electron impact to those atomic states which might result in

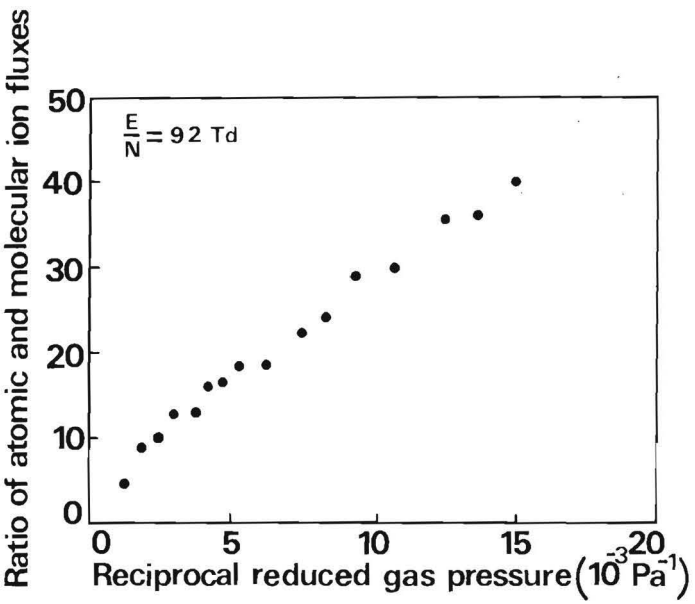

Figure 3.4 Associative ionization measurements at an E/N of 92 Td.

A.I., shows an increase by more than 2 orders of magnitude, from 0.6 at an E/N of 45 Td to a value of 160 at an E/N of 245 Td.

III.3.1.5 Discussion

Previous and present experimental results on the associative ionization process in neon, in terms of $k_r\tau$ and k_i/k_e, are given in table 3.2.

In figure 3.8 known experimental data on $k_r\tau$ are given on a logerithmic scale for helium, neon, argon, krypton and xenon. From this figure one can see immediately that the experimental results on $k_r\tau$ in noble gases disagree by 2 or 3 orders of magnitude for each gas. Dahlers experiment on A.I. is the only one in neon not carried out in a gas discharge. In this experiment electrons of a specific energy excite and ionize the gas atoms present in the ionization chamber, in contrast with gas discharges where the electron

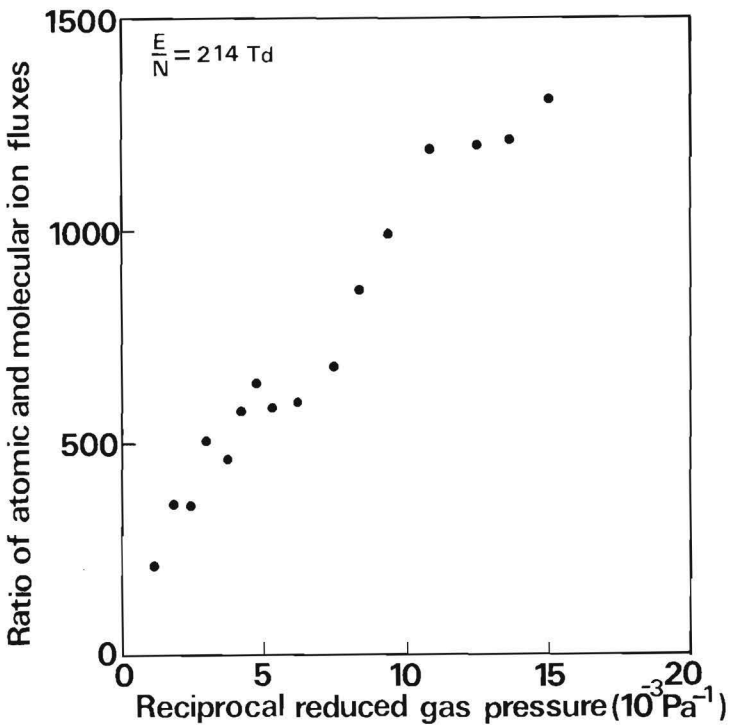

Figure 3.5 Associative ionization measurements at an E/N of 214 Td.

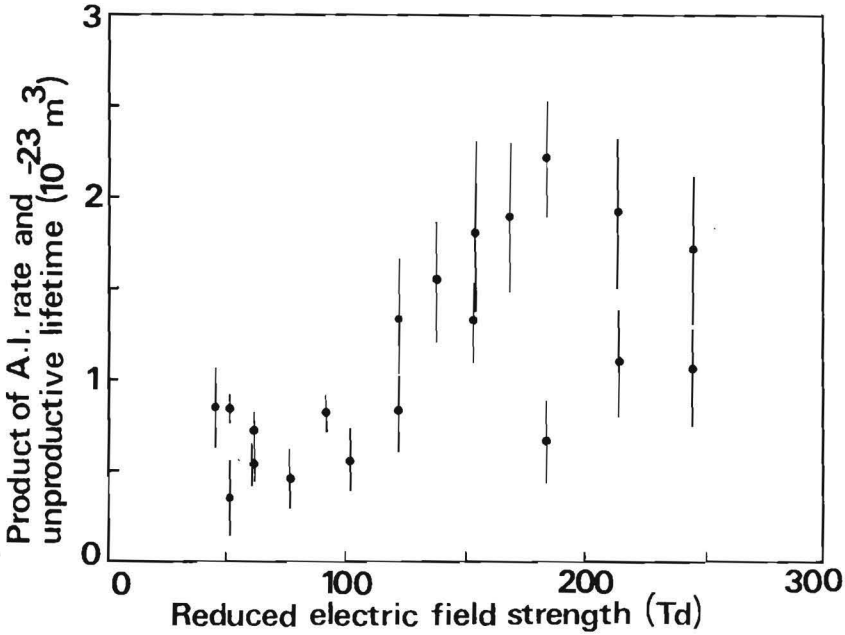

Figure 3.6 Measured dependence of $k_r\tau$ on E/N.

Table 3.2 Previous and present experimental results on associative ionization in neon.

reference	$k_r\tau$ (m^3)	k_i/k_e	method
Dahler, J.S. *et al.* (Dah62)	$(12 \pm 3)\times10^{-22}$ $(1.1\pm0.1)\times10^{-22}$	110±20 223±15	Ionization chamber + mass spectrometer. Results depend on electron energy (20 and 70 eV, respectively).
Hornbeck, J.A. (Hor51c)	3.0×10^{-24}	5	Pulsed T.D.; no mass spectrometer. E/N = 42 Td.
Pahl, M. von (Pah59)	$(0.33-1.1)\times10^{-24}$	1	Low pressure positive colum + mass spectrometer.
Present	$(0.6-1.9)\times10^{-23}$	0.7-200	T.D. + mass spectrometer. $45 < E/N < 245$ Td.

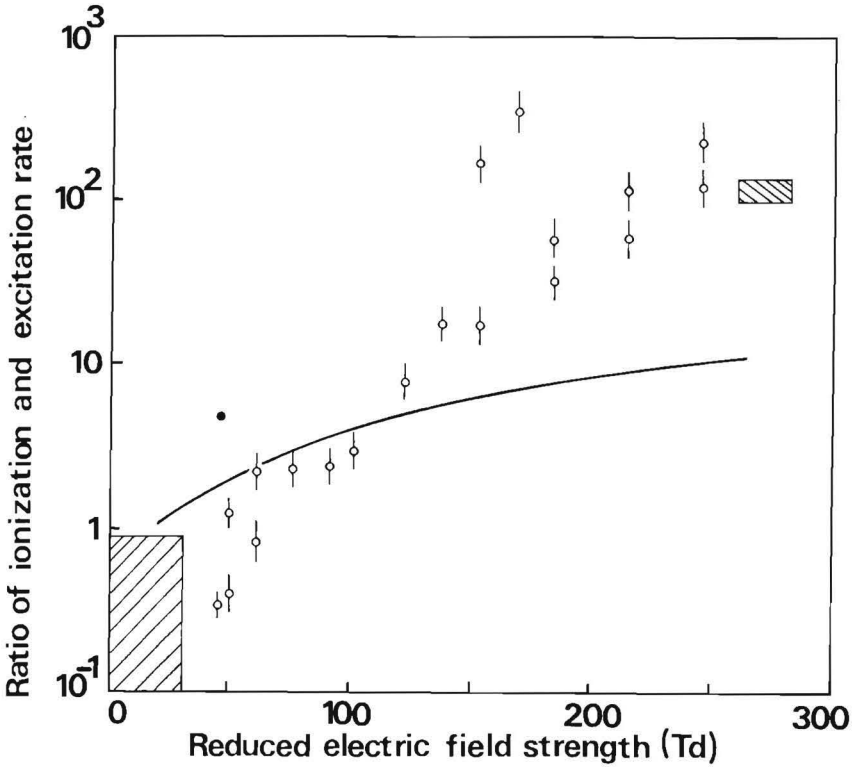

Figure 3.7 Measured ratio k_i/k_e as a function of E/N. ○ (present); ● (Hor51c); ▨ (Pah59); ▧ (Dah62); —— (calculations appendix).

energy has a broad distribution with a mean value usually much smaller than the electron energy Dahler used in his experiment. Becker and Lampe (Bec65) also investigated the A.I. process in argon with an experimental setup containing an ionization chamber. As can be seen from figure 3.8 the result of Dahler, and Becker and Lampe on $k_r\tau$ for He, Ne and Ar are about one order of magnitude larger than data obtained from gas discharge experiments. In the same experiment Dahler determined the termolecular association rate in neon which appeared to be a factor of 100 larger than generally accepted. We have too little knowledge on the experimental technique these authors used, to criticize their work. A comparison, however, of their results with data of other authors gives rise to the assumption that data on $k_r\tau$ and k_c, as found by Dahler *et al.*, are too large.

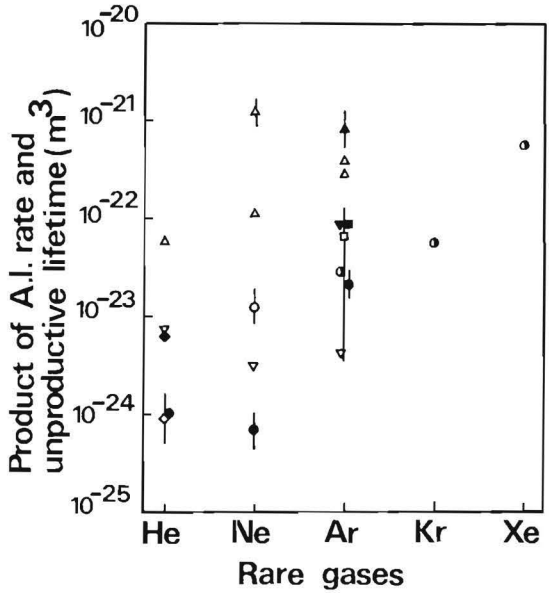

Figure 3.8

Data on previous and present values of $k_r\tau$.

○ *(present)*
△ *(Dah62)*
▼ *(Pah63)*
▲ *(Bec65)*
◑ *(Fit73)*
□ *(Huf66)*
● *(Pah59)*
■ *(Kau60)*
◆ *(Rob72)*
▽ *(Hor51c)*
◇ *(Wel72)*

The ratio of ionization and excitation as measured by Dahler cannot be compared directly with the present results, because in their experiments a monochromatic electron energy distribution exists. A mean electron energy of 20 eV, which is the lowest value used by Dahler, can only be achieved in gas discharges like the present T.D., at a reduced electric field strength of about 300 Td, as can be seen from calculations of Kitamori *et al.* (Kit78). Dahlers value of 110 for k_i/k_e at an electron energy of 20 eV is a reasonable agreement with present experimental results at the highest E/N. Only the lowest value used by Dahler can be compared with gas discharge experiments.

Although no identification of the formed ions was carried out by a mass spectrometer, the experiment by Hornbeck (Hor51c) was carried out in a discharge under well specified conditions. The author gives no accuracy interval for the experimental results obtained in this experiment, but only says that his measurements are rough. However, the data of $k_r\tau$ are in reasonable agreement with other experimental results, as is to be seen in figure 3.8. The value of k_i/k_e of 5 is about a factor of five larger than the present experimental results under comparable conditions.

The study of A.I. by Von Pahl (Pah59) in a stationary positive column, coupled to a mass spectrometer, is afflicted with a number of uncertainties as mentioned by the author, which might interfere in the analysis of the experimental data. Uncertainties in the determination of k_i/k_e are carried through in the determination of $k_r\tau$. In the experiment the gas density is varied, as a consequence of which the reduced electric field strength, determining the ratio of ionization and excitation, is no longer a constant. The transmission of the orifice for ion sampling, which was measured for helium in an earlier work of this author and his co-worker (Pah58, Wei58), and which varied between 30% and 50% with changing gas pressure, is assumed to be constant in the analysis of experimental data. The reduced electric field strength in this experiment is lower than 10 Td. Pahl estimated the value of k_i/k_e to be less than 1, which is in agreement with the present data on k_i/k_e, as is to be seen in figure 3.7.

From the results of the present study on the A.I. reaction, two main features can be noticed. Firstly the systematic increase of $k_r\tau$ as a function of reduced electric field strength, secondly the strong increase of k_i/k_e for increasing reduced electric field strength by more than two orders of magnitude.

Concerning the product of A.I. rate and lifetime of the excited reactant, one can say that $k_r\tau$, containing only atomic quantities when τ is supposed to be the mean radiative lifetime of highly excited states, is a constant and therefore should have no dependence on discharge parameters *e.g.* E/N. In the physical model describing the A.I. process, separate excited neon states within about 1 eV under the ionization potential, are all taken together into one excited level with one reaction rate and one unproductive decay time. In reality each single excited level, however, may have a specific A.I. rate and lifetime. The dependence of the measured value of $k_r\tau$ on E/N can physically be made plausible. The higher the excited neon state the longer the radiative lifetime (Afa75a, Afa75b) and the larger the reaction probability for this excited state to bring about the A.I. reaction (Dem66). At large reduced electric field strength when the electrons have a large mean energy, the higher lying neon states will be populated relatively more by electron impact in comparison to the lower lying states, than in the case of smaller reduced electric field strengths. Therefore at

increasing E/N the product $k_r\tau$ also may increase. This phenomenon is investigated in the appendix by taking into account each single excited neon state n_j^{**} in the model calculations. The assumptions made in these model calculations are (*i*) the unproductive decay time for each excited state is equal to its radiative lifetime; (*ii*) the reaction rate for associative ionization as a function of the energy of the excited state, is given by the expression from Demkov and Komarov; (*iii*) the absolute value of the cross section for electronic excitation to an excited state with principal quantum number n, is proportional to n^{-3}; (*iv*) the shape of the cross section above threshhold has an E^{-1}-dependence, with E the energy; and (*v*) a Druyvesteyn function is supposed to be the electron energy distribution. As a result of these calculations we found that $k_r\tau$ is independent of E/N, in contrast with the measurements.

III.3.1.6 Conclusion

Under well specified discharge conditions we have obtained experimental data on the product of the A.I. rate and the mean unproductive lifetime, $k_r\tau$, and the ratio of the ionization rate to the excitation rate, k_i/k_e, as a function of reduced electric field strength E/N.

The value of $k_r\tau$ ranges from 0.6×10^{-23} m^3 at an E/N of 45 Td up to 2.0×10^{-23} m^3 at an E/N of 245 Td. When we compare these results with previous experimental results, as indicated in figure 3.8, one should keep in mind that our experimental conditions are much better defined. The transmission of the sampling hole for both atomic and molecular ions was constant for the pressures we used. Also the discharge parameters in the T.D., *viz.* E/N, N and d could be chosen independently. Finally we used ultra-high vacuum techniques and cataphoretic cleaning of the gas in order to ensure an impurity content below 1 ppm.

The values of k_i/k_e show a strong increase from 0.6 at an E/N of 45 Td to 160 at an E/N of 245 Td. This strong increase of k_i/k_e at increasing E/N is in agreement with previous experimental results. From the slight increase of $k_r\tau$ and the strong increase of k_i/k_e as functions of E/N we conclude that the high energy tail of the electron energy distribution decreases more rapidly than that of the Druyvesteyn distribution.

III.3.2 Termolecular association (T.A.)

III.3.2.1 Introduction

The termolecular association of an atomic ion in a collision with two ground state atoms leading to the formation of a molecular ion is a three-body reaction, and therefore takes place predominantly at high gas densities. This process is studied in bulk experiments like afterglows and drift tubes. In drift tube experiments the rate for T.A., in combination with mobility measurements of atomic and molecular ions can be determined as a function of reduced electric field strength and hence as a function of mean ionic energy. Experiments of Beaty and Patterson (Bea68) and Orient (Ori73) in neon both were carried out in a similar way using a four-grid electrical shutter drift tube. Orient used a mass spectrometer for ion identification. In both studies the continuity equation for the ions, including diffusion, drift and the T.A. reaction, was solved. The theoretical expression was fitted to the experimental time of flight spectrum of both atomic and molecular ions with the diffusion coefficients, the mobilities and the reaction rate acting as unknown parameters. Beaty and Patterson measured the rate for T.A. for values of the reduced electric field strength from 5.6 Td to 17.8 Td and found a slight decrease of the rate k_c from 0.73×10^{-43} m^6s^{-1} at the lowest reduced field strength to about 0.50×10^{-43} m^6s^{-1} at the highest E/N values. Orient on the other hand obtained data for the reaction rate that were independent from the reduced electric field strength. His measurements were carried out from 5.3 Td to 28.3 Td, leading to a value of $k_c = (0.46 \pm 0.04) \times 10^{-43}$ m^6s^{-1}.

In neon afterglow studies the time dependence of the atomic ion density was measured and from that values for the rate of T.A. and the ambipolar diffusion coefficient were derived. These data, in contrast with results from drift tube experiments are obtained for ion temperatures equal to the gas temperature. Experiments of Sauter *et al.* (Sau66), Smith and Cromey (Smi68) and Vitols and Oskam (Vit72) only gave the T.A. rate for a gas temperature of 300 K. In all these studies a mass spectrometer was used for ion identification. Data on k_c range from 0.41×10^{-43} m^6s^{-1} to 0.79×10^{-43} m^6s^{-1}. Two experimental studies are known in which the temperature dependence of the T.A. rate was investigated. Hackam (Hac66) measured the temperature variation of electron density decay rates following

a pulsed discharge in neon by means of the microwave cavity method. No mass spectrometer was used. The measured reaction rate was found to be proportional to the gas temperature giving values of 0.092×10^{-43} m^6s^{-1} for a temperature of 195 K to 0.27×10^{-43} m^6s^{-1} for a temperature of 523 K. This is in contradiction to results of Niles and Robertson (Nil65) in helium who found the T.A. reaction to be inversely proportional to gas temperature.
Che Jen Chen (Che69) investigated mass spectrometrically the ion density in a decaying neon plasma for temperatures ranging from 300 to 1500 K, and obtained a $T^{-0,23}$ dependence for the reaction rate, where T is the gas temperature. His value at 300 K appeared to be 0.85×10^{-43} m^6s^{-1}.

As can be seen the results of previous experiments on the reaction rate for T.A. mutually disagree by almost an order of magnitude, whereas complete uncertainty exists on the temperature dependence of the reaction rate.

Theoretical calculations were carried out in several ways. Niles and Robertson (Nil65b) used a combination of an expression for the inverse dissociation reaction and the principle of detailed balancing to obtain the T.A. reaction rate around 300 K. For neon a value of 0.143×10^{-43} m^6s^{-1} was found, whereas a T^{-1} dependence on the gas temperature T was obtained. Mahan (Mah65) proposed the mechanism to proceed via a resonant charge transfer reaction, followed by the capture of the "slow" ion by the polarization interaction. A value of 0.62×10^{-43} m^6s^{-1} was obtained for the reaction rate. Dickinson *et al.* (Dic72) assume the reaction to proceed via the formation of a long lived complex of an ion and an atom, which is deactivated in a collision with a third atom. A value of 0.40×10^{-43} m^6s^{-1} was obtained. Smirnov (Smi67) calculated the reaction rate for T.A. in a similar way as done by Dickinson. A $T^{-3/4}$ law is found for the reaction rate, whereas at 300 K a value of 1.15×10^{-43} m^6s^{-1} was calculated. The scatter in the results of the theoretical calculations is about one order of magnitude. The theoretical data on k_c of Maham and Dickinson *et al.* agree fairly well with present experimental results. In the expression for k_c as calculated by Niles and Robertson the steric factor was treated as an adjustable parameter and was fit to obtain agreement between the theoretical and experimental results of k_c for He. A 50% larger value for this steric factor together with an increase of the dissociation energy of the molecular ion from 0.6 eV to 1.4 eV, as has been found in the present work, causes good

agreement with the present experimental result on k_c. Smirnov obtained relative rates for T.A. A fit of his expression to experimental results in He, gave a best value for the proportion constant. The difference between Smirnovs method and that of Dickinson *et al.* is that in the former method the excited molecular ion states were not specified (Dic72). In the present work a method is proposed with the aid of which the reaction rate for T.A. can be determined. The atomic and molecular ion fluxes at the cathode of a non-selfsustaining T.D. are measured as functions of the electrode distance with constant gas density and constant reduced electric field strength. The reaction rate for T.A. is calculated by fitting equation (3.21) to the experimental points for low values of E/N, and of equation (3.22) for higher values.

III.3.2.2 Analysis of the experiments

Expressions for the reduced atomic and molecular ion current densities at the cathode of a T.D. have been derived in section III.2.1. These expressions give the fundamental dependence of these current densities on the gas density N, the electrode distance d and the reduced electric field strength E/N. In the experiment described below, for reduced electric field strengths smaller than about 30 Td, the atomic ion flux, which is proportional to the atomic ion current density, and the total current through the discharge, which is proportional to the discharge current density, are measured as functions of the electrode distance, with the gas density and the reduced field strength acting as parameters. The gas density is kept constant in this experiment to ensure that the transmission of the sampling orifice is constant. The mean ionic energy is well defined and constant because the reduced electric field strength is fixed. The reaction rate for T.A. is calculated by fitting equation (3.21) to the experimental points by an iterative process. In the first round the dissociation rate is taken zero in equation (3.21) which is a good approximation because of the low value of the reduced field strength, and hence the low mean ion energy. For the associative ionization process, the first approximation, given by equation (3.30), is used. In the second round of iteration the dissociation rate, found in first approximation is used, together with the second approximation of the associative ionization rate. This scheme is repeated until a sufficiently accurate result for the T.A. rate is found. The three-body

nature of T.A. makes it necessary for these measurements to be carried out at relatively high gas pressures of more than about 2.5 kPa, in order to have an appreciable change in the reduced atomic ion current density with changing electrode distance. To provide for the non-selfsustaining character of the T.D. therefore, the reduced electric field strength must be smaller than about 40 Td. For larger reduced electric field strength the molecular ion current density is measured as a function of the electrode distance for constant gas density and reduced electric field strength. The gas pressure is of the order of a few hundreds of pascals. In a similar iterative process equation (3.22) is fitted to the experimental points using a value for the associative ionization rate found in the previous round. In this way data for the T.A. rate as well as for the dissociation rate are obtained. With these experiments data on the reaction rate for T.A. at high mean ionic energy, up to one electron volt, are obtained.

III.3.2.3 Experiment

The T.A. experiments have been carried out in the T.D. in neon with variable electrode distance at 295 K. In the non-selfsustaining discharge the atomic and molecular ion fluxes and the discharge current have been measured at constant values of E/N and constant gas pressure. For reduced electric field strengths from 9 Td to 45 Td, the atomic ion flux has been measured for pressures between 1.65 kPa and 4.0 kPa. The molecular ion flux has been measured for reduced electric field strengths of 150 Td and 210 Td and pressures of 0.40 kPa and 0.27 kPa, respectively.

III.3.2.4 Results

A typical plot of the measured atomic ion flux as a function of the electrode distance for a reduced electric field strength of 30 Td and a reduced gas pressure of 2.1 kPa is given in figure 3.9. A similar plot of the molecular ion flux as a function of the electrode distance for an E/N of 210 Td and a reduced gas pressure of 0.25 kPa is shown in figure 3.10. The results of these measurements in terms of the reaction rate for T.A., k_c, are shown in figure 3.11. In this figure also previous experimental and theoretical data on k_c are given. A note should be made on the measurements of the T.A. rate, obtained from the measured atomic ion flux dependence on

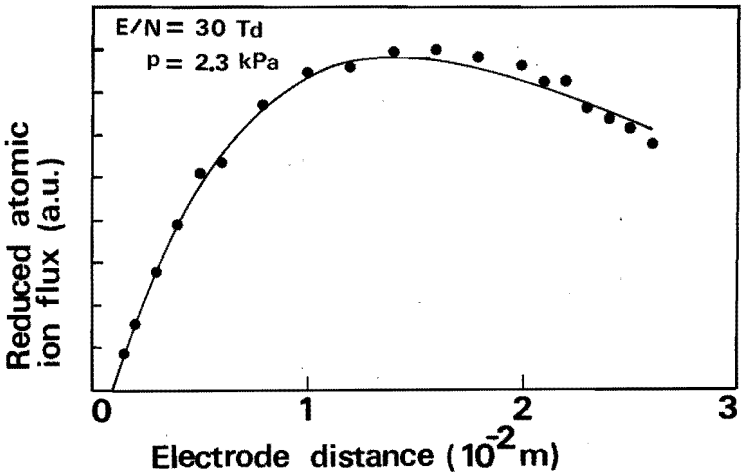

Figure 3.9

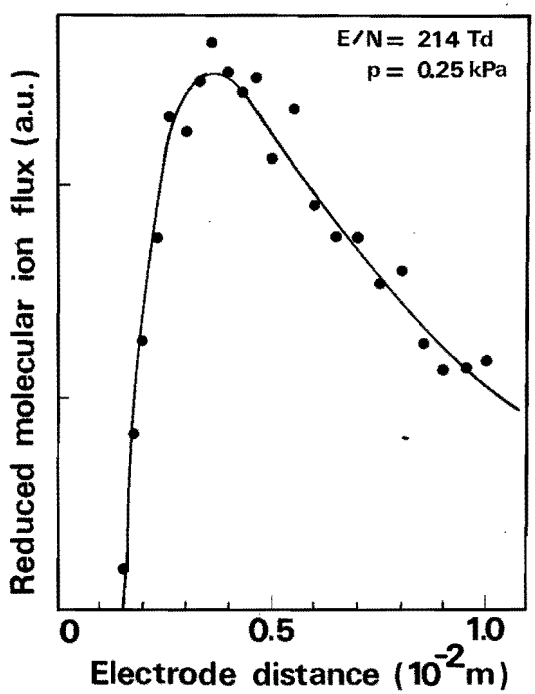

Figure 3.10

Figures 3.9 and 3.10 show comparisons of experimental results (●) with results from the model in which k_c and k_c,k_d are fitted, respectively.

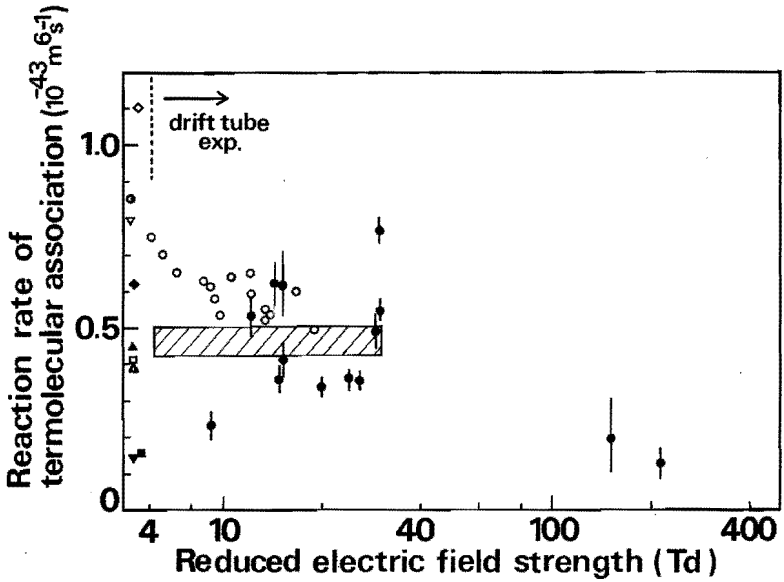

Figure 3.11 *Previous and present experimental and theoretical results on termolecular association in neon.*
Experimental: ● *(present)* ▽ *(Smi68)*
▨ *(Ori73)* ■ *(Hac66)*
○ *(Bea68)* ▲ *(Vit72)*
◑ *(Che68)* □ *(Sau66)*
Theoretical: △ *(Dic72)* ◆ *(Mah65)*
▼ *(Nil65b)* ◇ *(Smi67)*

the electrode distance, for reduced electric field strengths between 30 Td and 45 Td. Because of the large E/N and high gas pressure the T.D. operates close to breakdown at the largest electrode distance used and the electron current density becomes so large that space charge might disturb the ion density profile in the T.D.. The mathematical expression (3.21) fits the experimental points poorly. Therefore only the results for reduced electric field strengths smaller than 30 Td are given in this figure. No systematic dependence of k_c on the reduced field strength for E/N smaller than 30 Td can be seen from figure 3.11. The mean value of k_c is equal to $(0.47\pm0.05) \times 10^{-43}$ m^6s^{-1}. The two values of k_c, determined by a least mean square fit of the measured molecular ion flux as a function of electrode distance, indicate a decreasing dependence of the T.A. rate at increasing mean ionic energy.

III.3.2.5 Discussion

The present data on the termolecular reaction rate k_c are in very good agreement with data measured by Orient (Ori73) and Beaty and Patterson (Bea68). In the lower E/N range the scatter in the points agree with a constant value of $(0.47\pm0.05) \times 10^{-43}$ m^6s^{-1} for k_c, as was measured by Orient (Ori73). Present data on k_c in the complete range of E/N indicate a continuation of low E/N data found by Beaty and Patterson.

A direct comparison of afterglow experiments with drift tube experiments is not possible. Only a comparison of data on k_c from drift tube experiments for zero-field strength with results from afterglow measurements can be done. In drift tubes the temperatures of the neutrals and the ions are not identical and when the electric field strength is varied only the mean ion temperature changes. In afterglow experiments the temperatures of all reactants are the same and fixed to the environmental temperature. Thus at changing gas temperature the ionic as well as the neutral particle temperature varies. A good agreement exists with the experimental results of Vitols and Oskam (Vit72) and Sauter *et al.* (Sau66) obtained from afterglow experiments. A negative temperature dependence of k_c was found in afterglow experiments by Niles and Robertson (Nil65a) in helium and by Chen (Che69) in helium, neon and argon. This is in agreement with higher energy results in drift tube like experiments. A transformation of the reduced electric field strength, using the drift velocity of Ne^+-ions in neon (Bea68, Hor51d) and Wanniers formula (3.23), to an effective ion temperature T_{eff}, shows our data on k_c to have a temperature dependence of about $T_{eff}^{-0.5}$ in the range from 300 K to 3000 K.

III.3.2.6 Conclusion

Measurements of the atomic and molecular ion current densities at the cathode of a Townsend discharge by mass spectrometric sampling of the specific ion species have lead to the determination of the reaction rate for termolecular association. This rate varies from 0.47×10^{-43} m^6s^{-1} for a reduced electric field strength of 20 Td to 0.13×10^{-43} m^6s^{-1} for a reduced field strength of 210 Td. The present measurements have been carried out over a range of reduced field strengths larger than was done in previous drift

tube experiments and show the reaction rate to decrease by more than a factor of 3 for an increase of the mean ion energy by a factor of 8. This negative energy dependency of the reaction rate is in accordance with previous afterglow experiments which show a negative dependency of the T.A. rate on the gas temperature (Nil65a, Che68).

III.3.3 Dissociation

III.3.3.1 Introduction

We have found that the dissociation of a rare gas molecular ion in a collision with a ground state parent atom, is an important loss process for the molecular ions in a discharge at reduced electric field strengths larger than about 100 Td at intermediate gas pressures of a few hundred pascal. This reaction is the reverse of the termolecular association process. Under these discharge conditions, mostly at lower gas pressure, the molecular ions can gain such an amount of energy in the electric field that the dissociation reaction becomes possible. Up to now no experiments are known in which the reaction rate for the dissociative process in neon is determined as a function of the relative energy between the molecular ion and the colliding atom. Only experimental data on the dissociation energy of Ne_2^+ are available. In a mass spectrometrical study on the formation of homonuclear and heteronuclear diatomic ions of the rare gases, Munson *et al.* (Mun63) determined the dissociation energy from the difference of the ionization limit of the atom and the experimentally measured appearance potential of the molecular ion. A value of 0.7±0.2 eV for the dissociation energy of the neon molecular ion was obtained. Connor and Biondi (Con65) studied the 5852 Å emission line profile in the NeI spectrum of a neon afterglow by means of a Fabry-Perot interferometer and found this spectral line to be much broader in the afterglow than in the discharge. The broad component was ascribed by the authors to the radiation from excited, fast atoms formed by dissociative recombination of molecular ions. Assuming the Ne_2^+-ions to be in the vibrational ground state, the binding energy of the Ne_2^+-ion appeared to be 1.4 to 1.5 eV.

From scattering data of the Ne^+ ion by neon atoms, Mason *et al.* (Mas58) calculated the dissociation energy of Ne_2^+ and found this energy to be within 0.33 eV and 0.71 eV.

In a semi-empirical calculation Mulliken (Mul70) determined the dissociation energy of Ne_2^+ from known dissociation energies of He_2^+, H_2 and F_2, by putting the ratio of the dissociation energies of He_2^+ and H_2 equal to the ratio of the dissociation energies of Ne_2^+ and F_2. In this way an energy of 0.78 eV was obtained.

From ab initio configuration-interaction calculations on the several states of Ne_2^+, Cohen and Schneider (Coh74) determined the dissociation energy of the Ne_2^+ molecular ion. These authors found a value of 1.20 eV.

As can be seen the experimental and theoretical results on the dissociation energy of the neon molecular ion range from 0.33 to 1.5 eV, whereas no data are known on the reaction rate of the dissociation process (3.9) as a function of the relative energy of the colliding particles. In the present work an experiment in a T.D. is carried out in which this reaction rate is measured as a function of the reduced electric field strength.

III.3.3.2 Analysis

Expression (3.22) gives the functional dependence of the reduced molecular ion current density at the cathode of a T.D. on the discharge parameters. In the present experiment the reduced molecular ion flux is measured as a function of the electrode distance, for constant reduced electric field strength and gas pressure. The gas pressure is kept constant during a measurement to provide for the transmission of the sampling hole to be constant. A constant reduced electric field strength takes care of a constant mean ionic energy. By means of a least mean squares fit of expression (3.22) to the measured reduced molecular ion fluxes, the reaction rate k_d for dissociation can be calculated. In the first round of the iterative analysis the reaction rate k_c for T.A., appearing in (3.22), is taken constant over the whole range of E/N. For the associative ionization process, appearing as α_2 in (3.22), the first approximation, given by (3.30),

is used. A non-linear least mean squares fit of (3.22) to the experimental points gives the first approximation of the dissociative reaction rate. In the second round of the iterative analysis, the succeeding approximations of the iterative analysis for the T.A. rate and the A.I. rate are used. As a result of the second round, the least mean squares procedure gives a better value for the dissociation rate, etc.

III.3.3.3 Experiment

The experiments on the dissociation reaction of the molecular neon ion are carried out in a non-selfsustaining T.D. at 295 K. The molecular ion flux and the discharge current are measured as functions of the electrode distance d, with the reduced electric field strength and the gas pressure acting as parameters. The reduced electric field strength is chosen to range from 49 Td to 214 Td, whereas the gas pressure ranges from 0.27 kPa to 1.1 kPa. As mentioned before the gas pressure is kept constant during a set of measurements to provide for the sampling hole to have a constant transmission for ions.

III.3.3.4 Results

Typical plots of the measured reduced molecular ion fluxes as a function of the electrode distance for a reduced electric field strength and a gas pressure of 49 Td and 0.67 kPa, and 152 Td and 0.40 kPa, are shown in the figures 3.12 and 3.13, respectively. From these figures the influence of the dissociation process is obvious. The larger the reduced field strength, the larger the decrease in the reduced ion flux at increasing electrode distance. The results of these experiments for the dissociation rate k_d, as a function of E/N are shown in figure 3.14. As can be seen k_d increases more than 2 orders of magnitude for an increase of E/N from 50 Td to 200 Td. On the axis of abscissae also the mean molecular ion energy, calculated from Wanniers expression (3.23), is indicated. The ion swarm energy ranges from 0.26 eV to more than 1.50 eV.

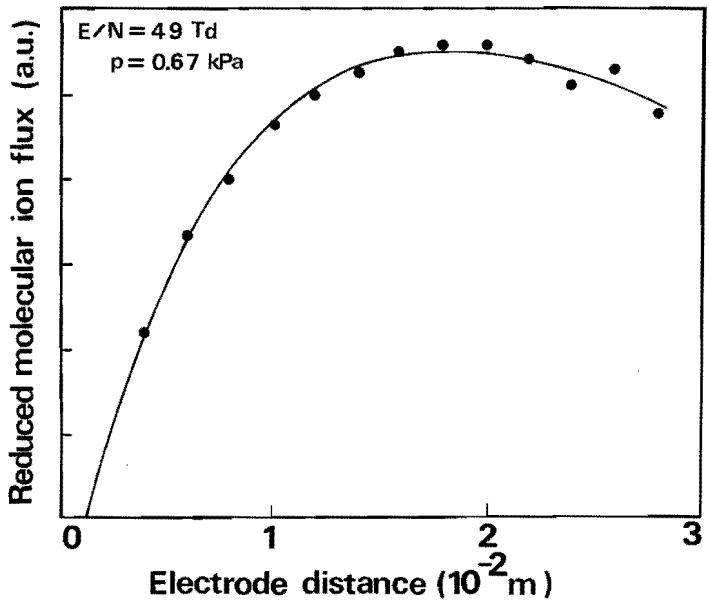

Figure 3.12

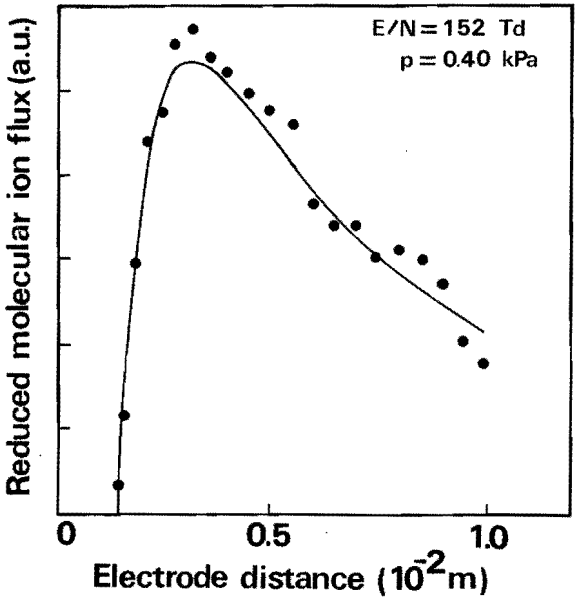

Figure 3.13

Figures 3.12 and 3.13 show comparisons of experimental results (●) with results from the model in which k_d and k_d,k_c are fitted, respectively.

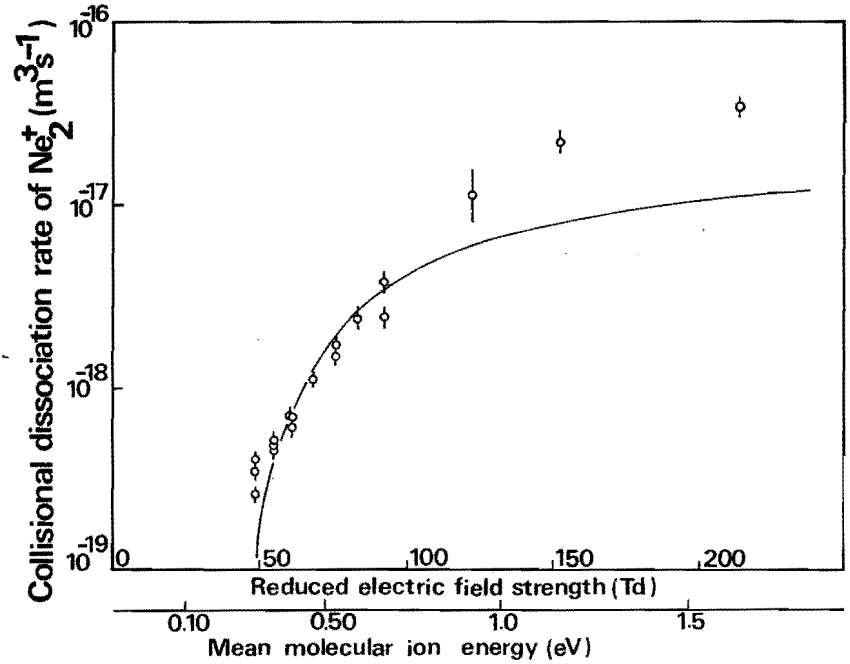

Figure 3.14 Comparison of experimental results (ϕ) with results from a model in which the depth D of the potential energy curve of Ne_2^+ is fitted to the corresponding dissociation rates.

III.3.3.5 Discussion

The range of the reduced electric field strength within which k_d is evaluated, is limited at the lower side by the small influence of the dissociation reaction on the reduced molecular ion flux, whereas for high *E/N* the measured flux of molecular ions, because of the dissociation, becomes too small for evaluation. Because no previous experimental results on this reaction are available, no direct comparison with the present data is possible. Other steps have to be taken in order to rate these data at their value. In a way, analogous to calculations of Niles and Robertson (Nil65a) for He_2^+, a theoretical formula can be derived in which the rate for dissociation, according to reaction (3.9), is expressed as a function of the kinetic energy of the molecular ion. The premisses of Niles and Robertson were twofold. Firstly, they supposed that the reaction rate can be written as a product of three terms, *viz.* (*i*) the rate at which two-body

collisions occur, (*ii*) the fraction of these events having enough energy to dissociate the Ne_2^+-ion, and (*iii*) the factor P, the steric factor, of these collisions actually giving rise to the dissociative reaction. Secondly, the molecular ions are assumed to have only translational energy, whereas rotational and vibrational excitation of the molecular ion are kept out of consideration. In other words, the Ne_2^+-ion is supposed to be in the vibrational ground state. In the T.D. we use, the mean energy of the molecular ions, calculated with Wanniers formula, increases at higher reduced electric field strength, so that this energy becomes larger than the energy difference of the excited vibrational states of Ne_2^+. So no use can be made of the second assumption of Niles and Robertson, that only the vibrational ground state is populated. An estimation of the ratio of the dissociation frequency to the collision frequency with neon atoms, shows this ratio for lower reduced electric field strengths to be much smaller than unity. The collision cross section is calculated as πR^2 where R is the interatomic distance of the Ne_2^+-ion, calculated by Cohen and Schneider (Coh74). From this estimation we assume the vibrational states to be populated according to a Boltzmann distribution with the mean energy of Ne_2^+-ions. For the energies of the vibrational states, an expression of Weizel (Wei58) is used in which the Morse potential, determining the anharmonic oscillator, is fitted to the Ne_2^+-potential energy curve calculated by Cohen and Schneider (Coh74). The energy E_v of the vibrational state with quantum number v can be written as

$$E_v = hc.w_e.v - \frac{h^2c^2w_e^2v(v+1)}{4D} \quad , \tag{3.31}$$

where D is the depth of the potential well, w_e a frequency containing the properties of the molecular ion, h Plancks constant and c the velocity of light. According to the Boltzmann distribution function, the fraction N_v/N of molecular ions in the vibrational state v, can be written as

$$\frac{N_v}{N} = \frac{e^{-E_v/kT}}{\sum_{v=0}^{s} e^{-E_v/kT}} \tag{3.32}$$

where $\frac{3}{2}kT$ represents the mean energy of the molecular ions and s is the number of vibrational states. The total fraction N_{diss}/N of the molecular

ions having enough energy to dissociate is the sum of the fractions in each single vibrational state that have sufficient translational energy to dissociate. According to Niles and Robertson (Nil65a) the total fraction can be written as

$$\frac{N_{diss}}{N} = \sum_{v=o}^{s} \frac{e^{-E_v/kT}}{\sum_{v=o}^{s} e^{-E_v/kT}} \left(1 + \frac{D-E_v}{kT}\right) e^{-\left(\frac{D-E_v}{kT}\right)} \quad . \tag{3.33}$$

The rate for dissociation k_d is then proportional to

$$(kT)^{\frac{1}{2}} e^{-\left(\frac{D}{kT}\right)} \frac{\sum_{v=o}^{s} \left(1 + \frac{D-E_v}{kT}\right)}{\sum_{v=o}^{s} e^{-E_v/kT}} \quad . \tag{3.34}$$

By means of a non-linear least mean squares procedure expression (3.34) for k_d is fitted to the experimental data, giving as best value for the depth D of the Ne_2^+-potential (1.4±0.2) eV. Vibrational states up to 0.01 eV below the ionization limit are considered. In figure 3.14 expression (3.34) for k_d is given as a solid line.

Previous and present experimental and theoretical results on the dissociation energy of the Ne_2^+-ion are given in table 3.3. As can be seen from this table the present result on the dissociation energy is in good agreement with previous experimental results of Connor *et al.* (Con65) and with theoretical data of Cohen and Schneider (Coh74). From figure 3.14 it is obvious that for mean molecular ion energies above about 0.9 eV the fit of expression (3.34) becomes poor. It is not astonishing that from equilibrium considerations too small values for the dissociation rate appear at relative energies larger than one half of the dissociation energy. In this energy range, at which a very large probability exists for dissociation when a collision between a molecular ion and a ground state atom takes place, an equilibrium concept will no longer be applicable. In the model calculations the energy distribution function of the Ne_2^+-ions is assumed to be Maxwellian. For low energies this distribution function is a good approximation, whereas

Table 3.3 Previous and present experimental and theoretical results on the dissociation energy of a Ne_2^+-ion.

Reference	D(eV)	Method
Mason and Vanderslice (Mas59)	0.33-0.71	Scattering experiment
Munson *et al.* (Mun63)	0.7 ±0.2	Ne_2^+-appearance potential measurement
Connor and Biondi (Con65)	1.4 -1.5	Measurement of emission line profile in afterglow
present	1.4 ±0.2	T.D. experiment
Gilbert *et al.* (Mul70)	1.65	Self consistent field approximation (theory)
Mulliken (Mul70)	0.78	Semi-empirical calculation
Cohen and Schneider (Coh74)	1.20	Ab initio Ne_2^+-potential calculation (theory)

for larger reduced electric field strengths the velocity distribution function deviates from a Maxwellian one. One should be aware that this latter phenomenon might be a second order effect.

III.3.3.6 Conclusion

The measurements of molecular ion fluxes at the cathode and the total discharge current in a non-selfsustaining T.D. in neon as functions of the electrode distance at constant reduced electric field strength and constant gas pressure, lead to a determination of the reaction rate for the dissociation of a Ne_2^+-ion in a collision with ground state neon atoms. The studied range of the reduced electric field strength from 50 Td to 200 Td corresponds with a rather broad range of molecular ion energies from 0.25 eV to more than 1.50 eV. Until now no experiments are known in which the dissociation rate is determined. Only experimental data on the dissociation energy of the Ne_2^+-ion exist, which, however, diverge from 0.33 eV to 1.65 eV. A theoretical expression for the dissociation rate in terms of the mean ion energy is derived in which the translational as well as the

vibrational energies of the Ne_2^+-ion are considered. This expression, when using a value of 1.4±0.2 eV for the depth of the Ne_2^+-potential energy curve, fits the experimental points very well, especially so at smaller reduced electric field strengths.

CHAPTER IV

DECAY OF METASTABLE NEON ATOMS

An experiment is described in which the decay of metastable Ne($^3P_2$)-atoms is studied as a function of gas density at 77 and 295 K. The results yield values for the diffusion coefficient, the de-excitation rate of the nearest resonant level and the excimer formation rate. The experimental method is a time sampling analysis of N_2^+-ions in the afterglow of a Townsend discharge in slightly impure neon. The N_2^+-ions are formed in a Penning ionization reaction with metastable neon atoms. The rate of formation of nitrogen molecular ions is proportional to the metastable atom density. Section IV.1 gives a historical introduction in the development of this subject and the present status of the experimental method is described. The analysis of the experiments is treated in section IV.2. Section IV.3 deals with the Penning ionization reaction, used as a tracer reaction for the experiments described in IV.4. Results of the measurements on the decay of metastable Ne($^3P_2$)-atoms are given in section IV.5. Section IV.6 gives a detailed discussion of the several reactions studied as well as a general conclusion.

IV.1 Introduction

IV.1.1 Recent developments

Several investigations on the destruction rate of metastable atoms as a function of gas density in neon and the other noble gases, were carried out since the first measurements of Meissner and Dorgelo (Mei25). Studies of the density dependence of the decay rates of metastable and resonant levels are made in order to gain an understanding of the destruction mechanism for these low lying excited energy levels. The level diagram is given in figure 4.1. From these measurements reaction rates for the several processes causing the destruction, were obtained. At this moment the mechanisms governing these decay rates are fairly well understood. Usually these processes are studied in afterglow plasmas, where only a limited

number of loss processes occur. In the afterglow the most important processes concerning the 3s-levels are diffusion of metastable atoms to the wall, followed by de-excitation, resonance radiation imprisonment, excitation transfer between the four 3s-levels in collisions with ground state atoms and three-body collision processes of 3s-atoms with two ground state atoms leading to the formation of quasi metastable molecules, excimers, (Phe59, Ste77). Various kinds of experiments have been carried out.

The most frequently used experimental method is the optical absorption technique used by Phelps (Phe59), Phelps and Molnar (Phe53), Dixon and Grant (Dix57) and Grant and Krumbein (Gra53). The relative absorption of characteristic line radiation by neon atoms in the 3s-level is measured as a function of time in the afterglow. The excited atoms are created by means of a high voltage pulse on two electrodes in the absorption cell. Line radiation emitted by a second discharge, the source, is collimated along the axis of the absorption cell. The radiation from the source is partially absorbed, selected by wavelength and detected by a photo multiplier. The absorption signal is measured with a time sampling technique. Under certain conditions the density of the absorbing atoms in a specific atomic level, is proportional to the measured fractional absorption of an emission line ending on that level. In the case of pure Doppler broadening (*i*) the ratio of the half-width of the emission line to the half-width of the absorption line, (*ii*) the absorption cross section at the centre of the line and (*iii*) the length of the absorption path are parameters is this proportionality. When these quantities are known, absolute determination of the densities of each of the 3s-levels as a function of time in the afterglow is possible. The values of the diffusion coefficients for the lowest metastable level of neon obtained experimentally with this method are in satisfactory mutual agreement. Only one reliable de-excitation rate is known from absorption measurements by Phelps (Phe59) for the transition from the lowest resonant $^3P_1$-level to the $^3P_2$-level in a collision with a ground state atom. Only few results exist for the excimer formation rate of Ne($^3P_2$)-atoms. (Phe59 at 300 K and Gra53, Phe53 at 77 K).

Some of the destruction processes we mentioned were also studied by a microwave technique. Biondi (Bio52) used this technique to study the electron density variation in an afterglow plasma. In these experiments lifetimes of

metastable atoms were determined at the same time by measuring the change in electron density during the afterglow caused by collisions of two metastable atoms, resulting in the ionization of one of them. The Penning ionization of argon was determined from such experiments with a well defined neon-argon mixture. In these experiments the discharge is placed in a microwave cavity. A magnetron pulse ionizes and excites the atoms in the discharge. The change in the resonant frequency of the cavity is proportional to the average electron density. From the determined electron density in the afterglow, the metastable density can be calculated. The value of the diffusion coefficient of the metastable neon atom found from these experiments is about 20% larger than those found from the optical absorption technique. The value of the de-excitation rate from the $^3P_1$- to the $^3P_2$-state in collision with a ground state neon atom was found to be a factor of 2 larger than obtained from other experiments.

In an experiment done by Steenhuysen (Ste79) the afterglow of a positive column is illuminated with a light pulse of 5-25 μs duration from a tunable dye laser, tuned at the frequency of an emission line from a 3p-level to one of the 3s-levels. The time between the end of the discharge, *i.e.* the start of the afterglow and the beginning of the laser pulse was varied. Non-resonant fluorescence was studied by measuring the line radiation from the upper level of the absorbing transition to another state of the 3s-group, with a time sampling photon counting detection system. Under certain physical conditions the intensity of the fluorescent light is proportional to the density of the lower level (3s) of the absorbing transition. In the analysis of his measurements Steenhuysen had to take into account quite a number of relevant processes. In addition to processes mentioned earlier, transitions between the four 3s-levels caused by collisions with electrons, production of 3s-states by dissociative recombination, termolecular association, and ambipolar diffusion of electrons and ions were taken into account. Gas pressures between 0.13 and 13 kPa were used. For the values of the physical quantities we are interested in, the authors found that the diffusion coefficient on the $^3P_2$-atom, the de-excitation rate from the $^3P_1$- to the $^3P_2$-state and the excimer formation rate of the Ne($^3P_2$)-atom agree within 30% with the results of the optical absorption experiments.

A time resolved study of the vacuum U.V. emission from the resonance $^1P_1$- and $^3P_1$-states of neon in a neon discharge was carried out by Leichner (Lei75). Along the axis of a cylindrical stainless steel emission cell atoms were excited by a pulsed beam of 250 keV electrons. In this way rapid energy injection is possible over a wide pressure range. The emitted photons were selected by a vacuum U.V. monochromator and detected by a single photon detector. Using a time sampling technique, time resolved measurements were made. From the 743 Å emission the pressure dependent lifetimes of the Ne($^3P_1$) and the Ne($^3P_2$)-atoms were obtained for pressures from 0.5 kPa to 130 kPa. The obtained values of the de-excitation rate for the transition from the $^3P_1$- to the $^3P_2$-state are the same as those found by the fluorescence experiment (Ste79), whereas the excimer formation rate of the Ne($^3P_2$)-atom is in good agreement with the optical absorption experiments. Moreover, the two-body de-excitation rate for the Ne($^1P_1$)-atoms, and the excimer formation rate for Ne($^3P_1$), which could not be measured by the absorption technique, were found with the vacuum U.V. experiment. A fast and slow component in the 743 Å-line decay enabled Leichner to solve the two coupled differential equations involving the densities of the $^3P_1$- and $^3P_2$-states, and from the solution he found the excimer formation rate of the $^3P_1$-state.

Few theoretical calculations are available on the diffusion of the lowest metastable level of neon. The same holds for calculations on the de-excitation rate from the resonant state nearest to this metastable state under the various experimental conditions.

Cohen and Schneider (Coh74, Sch74) have given a detailed description of the structure of the ground state and of some excited states of the Ne_2-molecule. Ab initio calculations of potential energy curves were carried out for the Ne_2^*-molecule, with semi-empirical treatment of spin-orbit coupling and long range forces. Spectroscopic properties and radiative lifetimes were also taken into account. From the results of these calculation the diffusion coefficient of the Ne($^3P_2$)-atom in neon was calculated (Coh75). For 300 K the value of the calculated diffusion coefficient is in good agreement with results of the optical absorption technique (Gra59), whereas for 77 K this quantity is about 20% larger than those measured by Phelps (Phe53) and Grant and Krumbein (Gra53) in their optical absorption experiments.

Another approach was used by Palkina *et al.* (Pal69). Here the diffusion coefficient of metastable atoms of noble gases in their parent gas, which is determined by the elastic scattering of the metastable atoms by atoms in the ground state, is calculated in the Chapman-Enskog approximation. The elastic collision cross section is calculated using an asymptotic expression for the interaction potential. The diffusion coefficient of the $Ne(^3P_2)$-atom determined in this way for 77 K is in good agreement (within 10%) with the results from optical absorption experiments of Phelps (Phe53) and Grant and Krumbein (Gra53).

Close-coupling calculations of cross sections for the excitation transfer between atomic states within the 3s-group of neon by collisions with ground state neon atoms were carried out by Cohen *et al.* (Coh78). The transitions $^1P_1 \rightarrow {}^3P_2$, $^3P_1 \rightarrow {}^3P_2$ and $^3P_0 \rightarrow {}^3P_2$ were studied for collision energies below 3 eV. The transition mechanism was assumed to be spin-orbit coupling. The calculated de-excitation rate for the $^3P_1 \rightarrow {}^3P_2$ transition was compared with experimental results (Phe59, Gra53, Lei75). For temperatures above 400 K the agreement with experiments is within 10%, whereas for 300 K and below the calculated values are about 50% and more below the experimental values. A possible explanation given by the authors is that low energy cross sections are very sensitive to small changes in the potential energy curve corresponding to the initial state.

IV.1.2 Present experiment

Because of the rather large discrepancy in the experimental values for the de-excitation rate of the $Ne(^3P_2)$-atom by collisions with ground state neon atoms and the few experimental data for the excimer formation rate as well as for the diffusion coefficient for the $Ne(^3P_2)$-atom at 77 K, an alternative experiment has been performed from which these physical quantities can be obtained. In this experiment the Penning ionization reaction

$$Ne^* + N_2 \rightarrow N_2^+ + Ne + e^- \qquad (4.1)$$

in which Ne^* is a 3s-atom, is used as a diagnostic method. The nitrogen molecular ion is used as a tracer for the determination of the decay

frequency of the metastable atoms. This is only possible if the nitrogen density in the neon gas is so small that it does not affect the decay frequency itself. The rate of formation of N_2^+ is proportional to the metastable density. With our time sampling technique, as described in section II.4, the flux of N_2^+-ions from the T.D. afterglow can be measured as a function of time. The present proposed method is possible in every afterglow but the use of a T.D. has several advantages. (*i*) The main advantage of a T.D. is that neither in the discharge nor in the afterglow cumulative processes occur because of the very low densities of excited and ionized particles and electrons. This implies *e.g.* that the dissociative recombination process gives a negligible contribution to the population of the 3s-states of neon in the discharge as well as in the afterglow. (*ii*) Because the Debeye length of a plasma with comparable densities is larger than the geometrical dimension of the T.D., no ambipolar diffusion of electrons and ions takes place, and electrons and ions drift to the electrodes independently in the applied electric field. Numerous processes, as mentioned by Steenhuysen (Ste77) and which thwart the analysis of the decay frequency data, are non-relevant. (*iii*) A third advantage is that the sampling of ions from the afterglow of a T.D. by means of a small orifice in the cathode will not be influenced by a Debye sheath, as will happen in positive columns. Under the influence of the electric field applied in the afterglow, electrons and ions formed in the discharge drift to the electrodes within tens of microseconds. Hence no ions are formed in the afterglow, except for the N_2^+-ions made in the Penning reaction (4.1) mentioned. After formation these ions drift also to the cathode within tens of microseconds. This drift time is at least 2 orders of magnitude smaller than the decay time of the metastables. A sufficiently good resolution in time for the afterglow measurements is thus obtained. (*iv*) The gas temperature in a T.D. is better defined than in a positive column used mostly for this kind of experiments.

The statement that no ions except the N_2^+-ions are made in the afterglow does not hold exactly for the following reason. Ne^+- and Ne_2^+-ions can be formed by secondary effects. Primary ions, metastable and resonant photons, formed in the discharge and colliding with the cathode, can release secondary electrons which again are accelerated in the electric field applied during the afterglow and are able to ionize and to excite neon atoms.

The results of this phenomenon can be seen when measuring Ne^+- and Ne_2^+-ions by the time sampling technique. After the bulk of primary Ne^+- and Ne_2^+-ions, formed in the discharge, has passed the sampling hole in tens of microseconds, still some ions are detected. This tail in the time sampled curves of the ions has a decay frequency exactly equal to the decay frequency of the $^3P_2$-metastable atoms. The explanation is that as long as metastables are present in the afterglow, secondary electrons are released from the cathode by these metastable atoms and thus secondary Ne^+- and Ne_2^+-ions will be formed in the afterglow. The influence of the extra amount of metastable atoms, formed in excitation reactions by the secondary electrons, on the $^3P_2$-decay frequency will be discussed in IV.2 and is found to be negligible.

IV.2 Analysis of the experiments

In this section the processes determining the decay frequency of the lowest metastable state of neon are described. In figure 4.1 the energy level diagram of the lowest atomic states of neon, the four 3s-levels, is shown. We shall use a notation for the excited states and the reaction rates originating from Phelps (Phe53, Phe59).

The four 3s-states of neon consist of 2 metastable states, the $^3P_2$- and $^3P_0$-state and 2 resonant states, the $^3P_1$- and $^1P_1$-states. The 2 metastable levels cannot radiate to the ground state, because of transitions forbidden by the selection rules, whereas the $^3P_1$- and $^1P_1$-states emit allowed electric dipole radiation, *viz.* the 743 and 736 Å lines, respectively. The atomic state of interest for the present work is the $^3P_2$-metastable state. In the afterglow of a T.D., the only processes governing the decay of this lowest metastable state, are diffusion to- and de-excitation at the wall, excitation transfer between the $^3P_1$-resonant and the $^3P_2$-metastable state by a two-body collision with a ground state neon atom, and three-body collisions of a $^3P_2$-atom with two ground state atoms leading to the formation of an excimer. As mentioned earlier in the introduction, cumulative effects are negligible because of the very low densities of excited atoms, ions and electrons in the T.D.. The dissociative recombination of an electron and a molecular ion, mentioned by Steenhuysen (Ste77) as an important process in the early afterglow of a positive column, is absent in the T.D. afterglow.

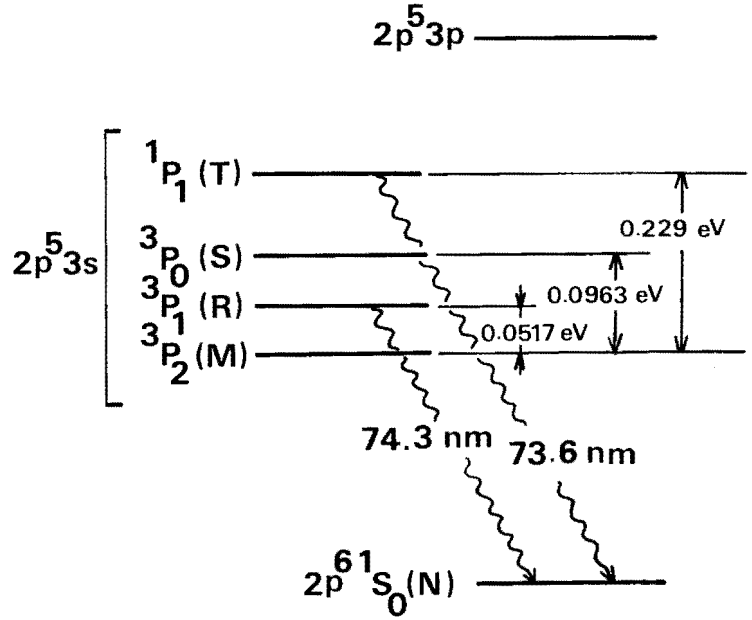

Figure 4.1 Energy level diagram of neon.

This follows from an estimate of the rate of formation of excited neon states via the dissociative recombination reaction

$$Ne_2^+ + e^- \rightarrow Ne^{**} + Ne \ . \qquad (4.2)$$

If we assume that all dissociative recombination ends up in the $^3P_2$-level, a value of 10^{14} $m^{-3}s^{-1}$, at the beginning of the T.D. afterglow is found. In this calculation we used a known reaction rate for (4.2) of 10^{-14} m^3s^{-1} (Oma72) and an estimated electron density of 10^{13} m^{-3} together with a molecular ion density of 10^{15} m^{-3}, as starting values in the afterglow. The rate of decay in the afterglow of the $^3P_2$-metastable state, having an initial density of the order of 10^{16} m^{-3} and a decay frequency of about 10^3 s^{-1} at 300 K, is 10^{19} $m^{-3}s^{-1}$, which value is orders of magnitude larger than the population rate of the $^3P_2$-state by dissociative recombination. This argument, valid at the onset of the afterglow, can be extended to any later time. The primary electrons and molecular ions which vanish from the afterglow within a few microseconds and tens of microseconds, respectively, can only be replenished by secondary electrons as described in IV.1.2, and this replenishment decays simultaneously with the metastable density as mentioned before.

The secondary effect mentioned in IV.1.2, which is able to influence the decay of metastable atoms, depends on the magnitude of the reduced electric field strength in the afterglow by which secondary electrons, released from the cathode, are accelerated and consequently are able to ionize and to excite. To investigate this effect, the decay rate of the $^3P_2$-state was measured as a function of the reduced electric field strength E/N in the afterglow. These measurements show that for values of E/N lower than a specific value, *e.g.* 15 Td for a pressure of 1.3 kPa, the value of the decay frequency found from the measurements is constant within the experimental accuracy. At higher E/N the frequency determined from the experiments decreases slightly, leading to an apparently larger metastable decay rate.

With regard to the four 3s-states of the neon atom, one wants to know which of these atomic states exert an influence on the decay of the $^3P_2$-metastable state. Concerning the $^1P_1$-state, Leichner (Lei75) concluded from time resolved U.V. spectra and available potential energy curves that the only important coupling of the $^1P_1$-state in two-body collisions with ground state neon atoms, is the coupling with the $^3P_1$-state, and not with the nearest $^3P_0$-state, as would be expected from energy consideration. From studies of the spectra of the 744 Å-line it was evident (Lei75) that the $^1P_1$-state plays no role in the decay of the $^3P_1$-state. Calculations of Cohen *et al.* (Coh78) show that the rate for the energy transfer reaction of $^1P_1 \rightarrow {}^3P_2$ is about 5 orders of magnitude smaller than the rate for the reaction of the $^1P_1$-state to the $^3P_1$-state, which implies that the influence of the $^1P_1$-state on the $^3P_2$-state is negligible. These considerations are in agreement with measurements of Phelps who found zero density for the $^1P_1$-resonant state. In the T.D. we use, no dissociative recombination takes place so the population of excited states is caused by direct excitation of ground state atoms only. The large energy gap between the $^3P_0$-state and the $^3P_2$-state in comparison with the thermal energy of the atoms at 300 K, implies that only de-excitation of the $^3P_0$-state to the $^3P_2$-state occurs. Cohen *et al.* calculated this rate to be a factor of 30 smaller than the rate for the de-excitation in two-body collisions from the $^3P_1$-state to the $^3P_2$-state. In the discharge Phelps used, the ratio of the $^3P_0$-state density to the $^3P_2$-state density was found to be smaller than 0.1. In the T.D. we use, this ratio will be even smaller. The arguments mentioned above show

that the $^1P_1$- and the $^3P_0$-states play no role in the decay of the $^3P_2$-state. The influence of the nearest $^3P_1$-state on the decay frequency of the $^3P_2$-atoms has, however, to be taken into account.

The density $R(t)$ of the $^3P_1$-state and the density $M(t)$ of the $^3P_2$-state as functions of time t in the afterglow can be calculated by solving two coupled differential equations,

$$\frac{dR(t)}{dt} = -(\beta_2 + A.N + \gamma_R.N^2)\,R(t) + a.A.N.M(t) \qquad (4.3)$$

and

$$\frac{dM(t)}{dt} = A.N.R(t) - (a.A.N + \gamma_M.N^2 + \frac{D_M}{N\Lambda^2})\,M(t)\,, \qquad (4.4)$$

where β_2 is the imprisonment decay rate, A the de-excitation rate from the $^3P_1$-state on the $^3P_2$-state, a the ratio of excitation to de-excitation, D_M the diffusion coefficient for the $^3P_2$-atoms at unit gas density, γ_R and γ_M are the reaction rates for excimer formation by $^3P_1$- and $^3P_2$-atoms at unit gas density, respectively, and Λ is the diffusion length. These equations only hold if the densities of the impurities in the neon gas are low enough so that Penning ionization of foreign atoms has no influence on the decay frequencies. These processes are shown in figure 4.2.

The densities $M(t)$ and $R(t)$ can be written as the sum of two exponentials, $\exp(-\nu_1 t)$ and $\exp(-\nu_2 t)$. The ratio of $R(t)$ to $M(t)$ is always smaller than the statistical value a. A calculation with available data for the sevaral reaction rates (Lei75), shows that in the final T.D. afterglow, both densities decay with the lowest frequency ν_1 only. *E.g.* at a reduced gas pressure of 1.4 kPa, this final afterglow is reached for the $^3P_1$-state and the $^3P_2$-state after a period of 100 μs and 50 μs, respectively.

The final decay frequency ν can be written as

$$\nu = -\tfrac{1}{2}[c_1 + c_4 + \sqrt{(c_1 + c_4)^2 - 4(c_1c_4 - c_2c_3)}\,] \qquad (4.5)$$

where c_1 and c_2 are the coefficients of R and M, respectively, in (4.3), and c_3 and c_4 are the coefficients of R and M, respectively, in (4.4).

For a gas temperature of 77 K, the thermal energy of the atoms is much smaller than the energy by which the $^3P_1$- and the $^3P_2$-states are sepatated.

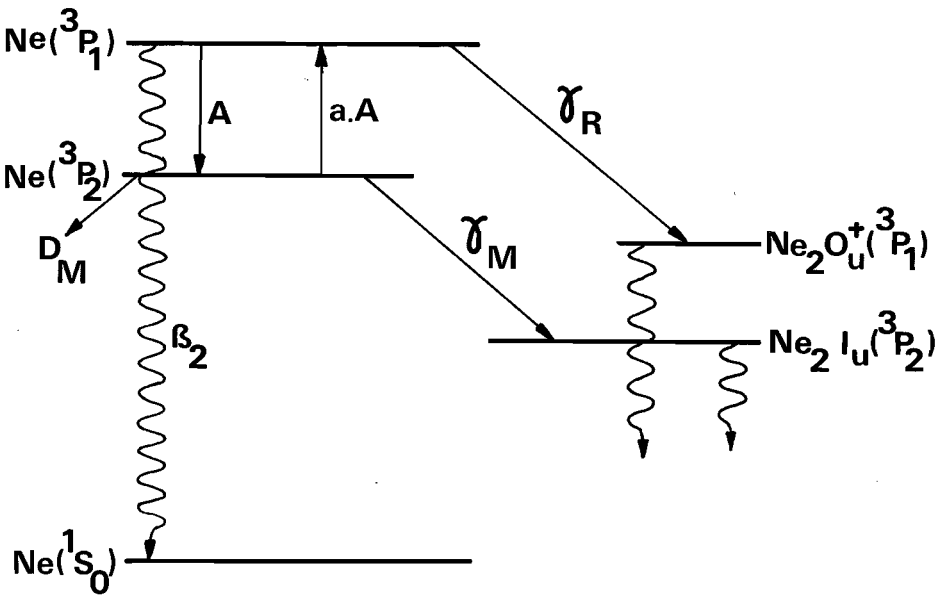

Figure 4.2 Processes governing the $^3P_1$- and $^3P_2$-state densities in a T.D. afterglow.

At this temperature the quantity a, the Boltzmann factor, becomes so small that the excitation of atoms in the $^3P_2$-state to atoms in the $^3P_1$-state by two-body collisions becomes negligible. From equations (4.3) and (4.4) one can calculate that the decay frequency of the $^3P_1$-atoms is constant during the afterglow and is much larger than the decay frequency of the $^3P_2$-atoms. In equation (4.4) the term A.N.R. becomes negligible in the final afterglow and the decay frequency of the $^3P_2$-atoms reduces to

$$\nu = \frac{D_M}{\Lambda^2}\frac{1}{N} + \gamma_M N^2 \ . \tag{4.6}$$

In the case of a discharge between flat parallel plates the diffusion length Λ satisfies the relation

$$\frac{1}{\Lambda^2} = \left(\frac{2.405}{r_o}\right)^2 + \frac{\pi^2}{d^2} \ , \tag{4.7}$$

where d is the electrode distance and r_o the radius of the electrodes. In the present experiment the value of $1/\Lambda^2$ is $1.355 \times 10^5\ m^{-2}$. When measurements of the decay frequency of the Ne($^3P_2$)-atoms in a neon afterglow

of a T.D. are carried out over a wide range of gas densities, values for the diffusion coefficient, the excitation rate and the excimer formation rate can be obtained. From measurements at different gas temperatures, one obtains the temperature dependence of several reaction rates, and hence the energy dependence.

IV.3 Penning ionization as a tracer reaction

As mentioned in the introduction of this chapter, the decay frequency of $Ne(^3P_2)$-atoms has been measured by making use of the capability of the $^3P_2$-atoms to ionize impurities. The impurity most often present in the neon gas we used was nitrogen. The concentration of the nitrogen is less than 1 ppm, as mentioned in II.2. The Penning ionization we use as a tracer reaction is

$$Ne^* + N_2 \rightarrow N_2^+ + Ne + e^- , \tag{4.8}$$

where Ne* is an atom in an excited state. From reaction (4.8) one can see that the rate of formation of N_2^+-ions, dN_2^+/dt, is proportional to the Ne* density, the nitrogen density N_2 and the Penning ionization rate $k_{P.I.}$. In case the Ne* density decays exponentially with a frequency ν, the rate of formation of N_2^+-ions can be written as

$$\frac{dN_2^+}{dt} = k_{P.I.}\, N_2\, Ne^*(0)\, e^{-\nu t} \tag{4.9}$$

where $Ne^*(0)$ is the Ne* atom density at the initiation of the afterglow *i.e.* for $t = 0$. The particle flux density of N_2^+-ions at the cathode is proportional to the rate of formation of N_2^+ and also the nitrogen ion flux at the detector is proportional to this rate of formation, because each decay measurement is carried out at constant gas density. From the measurement of this flux as a function of time in the afterglow of the T.D. one can calculate the decay frequency of the Ne* atoms.

At this moment it is important to establish in more detail which of the excited atoms play a preponderous role in the Penning ionization reaction. In principle every excited neon atom has a reaction probability for ionizing

a nitrogen molecule. In afterglow experiments, where relevant processes take place on a relatively long time scale, only metastable states and states that are very strongly coupled to these metastable states are of importance. Highly excited states cascade down by radiation within a microsecond. Also for the T.D. the important advantage of the absence of dissociative recombination causes no repopulation of these states.

From literature experimental not theoretical studies are known in which reaction rates for Penning ionization of nitrogen by the 3s-states of neon are studied separately. In one contribution of Illenberger and Niehaus (I1175) experimental and theoretical studies of the Penning ionization cross section of N_2 by He(2^1S) and He(2^3S) atoms, both metastable states, have been reported as functions of relative velocity, and hence of energy, of the colliding particles. At the gas temperatures we use, the cross section for Penning ionization of these various excited He-atoms, differ by a factor of 3 at 300 K to a factor of 6 when extrapolating to 77 K. Therefore, although no experiments concerning the separate 3s-states of neon are available, it is not unthinkable that the Penning ionization cross section of N_2 by atoms in the various excited states are different but probably not more than by these factors. As mentioned earlier, in the final afterglow the $^1P_1$-state and the $^3P_0$-state densities are too small in comparison with the $^3P_2$-state density to contribute to the formation of nitrogen ions by the Penning ionization process. In the final afterglow the decay frequencies of atoms in the $^3P_1$-state and the $^3P_2$-state are equal, so the absolute values of the Penning ionization cross sections are irrelevant.

IV.4 Experiments

All the measurements on the $^3P_2$-metastable state decay frequencies, those at 295 K included, have been carried out in the apparatus built for low temperature experiments. The experimental set-up was described in section II.2. Because these measurements have to be carried out at gas pressures as high as possible, a sampling orifice with a diameter of only 10 μm in the cathode of the T.D. is used. In this way a sufficiently low background density was obtained in the quadrupole and detector chamber for good operation of these elements. The experimental procedure for obtaining a

time resolved measurement of the formation of nitrogen ions by the Penning ionization reaction in the T.D. afterglow, is the time sampling technique which was extensively described in section II.3. After filling the T.D. with neon of the desires gas pressure, the T.D. is pulsed with a maximum frequency of about 100 Hz. In the selfsustaining mode of the discharge, the anode voltage is chosen barely larger than the breakdown voltage of the T.D. in order to keep the excited and ionized particle density as low as possible. a reverse drift field in the afterglow is necessary for the ions and electrons to move quickly towards the electrodes being then the cathode and the anode, respectively. After that the metastable states are the only excited states left. During their presence in the afterglow they may take part in Penning ionization collisions. In the drift field the formed N_2^+-ions move to the cathode and can be detected. The anode voltage in the afterglow is much lower than the burning voltage of the T.D.. Secondary electrons, released by ions and metastables which are formed in the discharge phase and impinge on the cathode during the afterglow, encounter a much lower electric field strength than in the discharge phase. In this way the amount of secondary metastables and ions formed in the afterglow is negligible. No disturbance of the measured decay curve takes place by these extra metastables, as is argued in IV.2.

While repeatedly pulsing the T.D. and processing the pulses from the formed N_2^+-ions, the micro-processor produced the decay curve of the $^3P_2$-metastable atoms. The pressure in the T.D. is measured with a membrane capacitance manometer (ATLAS MMCT) which is calibrated by means of an oil manometer. For the pressure range used the inaccuracy in the determination of the pressure is within a few percent. The pressure in the T.D. decreases only a few percent during the measurement of one decay curve, because the leak rate of neon gas through the sampling hole in the cathode is very small. For measurements taking more time, the pressure must be kept manually at the desired value.

The neon gas is cataphoretically cleaned before flowing into the T.D.. The densities of the impurities are low enough for the Penning reaction to have negligible influence on the decay frequency of the metastable atom.

Copper-constantan thermocouples are used to measure the temperature of the anode and cathode of the T.D. and of the inner and outer walls surrounding the liquid nitrogen. No deviation of the temperature of the gas in the T.D. from the real liquid nitrogen temperature of 77 K could be perceived. During the room temperature measurements, the temperature of the gas was 295±3 K.

Measurements of the decay frequency of the $^3P_2$-metastable neon atoms as a function of gas density have been carried out at two temperatures, 295 K and 77 K. At the gas temperature of 295 K these measurements were done for gas densities between 4.0×10^{22} m^{-3} and 3.4×10^{24} m^{-3}, whereas for the experiments at 77 K the gas densities range from 1.0×10^{23} m^{-3} to 2.0×10^{24} m^{-3}.

IV.5 Results

The results of the measurements described in section IV.4 are shown in the figures 4.3 and 4.4. Figure 4.3 shows typical plots of the detected N_2^+-ion fluxes at 295 K as functions of time in the afterglow for various gas pressures, as obtained from the time sampling measurements. The N_2^+-fluxes

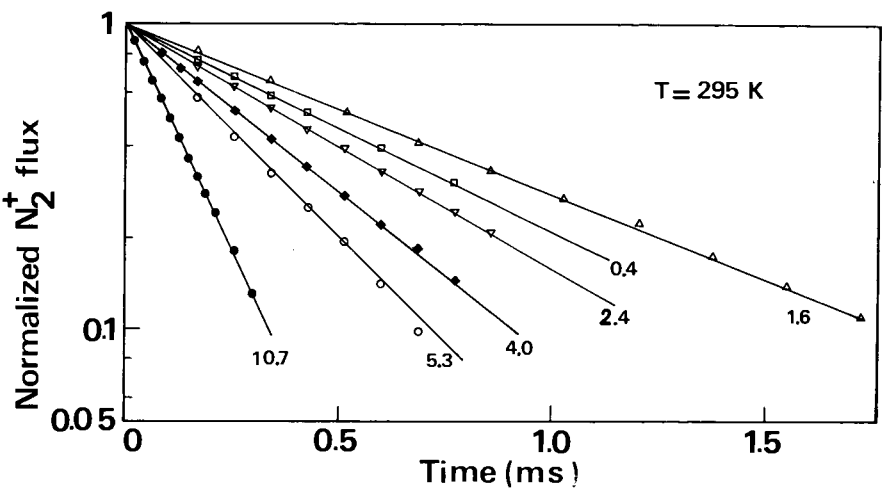

Figure 4.3 Measured normalized flux of N_2^+-ions vs. time in the afterglow at 295 K. Parameter is the reduced gas pressure (kPa).

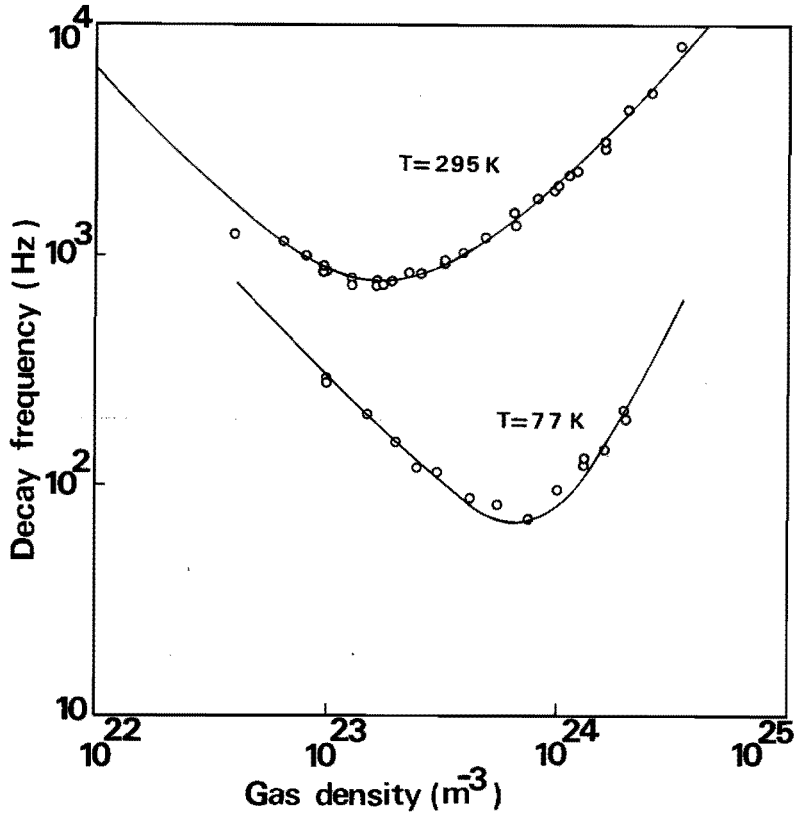

Figure 4.4 Comparison of experimental results (o) with results from the model in which the diffusion coefficient, the excitation rate and the excimer formation rate of the $^3P_2$-atoms and the imprisonment decay rate of the $^3P_1$-atoms are fitted to the experimental results.

vs. time are plotted on a log-linear scale and normalised to unity at $t = 0$. One can see that, within the experimental error, only one exponential decay is present in each of these graphs, as predicted by theory.

The determined decay frequencies as functions of gas density at 295 K and 77 K are shown in figure 4.4. The decay frequencies *vs.* gas density curves are plotted on a double logarithmic scale. The measured decay frequencies as functions of gas density at 295 K and 77 K are fitted by means of a nonlinear least mean square procedure ("MINIQUAD" on the Burroughs 7700 of the Eindhoven University) to equation (4.5) and equation (4.6), respectively. In this analysis the value of 0.47×10^{-44} $m^6 s^{-1}$ for γ_R, as

determined by Leichner (Lei75) from high density, time resolved vacuum U.V. spectra, is used. The best fits to the experimental data are shown as solid curves in figure 4.4. The diffusion coefficient D_M of the $Ne(^3P_2)$-atom in neon, the de-excitation rate A for de-excitation from $^3P_1 \rightarrow ^3P_2$ by two-body collisions with ground state neon atoms, the excimer formation rate γ_M and the imprisonment decay constant β_2 for the $Ne(^3P_1)$-atom, obtained from the least mean square procedures are given in table 4.1 for both temperatures.

Table 4.1 Results on the diffusion coefficient, the de-excitation rate and the excimer formation rate for the $^3P_2$-atom and the imprisonment decay constant for the $^3P_1$-atom in neon.

Temperature	295 K	77 K
D_M (10^{20} $m^{-1}s^{-1}$)	4.5±0.1	2.3 ±0.2
A (10^{-20} m^3 s^{-1})	3.5±0.1	-
γ_M (10^{-46} m^6 s^{-1})	3.3±0.2	0.52±0.04
β_2 (10^4 s^{-1})	4.8±0.4	-

IV.6 Discussion

The results of the measurements of the diffusion coefficient, the de-excitation rate and the excimer formation rate as given in section IV.5, shall be discussed separately in this section. The present value of the imprisonment decay rate β_2 for the $Ne(^3P_1)$-state is in good agreement with previous and recent experimental results of Phelps (Phe59) and Leichner (Lei75), respectively.

IV.6.1 Diffusion coefficient

The present results for the diffusion coefficient at unit gas density of the $Ne(^3P_2)$-atom in neon at 295 K and 77 K are compared to other experimental as well as theoretical results in table 4.2. From the results of other authors it can be derived that at 300 K the mean experimental value of D_M is 4.8×10^{20} $m^{-1}s^{-1}$ with a standard deviation of 0.4×10^{20} $m^{-1}s^{-1}$,

Table 4.2 Previous and present experimental and theoretical results on the Ne($^3P_2$)-diffusion coefficient in neon at different gas temperatures.

	Temperature (K)		D_M (10^{20} $m^{-1}s^{-1}$)		
Phe59	300		5.2		Experiment
Gra53	273	77	5.1±0.9	1.7±0.4	
Ste77	300		4.9±0.3		
Met72	300		5.1±0.4		
Dix57	300		5.5±0.3		
Gra51	300		4.0±0.7		
Mol51	298		3.9±0.4		
Bio52	300		6.4±0.4		
Phe53	300	77	5 ±1	1.9	
Present results	295	77	4.5±0.1	2.3±0.2	
Coh75	300	77	4.96	1.93	Theory
Pal69		77		1.80	

whereas for 77 K, at which only two experimental results are known, the mean value of D_M is 1.8×10^{20} $m^{-1}s^{-1}$, with a standard deviation of 0.4×10^{20} $m^{-1}s^{-1}$. As can be seen from table 4.2 the present result of the diffusion coefficient is in good agreement with previous experimental results at 295 K. At 77 K the present value of D_M seems to be somewhat larger than previous experimental data. In figure 4.5 the experimental and theoretical values of the diffusion coefficient are shown.

From ab initio calculations of potential energy curves for the Ne_2^*-excimers, Cohen and Schneider (Coh75) calculated the diffusion coefficient of the Ne($^3P_2$)-atom in neon at 77 K and 300 K. Measurements of the diffusion coefficient as a function of gas temperature might enable us to obtain the interaction potential between the $^3P_2$-atom and the ground state atom as a function of internuclear distance. Chapman and Cowling derived a first order approximation (Hir54) of the diffusion coefficient D of a neutral particle in a bulk gas at a certain temperature. The diffusion coefficient $[D]_1$ is, in first approximation, only a function of the collision integral $\Omega^{(1,1)}$,

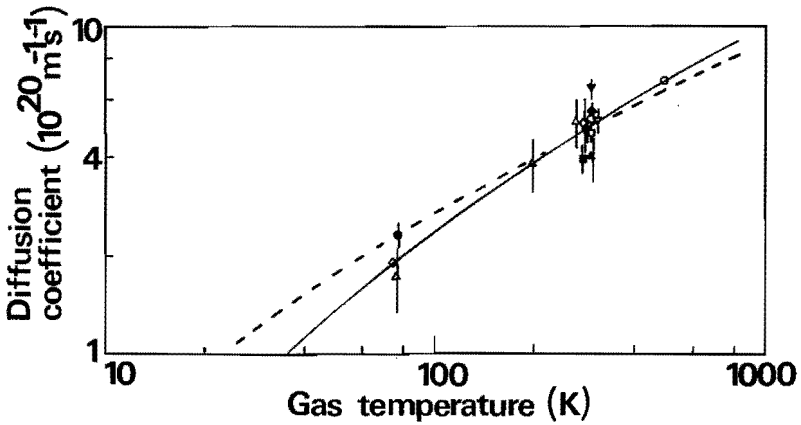

Figure 4.5 Previous and present experimental results on the diffusion coefficient for Ne($^3P_2$)-atoms in neon.
● *(present)*
△ *(Gra53)* □ *(Ste79)* ▲ *(Gra51)*
○ *(Phe59)* ▽ *(Met72)* ■ *(Mol51)*
◇ *(Phe53)* ◆ *(Dix57)* ▼ *(Bio52)*
Calculations with a 16-6- and 300-4-potential curve are shown by solid and dashed curves, respectively.

defined in section V.3, and reads

$$N[D]_1 = \frac{3\sqrt{\pi kT/2\mu}}{8\Omega^{(1,1)}(T)} \tag{4.10}$$

where N is the gas density, μ the reduced mass of the diffusing particle and the gas molecule, and k is the Boltzmann constant. For an interaction potential

$$V(r) = \frac{n\varepsilon}{n(3+\gamma) - 12(1+\gamma)} \left[\frac{12}{n}(1+\gamma)\left(\frac{r_m}{r}\right)^n - 4\gamma\left(\frac{r_m}{r}\right)^6 - 3(1+\gamma)\left(\frac{r_m}{r}\right)^4\right], \tag{4.11}$$

where ε and r_m are the depth and position of the potential minimum, respectively, and γ the parameter determining the relative strength of the r^{-6} and r^{-4} terms, Viehland *et al.* (Vie75b) calculated for various (n,γ)-combinations the reduced collision integral $\Omega^{(1,1)}/\pi r_m^2$ as a function of the reduced temperature kT/ε. Assuming an n-6-potential to be a good representation for the interaction, we calculated r_m and ε, using equation (4.10), the tabulated collision integrals (Vie75b) and the theoretical data for D_M at 77 K and 300 K (Coh75). The value of ε appeared to be at most 35 K for a 16-6-potential, which is equal to the value of ε in the case of

the interaction of two ground state neon atoms (Hir54). This small value for ε is in contradiction with the frequent occurrence in gas discharges of diatomic molecules (excimers), with rather long lifetimes.

Another phenomenon is the insensitivity of the diffusion coefficient to the potential energy curve. A calculation shows that divergent potential energy curves, *e.g.* 12-4, 16-6, 300-4, with various values for ε and r_m lead to diffusion coefficients as a function of temperature still within the error bars of the experimental data (see figure 4.5). The conclusion is that very accurate data on the diffusion coefficient over a wide range of temperatures must be available to obtain a unique potential energy curve with sufficiently accurate parameters.

IV.6.2 De-excitation rate

In table 4.3 the several experimental and theoretical results on the de-excitation rate A from the $^3P_1$-state to the $^3P_2$-state by two-body collisions with ground state neon atoms at 295 K, are given.

When leaving out of consideration the value of Biondi (Bio52) the present value of 3.5×10^{-20} m^3s^{-1} is about 25% smaller than the mean value of the three other experiments, giving a value of $(4.6\pm0.5) \times 10^{-20}$ m^3s^{-1}. In figure 4.6 the known experimental (Phe59, Gra53, Bio52, Ste79, Lei75), theoretical (Coh78) and the present results on the de-excitation rate are shown in a double logarithmic plot as a function of gas temperature. As can be seen

Table 4.3 Previous and present experimental and theoretical results on the de-excitation rate A.

	Temperature (K)	A (10^{-20} m^3s^{-1})	
Phe59	300	4.1	
Ste77	300	4.2±0.5	
Lei75	300	5.59	Experiment
Bio52	300	9.2	
Present result	295	3.5±0.1	
Coh78	300	3.5	Theory

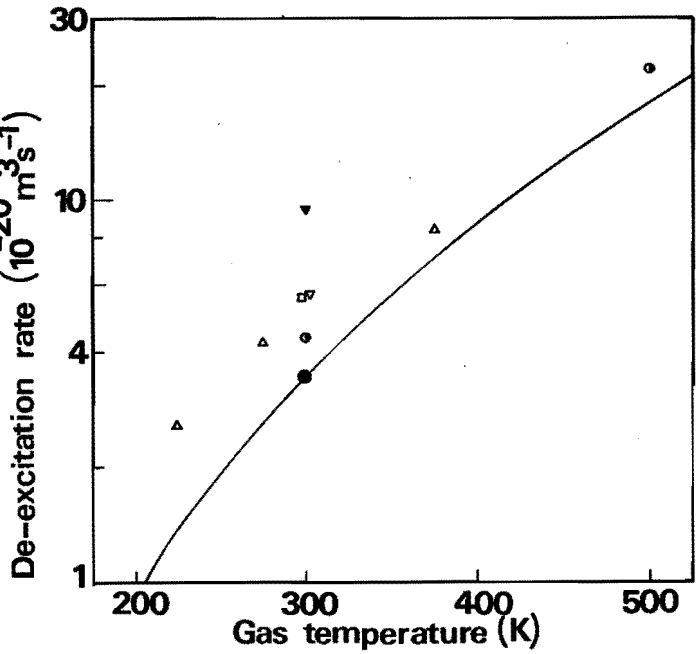

Figure 4.6 Previous and present experimental results on the de-excitation rate A from the $^3P_1$- to the $^3P_2$-state in collision with ground state neon atoms.
● *(present)* △ *(Gra53)* □ *(Ste79)*
◑ *(Phe59)* ▼ *(Bio52)* ▽ *(Lei75)*
Solid curve: calculations from (Coh78).

in this figure for temperatures above 400 K the agreement between theory and experiment is within about 10%. For temperatures below 400 K the deviation of results from previous experiments with theory increases to more than 40%. As discussed by Cohen *et al.* this latter discrepancy is somewhat larger than could be expected from inaccuracies in the calculated potential energy curves they used for their calculations. As can be seen from figure 4.6 a strong dependence of the de-excitation rate on gas temperature exists. A slight underestimation of the gas temperature in previous experiments, due to mA-currents in those discharges in contrast with μA-currents in a T.D., might diminish the deviation from the theoretical curve. The present result at 295 K is in good agreement with the theory of Cohen *et al.* (Coh78).

IV.6.3 Excimer formation rate

The results of the experimentally determined excimer formation rate at 77 K and 295 K, are shown in table 4.4. As can be seen from this table, the present result on γ_M at 77 K is in good agreement with previous experimental data. At 300 K the value for γ_M is about 40% smaller than previous results found by Phelps (Phe59), Steenhuysen (Ste79) and Leichner (Lei75). In the foregoing analysis a value of 0.47×10^{-44} m^6s^{-1} for the excimer formation rate γ_R through the $^3P_1$-resonant state, as found by Leichner, has been substituted in the expression for the decay frequency (equation (4.5)). The least mean square fit of equation (4.5) to the measured decay frequencies, shows a large dependence of γ_M on the substituted value of γ_R. This effect is caused by the strong atom coupling between the metastable and the resonant state. When we assume that the resonant $^3P_1$-state cannot form excimers, as is supposed by Steenhuysen (Ste79), a value of $(5.0\pm0.2) \times 10^{-46}$ m^6s^{-1} is found for γ_M. When varying the value of γ_R from 0 to 1.0×10^{-44} m^6s^{-1}, the diffusion coefficient D_M and the de-excitation rate A, determined from the least mean square analysis, appear not to depend on γ_R, whereas the imprisonment decay rate β_2 only increases 20%.

In the experiments of Phelps and Steenhuysen an accurate measurement of the ratio of the $^3P_1$- and $^3P_2$-state densities at high gas pressures is required. In their analysis the quantity $(1 - R/aM)$ is used. The deviation of R/M with respect to the Boltzmann factor is of importance.

Table 4.4 Previous and present experimental results for the excimer formation rate γ_M at various temperatures.

	Temperature (K)	γ_M (10^{-46} m^6s^{-1})
Phe59	300	5.0
Ste77	300	6.0±0.4
Lei75	300	5.79
Gra53	77	0.50
Phe53	77	0.50
Present result	295	3.3±0.2
	77	0.52±0.04

When an activation energy of E_o for the three-body collision reaction is assumed, the collision coefficient as a function of temperature can be written as

$$\gamma_M = C \exp(-\frac{E_o}{\frac{3}{2} kT}) \quad , \tag{4.12}$$

where C is a proportion constant, k the Boltzmann constant and T the absolute temperature of the gas. Substitution of the measured values of γ_M at 77 K and 295 K in equation (4.12) gives for the activation energy the value of 0.025 eV. The calculation of potential energy curves, as a function of internuclear distance R, for the ground and excited states of Ne_2 by Cohen and Schneider (Coh74), as is to be seen in the figures 4.7 to 4.9, shows for the interaction of $Ne(^3P_2)$ with a ground state neon atom one attractive curve and three repulsive ones. The attractive potential energy curve, without taking into account spin-orbit coupling, shows a hump in the potential curve of 0.086 eV, whereas for the $0_u^-(^3P_2)$- and $I_u(^3P_2)$-potential curves, which were calculated with spin-orbit coupling, humps of 0.11 eV are to be seen at intermolecular distances of about 0.25 nm. However, these data are only an indication for the order of magnitude of the potential hump, because the real potential energy curve is a linear combination of the separate potential curves as calculated by Cohen and Schneider (Coh74). It is reasonable to assume that the true value of this hump is smaller than the data found by Cohen and Schneider for the separate bondings. Studies of the emission band spectrum of the Ne_2 molecule in the visible and near infrared spectral region by Gritsina *et al.* give rise to the assumption that a hump in the potential energy curve of the upper electronic state of these molecules exists of several hundredths of electron volts (Gri74).

IV.6.4 General conclusion

From the present work we can draw the conclusion that the data on the diffusion coefficients, the de-excitation rate and the excimer formation rates at 77 K and 295 K are in good agreement with results of other experimentators and theoreticians. The slightly smaller value of the de-excitation rate at 295 K, as found in the present work, in comparison with results of Leichner, Biondi and Steenhuysen, might be caused by an underestimation of the gas temperature in these previous experiments. A good

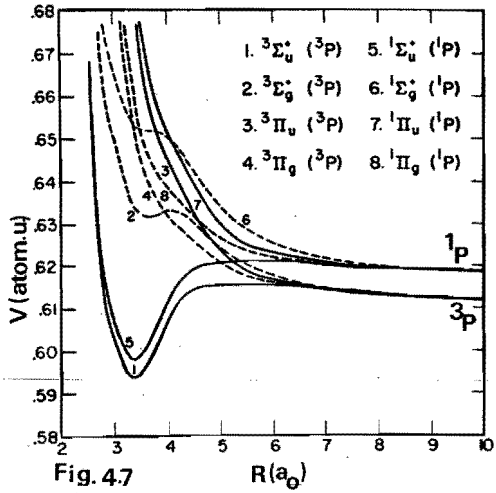

Fig. 4.7

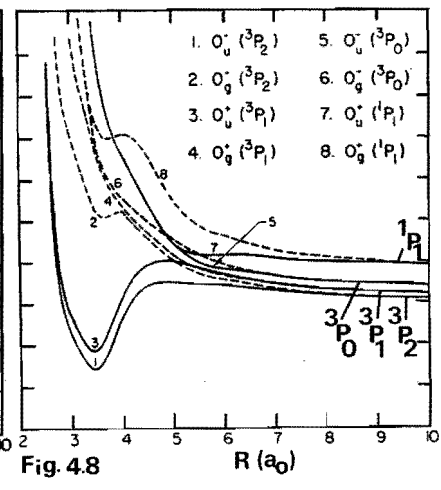

Fig. 4.8

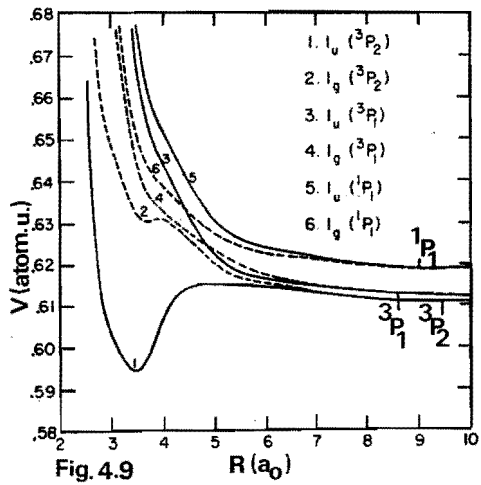

Fig. 4.9

Figure 4.7 *Potential curves for the excited states of Ne_2 formed in the interaction of Ne(3s, ^{1}, ^{3}P) with ground state Ne, not including spin-orbit coupling. The zero of the energy scale is the separated-atom limit of ground state Ne_2. After Cohen and Schneider (Coh74).*

Figure 4.8 *Potential curves of excited states of Ne_2 with $\Omega = 0$, including the effects of spin-orbit coupling, after (Coh74).*

Figure 4.9 *Potential curves of excited states of Ne_2 with $\Omega = 1$, including the effects of spin-orbit coupling, after (Coh74).*

conformity of the present value of the de-excitation rate with calculations of Cohen *et al.*, however, has been obtained. The excimer formation rate γ_M of the $^3P_2$-state at 295 K is 40% smaller than previous data of Phelps (Phe59), Steenhuysen (Ste79) and Leichner (Lei75). We showed that the precize value of γ_M depends strongly on the value of the excimer formation rate γ_R for the resonant $^3P_1$-state, a process which was neglected by Steenhuysen. *E.g.* at Steenhuysen γ_M would be $(4.0\pm0.4) \times 10^{-46}$ m^6s^{-1} when Leichners result on γ_R of 0.47×10^{-44} m^6s^{-1} was used in his calculations. Leichner, however, measured both the values of γ_R and γ_M and still obtained a large value of 5.8×10^{-46} m^6s^{-1} for γ_M.

The general conclusion is that the present method in which the nitrogen molecular ions, formed by the Penning ionization reaction, act as tracers for detecting the metastable atoms, is a reliable one for the measurement of the decay of $Ne(^3P_2)$-atoms. In the T.D. with its very low current densities, cumulative processes can be ruled out. No repopulation of 3s-states by dissociative recombination occurs in the T.D. afterglow. Velocity distributions are fairly well known. No space charge distortion is present and sampling of ions from the discharge is sound. The gas temperature in the T.D. has a well known value.

Measurements at intermediate gas temperatures, in combination with fluorescence techniques, will give more insight in the influence of the coupling between the $^3P_1$- and $^3P_2$-state.

CHAPTER V

MOBILITIES OF POSITIVE IONS IN NEON

In this chapter an experimental method is described using a Townsend discharge in which the mobilities of positive ions in neon can be measured over a large range of the reduced electric field strength. Section V.1 gives an introduction on experimental techniques used to determine this mobility. Also a short review is given of the existing method to calculate from mobility data the interaction potential between the ion and the gas molecule as a function of intermolecular distance. The experimental method we used is described in section V.2. Section V.3 deals with the application of the calculation method to find the potential energy curve from the measured mobility data. The results of the experiment and the calculations on the mobility of Ne^+ and N_2^+ in neon at gas temperatures of 77 K and 295 K, are given in section V.4. Sections V.5 and V.6 present the conclusions drawn from the experimental results and discuss the applicability of the present experimental method for measuring mobilities.

V.1 Introduction

Measurements of macroscopic transport properties of ions in neutral gases as functions of the electric field strength, are important for the determination of the microscopic interaction between ions and molecules. The intermolecular forces between an ion and a molecule, playing an important role in the physical and chemical properties of matter, are not directly measurable in an experiment. Ab initio calculations of these forces are tremendously difficult to carry out. Only with the introduction of fast computers, extensive calculations on solving intermolecular problems could be done. Because of the functional dependency of the macroscopic transport properties on intermolecular forces, measurements of the transport properties are a useful tool in getting qualitative and quantitative information on the potential energy functions between the molecules.

We limit ourselves to the case of the binary interaction of an ion and a molecule. The macroscopic quantities, *e.g.* diffusion of an ion in a gas and the mobility of an ion in the presence of an electric field, are determined by collisions between the ion and the molecules. The collision cross section is directly coupled to the interaction potential between the colliding particles. Measurements of the macroscopic quantities *e.g.* the diffusion coefficient and the mobility of ions in gases as functions of gas temperature and reduced electric field strength, and the availability of an inversion method for obtaining the interaction potential between an ion and a molecule from these measured data, enable us to calculate the interaction potential.

Viehland *et al.* (Vie76) give in their work criteria that must be satisfied to obtain an interaction potential in numerical form over a wide range of nuclear distances from the above mentioned measurements. (*i*) The data must be sufficiently accurate, (*ii*) the data on the macroscopic property should be obtained over a wide range of energy *e.q.* temperature, (*iii*) a theory must exist on the functional dependence between the macroscopic properties and the interaction potential and finally (*iv*) a mathematical scheme must be available to invert the functional dependence. The results of our measurements are not accurate enough to apply Viehlands inversion scheme with any success. It is possible, however, to use our results for the determination of the parameters of a potential energy function, the general shape of which is chosen for a variety of obvious reasons.

In this chapter we limit ourselves to the determination of the mobilities of positive ions in gases and the determination of the interactic potential from this mobility. An extensive description of the measurements c mobilities of positive ions with different experimental methods is given by McDaniel (McD72). In this section the several techniques will only be mentioned in short.

Measurements of mobilities are mostly carried out in drift tubes, ofter connected to a mass spectrometer for ion identification. The mobility K of an ion in a gas under the influence of an electric field strength E is per definition directly related to the drift velocity v_d according to

$$v_d = K.E \ . \qquad (5.1)$$

The determination of the mobility is done by measuring the drift velocity of the specific ions. Nowadays an ionic drift tube almost always consists of a cylindrical chamber containing an ion source on its axis, several ring shaped electrodes to obtain a homogeneous axial field, and a sampling orifice in the wall at the end of the tube. A swarm of specific ions which acquires in the drift field E a drift velocity dependent on the kind of ions and gas molecules, the gas density, the electric field strength and the temperature, passes the sampling orifice. Ions are selected by a mass spectrometer and detected. The source of ions is operated in a pulsed mode. The drift velocity is determined from an arrival time spectrum of the swarm of ions at the detector. Because of the large length of a drift tube - up to 0.5 m - gas pressures of a few hundred pascal or more lessen the influence of the diffusion of ions. This diffusion interferes with the analysis of the arrival time spectrum and reduce the accuracy of the measurements. The pressures commonly used in drift tubes range from 10 Pa to 1 kPa while E/N can vary between 0.3 Td to 5000 Td. This maximum value for E/N is always lower than that at which breakdown in the drift tube occurs and usually not higher than the value where the corresponding mean ion energy exceeds the treshhold for inelastic collisions. So the average energies of the ions range from thermal kinetic energy to a few electron volt. The possibility of ion-molecule reactions taking place in the drift tube, which thwarts the determination of transport properties, is not considered in this chapter. The accuracy of the data is usually better than 5%, whereas the best data have an accuracy better than 2% over the whole energy range (Hel77a, Gat77). As mentioned earlier, the range of energies of the ions at which mobility data can be obtained in drift tube experiments is still wide enough to acquire the interaction potential over a large range of internuclear distances.

A typical drift tube experiment without the use of a mass spectrometer is the four-grid, electrical shutter method developed by Tyndall (Tyn38) and used by Beaty (Bea62). Briefly indicated, the advantage of the method of pulsing is that the electric field is not affected by the pulse anywhere except between the grids of the shutters. Hornbeck (Hor51a+b) also used a drift tube without a mass spectrometer. A 0.1 μs pulse of photo electrons is released from the cathode of a gas filled tube with two parallel electrodes.

At high electric field strength an avalanche of electrons developes in the direction of the anode. The spatial distribution of the ions which were formed through ionization by the electrons, drifts much slower to the cathode and gives rise to an electric current that can be measured and displayed on an oscilloscope. The drift time can be seen as a break in the current signal on the oscilloscope. The Hornbeck technique is particularly useful for obtaining data at high E/N values up to 2000 Td.

The kinetic theory for the calculations of the mobility of ions in gases at arbitrary field strength for any interaction potential is developed by Viehland and Mason (Vie75a). In lowest approximation, where the expressio for the mobility is about the same as the one obtained from the free-flight theory, these calculations are accurate within about 10%. Higher approximations can reduce the error to within a percent. This theory was checked on data of the mobility of K^+-ions in He, Ne and Ar. Up to effective temperatures as high as 20,000 K the results agree with scattering experiments carried out with ion beams. An inversion scheme suitable for the calculation of the intermolecular potential energy curve from experimental data of ion mobility measurements is presented by Viehland *et al.* (Vie76). Based upon experimental data from Akridge *et al.* (Akr75) of Li^+ in He, and using their inversion scheme, they obtained numerical values for the interaction potential. This potential was compared with an analytical expression obtained by Morrison *et al.* (Mor75) which exactly fits the same experimental data. The discrepancy of the potential obtained by Viehland with the analytical expression in the vicinity of the potential well, is less than 3% Viehland states that in favourable cases the inaccuracy in the obtained interaction potential from gaseous ion mobility measurements is less than 5%

The reduced mobility K_o is defined as

$$K_o = 2.696 \times 10^{-3} \frac{p}{T} K \ , \qquad (5.2)$$

where p is the gas pressure in pascal and T the gas temperature in kelvin. In the present work K_o is measured for Ne^+ as well as for N_2^+-ions in neon at 77 K and 295 K, for reduced electric field strengths between 10 Td and 900 T and between 10 Td and 250 Td, respectively. The reduced mobilities of the Ne^+-ion in neon at 295 K are extensively measured by several authors.

Accurate measurements of Helm and Elford (Hel77a) carried out in a drift tube experiment gives values of K_o up to a reduced field strength of 300 Td. Hölscher (Hol73) obtained reduced mobility data of Ne^+ in neon by measuring the impedance of a T.D.. His data for K_o were given for E/N values up to 400 Td. Hornbeck obtained less accurate data for E/N from 30 to 1700 Td (Hor51b). At 77 K the measurements done by Helm and Elford (Hel77a) show, up to a reduced field strength of 30 Td, different reduced mobilities for $Ne^+(^2P_{3/2})$ and $Ne^+(^2P_{1/2})$. The mobility of $Ne^+(^2P_{1/2})$ is smaller than that of the $Ne^+(^2P_{3/2})$-ion. In the range from 30 Td to 70 Td these effects could not be observed and only a single value for the mobility was found.

In our experiment we determined the reduced mobilities of the Ne^+-ion in neon at temperatures of 77 K and 295 K for maximum values of E/N of 350 Td and 900 Td, respectively. Because the existence of very reliable results in literature on the mobility of Ne^+ in neon, our experiments have not been carried out on a very extensive scale. Apart from showing that the present experiment is suitable for mobility measurements at very high reduced electric field strengths, the present results mainly are a check on the reliability of our experimental method. In the present work more extensive experiments have been done on the mobilities of N_2^+-ions in neon at 77 K and 295 K. From the mobility data over the wide range of reduced field strength from 10 Td up to 200 Td, the intermolecular potential between a N_2^+-ion and a Ne atom as a function of nuclear distance was inferred. The only known value in the literature on the mobility of a nitrogen molecular ion in neon is the zero-field reduced mobility by Märk and Oskam (Mar71). From experiments in the afterglow of a Ne-N_2 plasma they determined the ambipolar diffusion coefficient of N_2^+ in neon. Because this ambipolar diffusion coefficient is directly related to the reduced mobility at very low electric field strength it was possible to calculate the zero-field reduced mobility from the mentioned value. Previous measurements on the mobility of N_2^+-ions in neon for E/N from 30 Td to 80 Td with the present experimental setup were carried out by van der Laarschot and de Hoog (Laa74). The experimental technique used in the present work resembles the experiments of Hornbeck (Hot51a+b) as mentioned above. In section V.2 the experimental method will be described.

V.2 Experimental method

The experimental technique is based on the measurement of the time of flight of a specific positive ion from the anode to the cathode containing the sampling hole. As can be seen in chapter III, the density distribution of positive ions, *c.q.* the N_2^+-ions, in a stationary T.D. is a monotonically increasing function of the distance to the positive electrode. At the negative electrode the density reaches a minimum value, whereas at the anode the positive ion density should be zero. In section II.4 the measuring technique is extensively described. With the aid of the time sampling apparatus, the time of flight of the positive ions from the moment the electric field is reversed, to their arrival at the detector is measured. A histogram of the spatial ion density distribution in the discharge is obtained by periodically repeating this experiment, while storing the measured times in the micro processor memory. Because the ion density distribution in the discharge mode has a positive gradient at the positive electrode and a steep flank at the negative electrode, the mean transit time of an ion species can easily be obtained from the histogram. This can be seen in figure 5.1.

The drift velocity of this ion species then equals the ratio of the electrode distance d and the time Δt, representing the average maximum drift time, which is measured from the histogram. The ratio of the diffusive spreading $\langle x \rangle$ of an ion swarm and the length L of the drift tube, at 273 K and low electric field strength, can be written as (McD72)

$$\frac{\langle x \rangle}{L} = \frac{0.173}{\sqrt{V}} \quad , \tag{5.3}$$

where V is the potential difference in volts over the drift tube. In the present experiments the maximum value of this ratio is 0.03 and the influence of diffusion of ions on the spatial distribution can be neglected. The reduced electric field strength, E/N, can be chosen by varying the gas density and the drift voltage between the electrodes. This drift voltage has to be less than the voltage at which breakdown in the gas occurs. The drift velocities and hence the reduced mobilities are measured in the experimental setup which could be operated at 77 K. Here the distance between the electrodes is fixed at a value of $(8.90 \pm 0.05) \times 10^{-3}$ m.

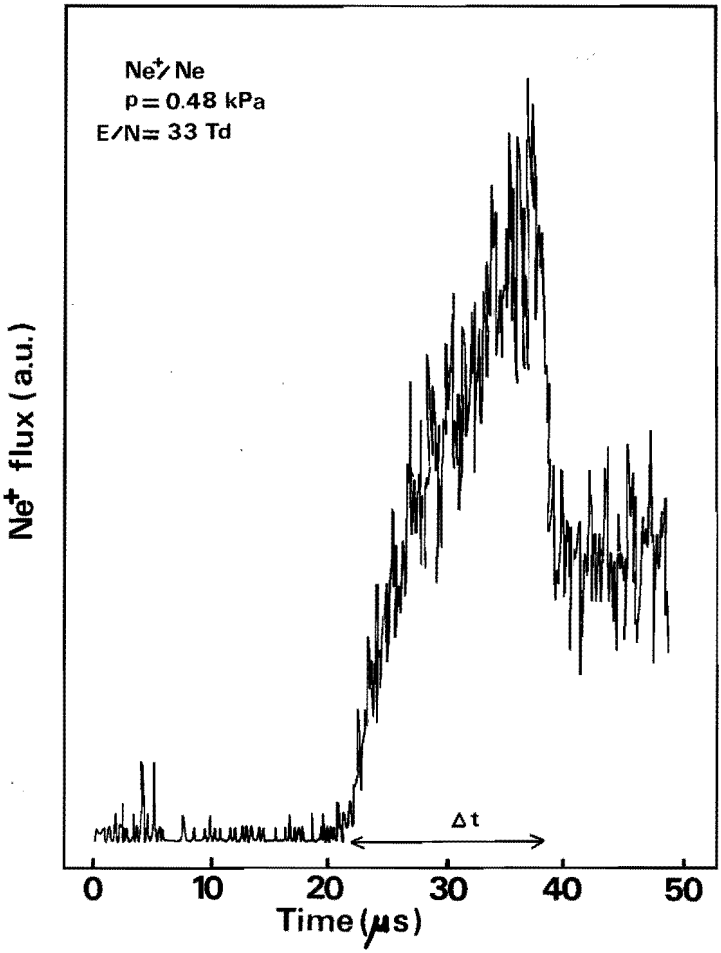

Figure 5.1
Typical plot of a time of flight spectrum.

V.3 Calculation of the intermolecular potential

As mentioned in the introduction Viehland *et al.* (Vie76) developed an inversion scheme for the calculation of the intermolecular potential between an ion and a molecule from mobility data. In this procedure it is necessary to calculate in each step an inversion function which is in general a complicated combination of the interaction potential, the collision integral and the relative energy. When the experimental mobility data are sufficiently accurate, the interaction potential calculated with this method can reach an accuracy of better than 3% in third approximation. The results

of our measurements are not accurate enough to use Viehlands inversion method. When one chooses a potential energy curve of a specific shape containing 3 parameters, it is possible to calculate these, so that the result fits the experiments. We describe the interaction of a N_2^+-ion and a Ne-atom with a 12-6-4-potential

$$V(r) = \frac{\varepsilon}{2}\left[(1+\gamma)\left(\frac{r_m}{r}\right)^{12} - 4\gamma\left(\frac{r_m}{r}\right)^{6} - 3(1-\gamma)\left(\frac{r_m}{r}\right)^{4}\right] , \tag{5.4}$$

where ε and r_m are the depth and position of the potential minimum, respectively, and γ is a dimensionless parameter giving the contributions of the r^{-6} and r^{-4} terms, as a representative of the true potential energy curve. The r^{-4} term describes the ion-induced dipole interaction, whereas the r^{-12} and r^{-6} terms give the normal Lennard-Jones potential.

The deflection angle in a central force collision with potential energy $V(r)$ as a function of the impact parameter b and the relative energy E can be written as

$$\theta(b,E) = \pi - 2\int_{r_a}^{\infty}\left(1 - \frac{b^2}{r^2} - \frac{V(r)}{E}\right)^{-1/2}\frac{dr}{r^2} , \tag{5.5}$$

where r is the nuclear distance and r_a the distance of closest approach given by

$$1 - \frac{b^2}{r_a^2} - \frac{V(r_a)}{E} = 0 \tag{5.6}$$

Integration of $(1 - \cos^1(\theta))$ over all impact parameters b gives the transport cross section

$$Q^{(1)}(E) = 2\pi\left(1 - \frac{1+(-1)^1}{2(1+1)}\right)^{-1}\int_0^{\infty}(1 - \cos^1(\theta))\, b.db . \tag{5.7}$$

Integration of this expression over E gives the collision integral

$$\Omega^{(1,s)}(T) = \left((s+1)!(kT)^{s+2}\right)^{-1}\int_0^{\infty} Q^{(1)}(E)\, e^{-E/kT}\, E^{s+1}\, dE \tag{5.8}$$

as a function of the temperature T. The collision integral $\Omega^{(1,s)}$ and the temperature T are written mostly as dimensionless quantities. The reduced collision integral and reduced temperature are written as

$$\Omega^{(1,s)*} = \frac{\Omega^{(1,s)}}{\pi r_m^2} \tag{5.9}$$

and

$$T^* = \frac{T}{\epsilon} \tag{5.10}$$

respectively. Here ϵ is the depth of the minimum of the potential in kelvin. For several types of potential energy curves the integrals $\Omega^{(1,s)*}$ have been calculated and tabulated as functions of T^*. Viehland *et al.* (Vie75b) calculated these collision integrals $\Omega^{(1,s)*}$, for a 12-6-4-potential and for values of 1 and s of 1, 2 and 3, as functions of the reduced temperature T^*. In first approximation several transport coefficients, such as the viscosity, the thermal conductivity and the diffusion coefficient can be expressed in the collision integrals $\Omega^{(1,1)}$ and $\Omega^{(2,2)}$ etc. (*c.f.* IV.6.1).

The reduced mobility K_o can, in first approximation, also be expressed in $\Omega^{(1,1)}$. For the sake of convenience we shall proceed in the reversed order and express the collision integral in terms of the reduced mobility. The first order approximation of the collision integral as a function of an effective temperature, given by Viehland and Mason (Vie75a) and mentioned in section V.1 can be written as

$$\Omega^{(1,1)}(T_{eff}) = 497.4 \left(\frac{z}{v_d}\right)\left(\frac{m+M}{mMT_{eff}}\right)^{1/2} \frac{E}{N} , \tag{5.11}$$

with $\Omega^{(1,1)}$ in $\mathring{A}^2$, E/N in Td, T_{eff} in kelvin, ionic mass m and atomic mass M in kg/kmole, the drift velocity v_d in 100 ms^{-1}; z is the number of elementary electronic charges. The effective temperature is given by

$$T_{eff} = T + 0.4009\ M\ v_d^2 , \tag{5.13}$$

where T is the gas temperature in kelvin. This equation gives $\Omega^{(1,1)}$ with an accuracy better than 10%. Using the relation

$$v_d = 0.02687\ K_o \frac{E}{N} , \tag{5.14}$$

with v_d in 100 ms^{-1}, K_o in $cm^2V^{-1}s^{-1}$ one can write (3.9) and (3.10) as

$$\Omega^{(1,1)}(T_{eff}) = 18.511 \times 10^3 \frac{1}{K_o} \left(\frac{m+M}{mMT_{eff}}\right)^{1/2} \tag{5.15}$$

and

$$T_{eff} = T + 5.789 \times 10^{-3} K_o^2 \left(\frac{E}{N}\right)^2 \qquad (5.16$$

The first order approximation of the collision integral as a function of mobility and reduced field strength is sufficiently accurate for treating the reduced mobility data obtained from our experiments.

V.4 Results

As mentioned in the introduction the drift velocities of Ne^+ and N_2^+-ions in neon at 77 K and 295 K have been measured as functions of reduced electric field strength, and from these data the reduced mobilities have been calculated.

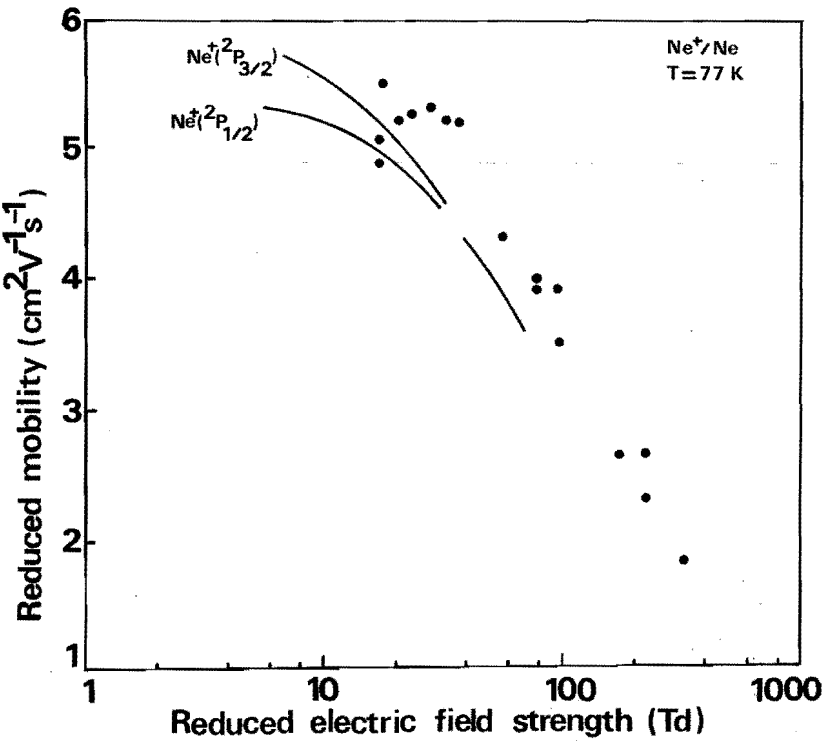

Figure 5.2 Previous and present (●) experimental results on the reduced mobility of Ne^+ in Ne at 77 K; —— (Hel77a).

V.4.1 Mobility of Ne^+ in neon

The reduced mobilities of Ne^+ in neon at 295 K have been measured for values of E/N from 20 Td to 900 Td. Gas densities ranged from 1.6×10^{22} m^{-3} to 6.4×10^{23} m^{-3}. In figure 5.3 these data are shown and compared with experiments by Helm and Elford (Hel77a), Hölscher (Hol73) and Hornbeck (Hor51b). Figure 5.2 gives the reduced mobilities of Ne^+ in neon at 77 K, measured from 17 Td to 320 Td. Gas densities ranged from 5.0×10^{22} m^{-3} to 2.2×10^{24} m^{-3}. These data are also compared with the results of experiments

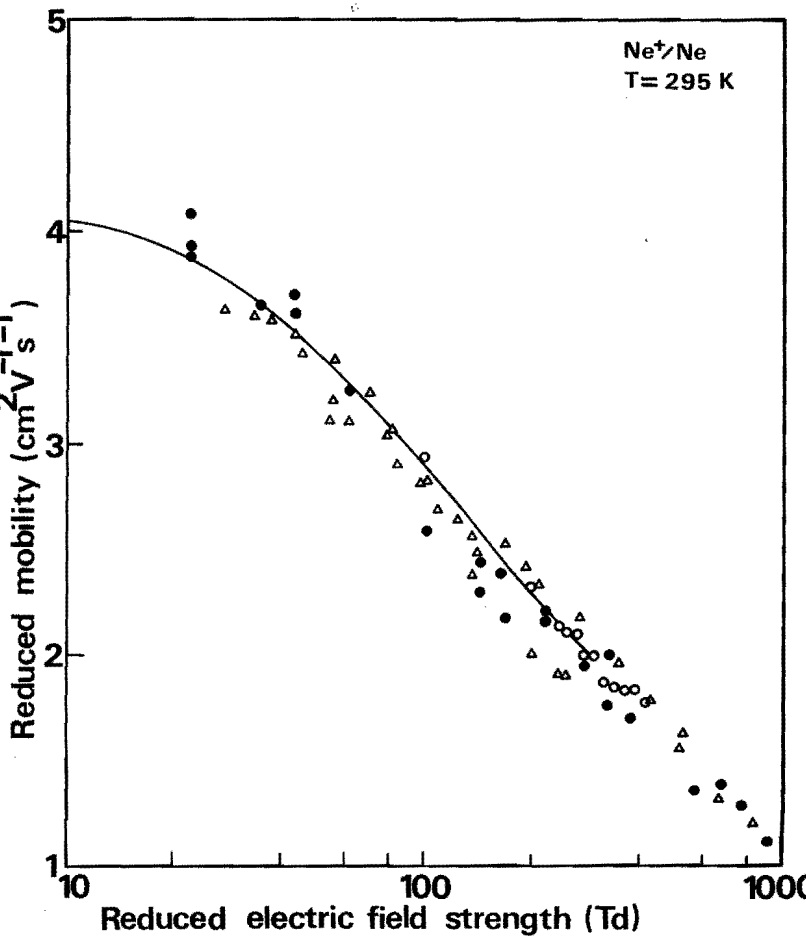

Figure 5.3 Previous and present (●) experimental results on the reduced mobility of Ne^+ in Ne at 295 K; —— (Hel77a), O (Hol73), Δ (Hor51b).

by Helm and Elford (Hel77a). As can be seen from these figures the present measurements of the Ne^+ mobilities in neon are in good agreement with the very accurate data of Helm. At this point the conclusion is justified that the present experimental method is suitable for the determination of mobilities of positive ions in gases, especially at higher reduced electric field strengths.

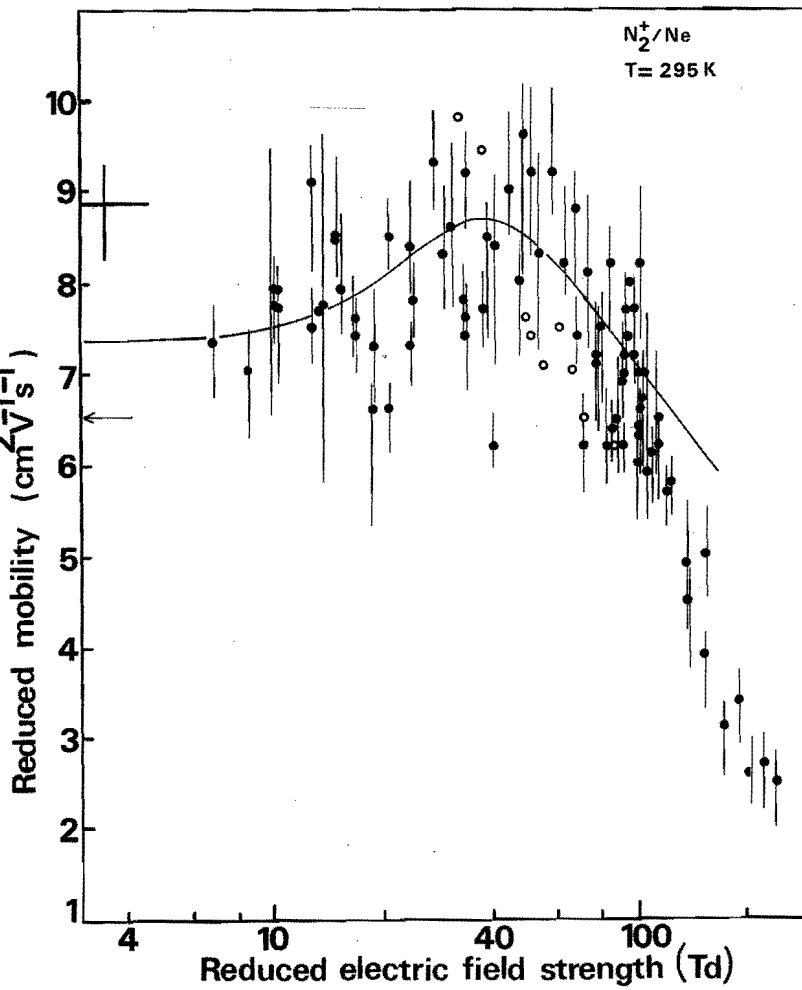

Figure 5.4 Comparison of the experimental results (●) with results from the model in which the depth and the position of the 12-6-4-potential energy curve are fitted to the experimental points at 295 K; O(Laa74), +(Mar71).

V.4.2 Mobility of N_2^+ in neon

From measured drift velocities reduced mobilities of N_2^+-ions in neon were determined as a function of reduced electric field strength at 77 K and at 295 K. At 295 K the reduced mobilities of N_2^+ in neon were measured in the range of the reduced electric field strength from 7 Td to 250 Td. In figure 5.4 these mobility data are shown on a linear-logarithmic plot as a function of the reduced electric field strength. Also is shown the zero-field reduced mobility measured by Märk and Oskam (Mar71). As is the case for Ne^+, the N_2^+-mobility shows a strong dependence on the reduced electric field strength. As can be seen from extrapolating these data to lower E/N the value found by Märk and Oskam is about 20% higher than the present zero-field reduced mobility. The reduced mobilities of N_2^+ in neon at 77 K have been measured

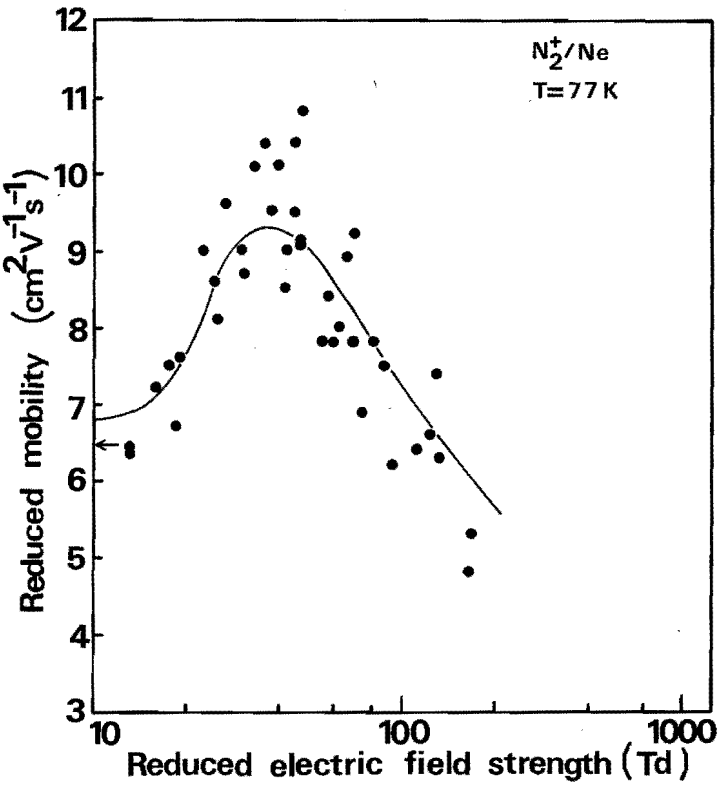

Figure 5.5 Comparison of the experimental results (●) with results from the model in which the depth and the position of the 12-6-4-potential energy curve are fitted to the experimental points at 77 K.

for values of E/N from 13 Td to 130 Td. In figure 5.5 these data are shown in a linear-logarithmic plot. No other experimental values are known in literature.

V.4.3 Molecular ion-atom potential energy curve

In this section the theory of Viehland and Mason (Vie75a) as treated in section V.3, will be applied to the interaction of a N_2^+-ion with a Ne-atom. By using the equations (5.15) and (5.16) the mobility data of N_2^+ in neon as a function of E/N are transformed to values of the collision integral $\Omega^{(1,1)}$ as a function of temperature T_{eff}. In the figures 5.6 and 5.7 the calculated $\Omega^{(1,1)}$ is shown on a linear-logarithmic plot as a function of the effective temperature T_{eff}. In the second step we start from the interaction potential $V(r)$ given by relation (5.4) with γ between 0 and 1. For this 12-6-4-potential, the reduced collision integral $\Omega^{(1,1)*}$ was tabulated by

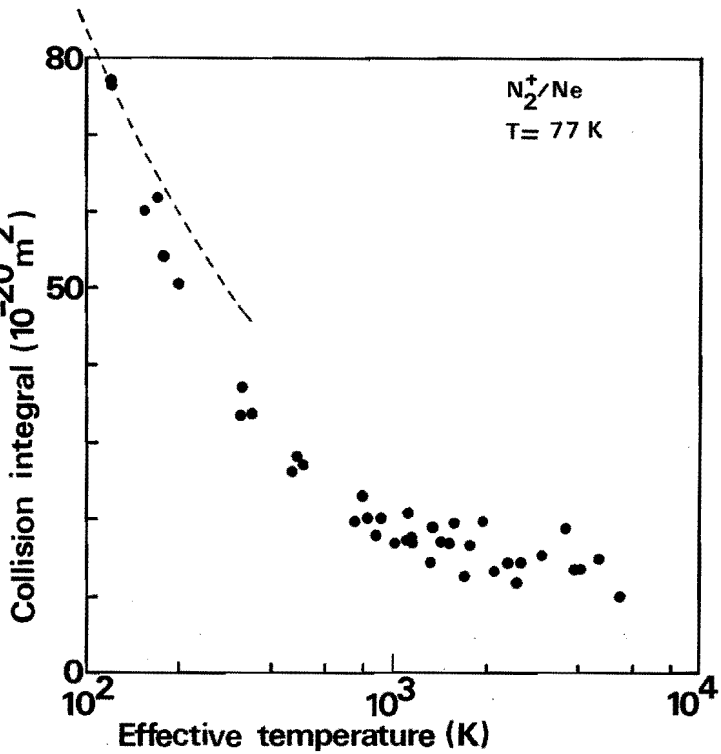

Figure 5.6 The collision integral $\Omega^{(1,1)}$ v. the effective temperature T_{eff} for N_2^+ in Ne at 77 K. The dashed curve shows the polarization limit.

Viehland *et al.* as a function of the reduced effective temperature T^*_{eff} (Vie75b). The third step consists of a determination of the parameters ε, r_m and γ. By means of a non-linaer least square method ("MINIQUAD" on the Burroughs 7700, THE Eindhoven), the best values of ε, r_m and γ are obtained, by fitting the tabulated $\Omega^{(1,1)}$ to the experimentally determined $\Omega^{(1,1)}$ values, as calculated from the mobility data. The results of these calculations are given in table 5.1. From this table we give for the best values of ε and r_m:

ε = 0.051±0.005 eV

r_m = 0.261±0.005 nm

With the values of ε and r_m, as given in table 5.1, the reduced mobility as a function of the reduced electric field strength can be calculated by using (5.15) and (5.16).

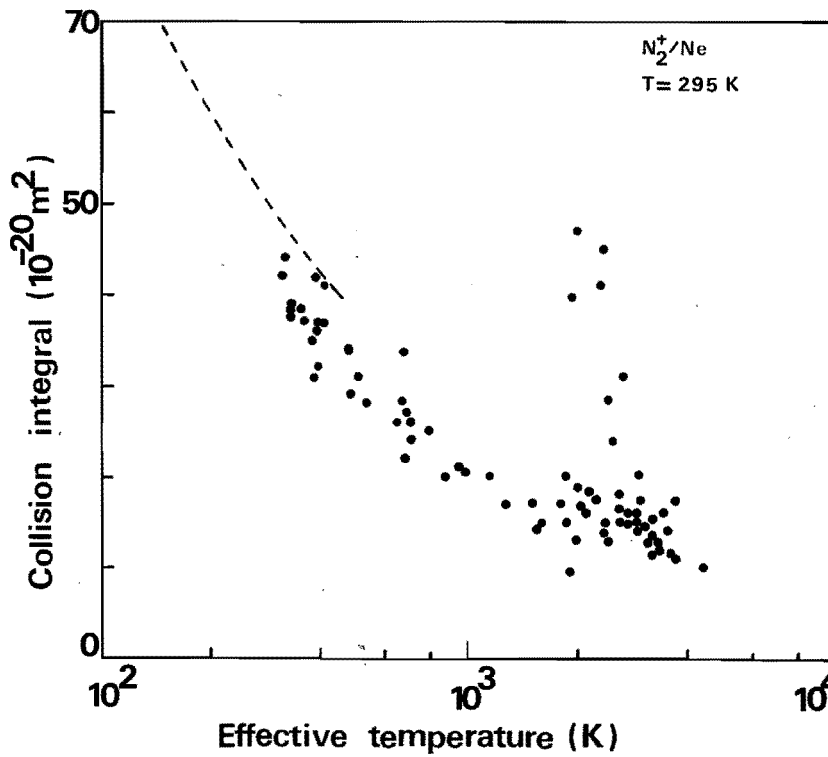

Figure 5.7 The collision integral $\Omega^{(1,1)}$ v. the effective temperature T_{eff} for N_2^+ in Ne at 295 K. The dashed curve shows the polarization limit.

Table 5.1 Calculated values for the parameters of a 12-6-4-potential energy curve for the interaction between a N_2^+-ion and a neon atom.

Gas temperature (K)	γ	ε (K)	r_m (Å)
77	$0^{+0.2}$	540±60	2.63±0.07
295	$0^{+0.1}$	660±50	2.60±0.05

Another quantity of interest is the polarization limit of the reduced mobility. The inverse r^4 term in the potential energy curve, the contributio due to polarization, is a long range component and will therefore dominate th scattering at low energies, *i.e.* at infinitely small E/N and low temperature T. The polarization limit of the mobility is given by

$$K_p = \lim_{\substack{E/N\to 0 \\ T\to 0}} K_o = \frac{13.876}{\sqrt{\alpha\mu}} \text{ cm}^2\text{V}^{-1}\text{s}^{-1} \quad , \tag{5.17}$$

where α is the dipole polarizibility of the Ne atom in 10^{-30} m^3 and μ the reduced mass in g/mole (McD72). Using the value of 0.395×10^{-30} m^3 (McD72) for the dipole polarizibility of the neon atom, equation (5.17) gives for K_p the value of 6.46 cm^{2}V^{-1}s^{-1}. This value is indicated in figures 5.4 and 5.5 with an arrow for low E/N.

V.5 Conclusions

With respect to the measurements of the reduced mobilities of Ne^+ in neon as a function of the reduced electric field strength, one can say that at 295 K the present results are, within the experimental error, in good agreement with previous measurements of Helm and Elford (Hel77a), Hölscher (Hol73) and Hornbeck (Hor51a). At a gas temperature of 77 K the scatter in the present experimental data, concerning the mobility of Ne^+ in neon as shown in figure 5.2, is somewhat larger than at 295 K. Also in comparison with Helms data a significant deviation of about +8% is to be seen in figure 5.2. Although this systematic deviation is small, it cannot be explained by experimental errors because a comparison of our measurements at 295 K with those of Helm and Elford shows no systematic error. The measurements at 77 K were carried out up to higher reduced electric field

strength than previous experiments. Measurements of Helm on Ne^+ in neon at 77 K are performed up to a maximum value for E/N of 70 Td, while in the present experiment mobility data can be obtained to at least a value of 300 Td for the reduced electric field strength. In previous experiments by Helm and Elford and Hölscher at 295 K mobility data of Ne^+ in neon are obtained for maximum values of 300 Td and 400 Td, respectively. With the present experimental method high values of E/N up to at least 900 Td can, as in Hornbecks experiment, be reached. From the above mentioned arguments the conclusion is justified that the present experimental method for measuring the mobility of positive ions in gases, which essentially consists of sampling an ion density distribution with specific features at both discharge electrodes, is a reliable method and particularly suitable for measurements at high reduced electric field strength.

As was reported before in the introduction only one experimental value exists on the mobility of nitrogen molecular ions in neon, apart from previous experiments by van de Laarschot and de Hoog (Laa74). Märk and Oskam (Mar71) calculated the zero-field reduced mobility from the ambipolar diffusion coefficient measured in a Ne-N_2 afterglow. In the present experiment, as can be seen in section V.4, the mobility of N_2^+-ions in neon is measured over a wide range of reduced field strengths, at two temperatures, *viz.* 77 K and 295 K. A non-linear least mean square fit to the experimental data of a 12-6-4-potential with parameters ε, r_m and γ, gives for both temperatures a satisfactory mutual agreement with regard to the calculated values of the depth ε and position r_m of the potential energy curve minimum. A note should be made about the measurements of the drift velocity of N_2^+ in neon at 295 K and hence on the determination of the mobility and the collision integral. For reduced electric field strength larger than 130 Td, the drift velocity of N_2^+ in neon shows no longer an increase with increasing E/N, but stays roughly the same. This implies the mobility to decrease more strongly at increasing values of E/N than in the range below 130 Td, as can be seen in figure 5.4. The collision integral calculated from mobilities for $E/N > 130$ Td appears to be larger than the collision integral calculated from data for $E/N < 130$ Td, while both are at the same effective temperatures. This is to be seen in figure 5.7. This effect cannot be explained by any of the tabulated potential energy curves

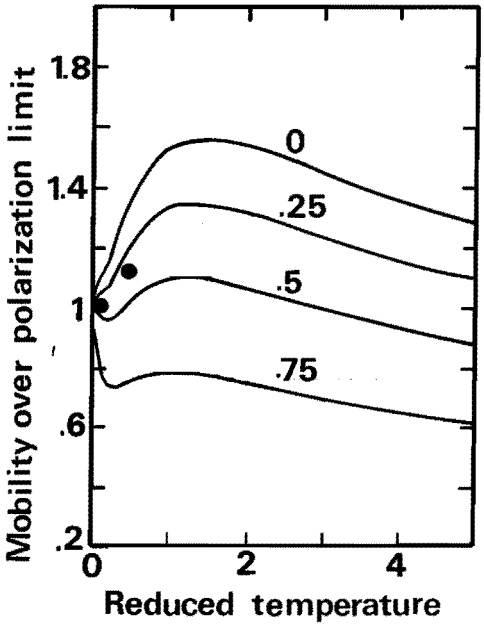

Figure 5.8

Ratio of the zero-field reduced mobility $K_0(0)$ and the polarization limit of the reduced mobility K_p, as a function of the reduced temperature T/ε, after Mason and Schamp (Mas58b); parameter is γ.
—— theory Mason and Schamp (Mas58).
● present experiment.

and therefore mobility data for E/N above 130 Td are not taken into account in the least mean square fit.

Mason and Schamp (Mas58b) investigated the behaviour of the ratio of the zero-field reduced mobility $K_o(0)$ and the polarization limit of the mobility K_p as a function of the ratio of the gas temperature and the depth of the potential curve, T/ε, with γ as a parameter. This can be seen in figure 5.8. When comparing our experimental results indicated in figure 5.8, with his data, it seems that our result for γ is too low to fit his curve. Also from interpolation one might conclude that in our case a γ of 0.3 could be possible. This, however, is outside the uncertainty interval we accept for γ in our potential energy curve calculation from mobility data. According to Helm and Elford (Hel77b) at low energies the measured mobilities of all diatomic rare gas ions in their parent gas fall below the polarization limit, as is to be seen in figure 5.9. This feature is not explainable in terms of ion transport theories which are based on the assumption of a spherical symmetric interaction potential and elastic scattering. Although until now this effect is only observed for diatomic rare gas ions, the discrepancy of the present data of γ with the calculations of Mason and Schamp is not considered to be dramatic.

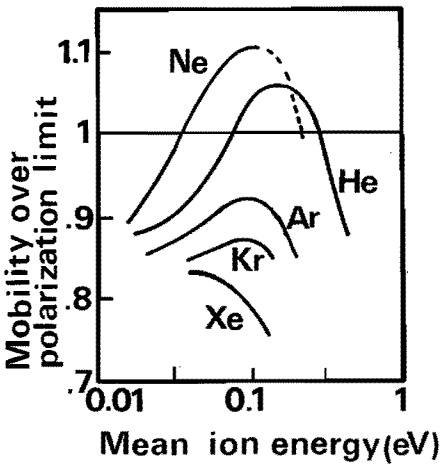

Figure 5.9

Ratio of the zero-field reduced mobility and the polarization limit v. mean ion energy after Helm and Elford (Hel77b).

Finally we can conclude that Märks value for the zero-field reduced mobility of 8.9±0.6 $cm^2V^{-1}s^{-1}$ is about 20% larger than the present value of 7.3 $cm^2V^{-1}s^{-1}$. However, in the evaluation of the ambipolar diffusion coefficient from which they calculated the zero-field mobility, Märk and Oskam experienced difficulties in interpreting their data. These difficulties were mainly caused by a large number of processes generating and destructing N_2^+-ions. These processes obscured a straight-forward interpretation of N_2^+-lifetimes especially at lower gas densities.

V.6 Concluding remarks

In the preceeding section the conclusion was drawn that the present experimental method is suitable for determining the mobilities of ions in gases, especially at high reduced electric field strength. Because of the small distance of about 1 cm between the electrodes in the present experiment in comparison with the lengths of 10 cm to 50 cm in drift tubes, the transit times for ions from one electrode to the other are 10 to 50 times smaller than drift times in drift tubes. This implies that in the present experiments the influence of ion-molecule reactions and diffusion of ions, interfering with the analysis of the arrival times spectrum, is much less than in the longer drift tubes. The advantage of these longer drift paths, however, is

the better accuracy which can be achieved in the determination of the mobility of positive ions in the relative seldom cases when no interfering reactions occur.

APPENDIX

In this appendix the value of $k_r\tau$ is calculated when a large number of excited states is considered. Also the dependence of $k_r\tau$ on E/N is investigated. Equations (3.5) to (3.7) give

$$N_j^{**}(x) = \frac{k_{ej} N n^-(x)}{1/\tau_j + k_{rj} N} \cdot \tag{A.1}$$

When we neglect the influence of dissociation of Ne_2^+ and the termolecular association of Ne^+ on the reaction of A.I., equations (3.29), (3.27), (3.28) and (3.11) reduce to

$$\frac{j^+(0)}{j_2^+(0)} = \frac{k_i}{\sum_j k_{ej} \frac{k_{rj} N \tau_j}{1 + N k_{rj} \tau_j}} \cdot \tag{A.2}$$

From this equation one can see that the measured value of $k_r\tau$ is not the mathematical average of the single values of $k_{rj}\tau_j$ over all j involved. Because a linear dependence of the ratio of atomic and molecular ion fluxes on the reciprocal gas density is measured experimentally in a specific gas density range, expression (A.2) is also supposed to have in first approximation a linear dependence on $1/N$ in that density range. In the same way as calculating the values of $k_r\tau$ in the foregoing by dividing the inclination of the straight line by the cut-off of the axis of ordination, according to (3.30), this is done for relation (A.2). The inclination is determined as the first derivative of $j^+(0)/j_2^+(0)$ to the reciprocal gas density in the point $1/N_o$. $1/N_o$ is the mean reciprocal gas density used in the present experiment. The expression for $k_r\tau$, derived in this way, reads

$$k_r\tau = \frac{\sum_j \frac{k_{ej}}{k_i} \left(\frac{k_{rj}\tau_j}{1/N_o + k_{rj}\tau_j} \right)^2}{\sum_j \frac{k_{ej}}{k_i} \frac{k_{rj}\tau_j}{(1/N_o + k_{rj}\tau_j)^2}} \cdot \tag{A.3}$$

For $j = 1$ equation (A.3) becomes identical to (3.30). The quantities which ought to be known for each specific excited level j are the A.I. reaction rate k_{rj}, the unproductive decay time τ_j and the rate of excitation by

electron impact k_{ej}, from a ground state neon atom to that excited state. The excitation k_{ej} depends on the reduced electric field strength.

The unproductive decay time τ_j

The excited atoms in state j can decay to lower energy levels by the emission of radiation and by de-excitation in collisions with ground state atoms. The problem is to calculate the collisional de-excitation rate for highly excited levels. Measurements of Smits (Smi78) of the coupling-coefficients between 2p-states in neon by collision with ground state atoms show the de-excitation rate to be about 10^{-17} m^3s^{-1} for energy differences of the transitions of a few hundredths of electron volts. At gas densities of about 3×10^{22} m^{-3} as used in our measurements of A.I., this implies the collisional de-excitation time to be about 3 μs. The cross section for collisional de-excitation will decrease at increasing energy difference between initial and final state and vice versa.

Afanaseva and Gruzdev (Afa75a+b) calculated the radiative lifetimes for the $2p^5ns$ states of neon for n = 3 through 10 and for the $2p^5np$, $2p^5nd$ and $2p^5nf$ states for n = 3 through 8. These radiative lifetimes are plotted in figure A.1, as functions of the energy difference between the ionization limit and the energy of the initial state. For each of the s, p, d and f states an empirical relation for these radiative lifetimes can be obtained as a function of the principal quantum number n according to

$$\tau_n = C\, n^k . \qquad (A.4)$$

Table A.1 gives the values of C and k for the s, p, d and f states of neon.

Table A.1

	s	p	d	f
C	0.16	0.126	0.99	1.22
k	3.7	4.9	3.0	2.9

As can be seen from equation (A.4) for the s states the radiative lifetime becomes equal to a de-excitation lifetime of 3 μs for a principal quantum number of 15. For the p state this equality is reached already for

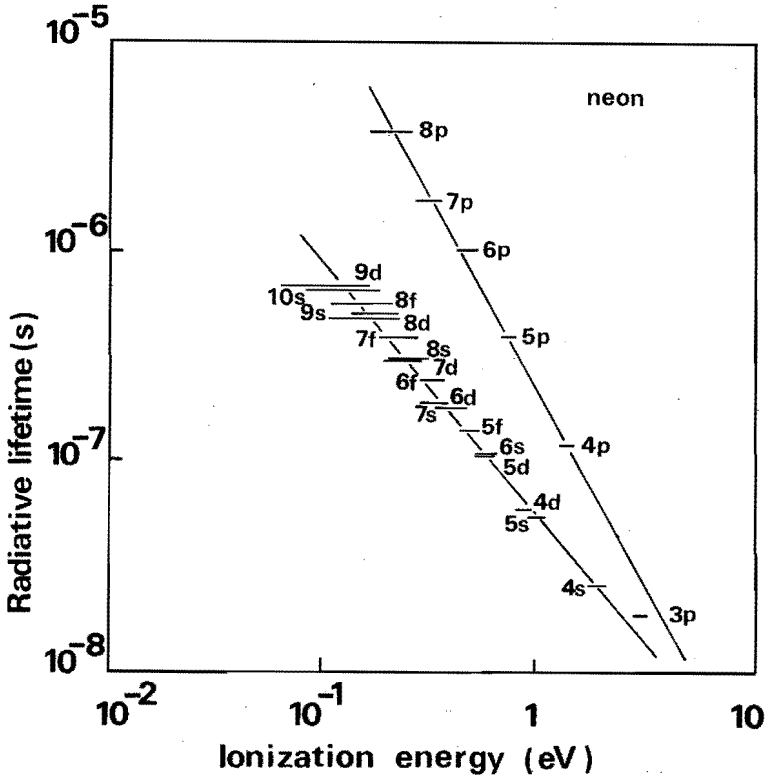

Figure A.1 Dependence of the radiative lifetimes τ_j of highly excited states in neon on the energy differences with respect to the ionization limit, after Afanaseva and Gruzdev (Afa75a+b).

n = 8. At high principal quantum numbers the difference in energy between the n state and the $(n-1)$ state decreases as a consequence of which the collisional de-excitation rate for these states increases and the de-excitation time becomes smaller. Still for the following calculations we only take into account the radiative lifetimes of the excited states, because this will give a maximum influence of the highest energy levels and so a maximum effect of E/N on $k_r\tau$.

Reaction rate for associative ionization k_{rj}

In order to estimate the reaction rate of A.I. for a specific energy level j, use has been made of the model developed by Demkov and Komarev (Dem66) for the reaction

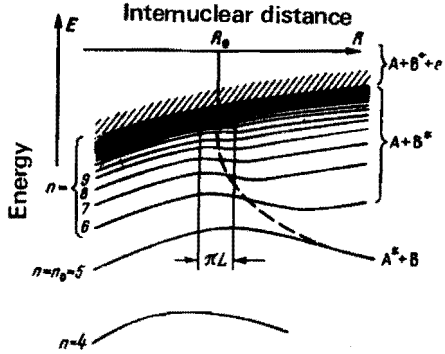

Figure A.2

Diagram of potential energy curves near the ionization limit according to Demkov and Komarov (Dem66).

$$A^* + B \rightarrow A + B^+ + e^- \,. \qquad (A.5)$$

In figure A.2 a diagramatic plot is given of the potential energy curves of reactants and reaction products as a function of intermolecular distance R. Demkov considers a system (A*-B) in an energy level n_o situated under an area of parallel energy levels very close to ionization. This area is called the Coulomb crowded region. The crossing of the system (A*-B) with this Coulomb crowded region into the ionized system ($A\text{-}B^+$) is described and the transition probability to the ionization level $E = 0$ is calculated and given by

$$W(0) = W_o \exp(-2BE) \,, \qquad (A.6)$$

where W_o is the probability for a system (A-B) to pass into a level n_o with energy E_o, E is the energy distance for state n_o to the ionization limit and B a constant equal to

$$B = \frac{2\pi eL}{hv} \,. \qquad (A.7)$$

In this relation e is the electronic charge, h Plancks constant, v the velocity of internuclear approach and $2L$ the interval of R around R_o, the point of crossing, at which the principal quantum number n changes with an amount of $^1/_2$. As mentioned in the introduction expression (A.6) has a similar form as the Landau-Zener expression and contains only one quantity B. Assuming the system ($A\text{-}B^+$) to be a stable molecule AB^+, the reaction rate k_{rj} for associative ionization in neon can be written as

$$k_{rj} = k_{bj} \exp(-2BE) \,, \qquad (A.8)$$

where k_{bj} is the collision rate between an excited Ne_j^{**} atom and a ground state neon atom. In the further calculations k_{bj} is chosen equal for all j. The probability for the Ne atom to attain the excited level j, given by W_o, is taken into account by the excitation rate k_{ej}.

Electronic excitation rate k_{ej}

The excitation k_{ej} is defined by

$$k_{ej} = \int_{E_{thr}}^{\infty} \sigma_j(E) \sqrt{2E/m}\, f(E)dE \ , \qquad (A.9)$$

where $\sigma_j(E)$ is the cross section for excitation to state j by electron impact at an energy E, m the electronic mass, $f(E)$ the electron energy distribution and E_{thr} the threshold energy for this excitation process. In a T.D. as is used in the present experiments, the energy distribution is not Maxwellian because the electron-electron collision frequency is much smaller than the electron-neutral collision frequency. A Druyvesteyn distribution should be a better representation in neon, because the elastic scattering cross section for electron-neutral collisions is fairly constant for the energies concerned. However, above the lowest excitation threshold (16.5 eV) inelastic collisions have a large influence on the high energy tail of the distribution, especially at lower reduced electric field strengths. In the estimation of the experimental values of $k_r\tau$ and k_i/k_e, we used the Druyvesteyn distribution.

Cross sections for the excitation to highly excited states by electron impact of ground state neon atoms are not known in literature. From results of Sharpton *et al.* (Sha70) we use as an approximation for the excitation cross section σ_j as a function of energy E

$$\sigma_j(E) = \begin{cases} 0 & \text{for } E < E_{thr} \\ \dfrac{E_{thr}}{E}\,\sigma_{oj} & \text{for } E \geq E_{thr} \ , \end{cases} \qquad (A.10)$$

where E_{thr} is the minimum energy necessary to excite and σ_{oj} the maximum value of the cross section for excitation to a state j. According to Goedheer (Goe78) for a principal quantum number $n \geq 4$, σ_{oj} is proportional

to $1/n^3$. In this way the cross section $\sigma_j(E)$ can be written as

$$\sigma_j(E) = \frac{E_{thr}}{E} \frac{\sigma_o}{n^3} \cdot \qquad \text{(A.11}$$

The value of σ_o is calculated by calibration of $\sigma_j(E_{thr})$ to known values for the excitation cross section for low states with $n = 4$ (Lab68). The excitation rate k_{ej} is calculated using (A.9) with $f(E)$ the Druyvesteyn distribution function.

Product of A.I. rate and mean lifetime, $k_r\tau$

The only input parameter, influencing the dependence of $k_r\tau$ on E/N is clearly the drop-off of the electron energy distribution about the ionizati limit. Taking this to be a Druyvesteyn distribution we calculated the value of $k_r\tau$, as given by equation (A.3), by means of equations (A.4), (A.8), (A. and (A.11), with the collision rate k_{bj} and the factor B acting as parameter These calculations have been carried out for p and s states and principal quantum numbers ranging from 4 to 20. As a result we found that $k_r\tau$ is independent of E/N in contrast with the results of the experiments. In orde to explain the observed variation it is clear that a distribution with a sharper drop-off for energies E about the ionization limit should be used. We found that $f(E) \sim \exp(E/\varepsilon)^{3.5}$, where ε is proportional to the mean electron energy, can explain the observed variations in $k_r\tau$ with E/N. The results on $k_r\tau$ are given in table A.2, for s states, with the collision rat k_{bj} varying from 10^{-16} m^3s^{-1} to 10^{-19} m^3s^{-1} and B running from 0.42 eV^{-1} to 4.2 eV^{-1}.

Another measured quantity is the ratio k_i/k_e of the ionization rate an the excitation rate. An increase by more than two orders of magnitude of k_i/k_e at increasing E/N can be seen from figure 3.7. The total excitation rate k_e is calculated by using

$$k_e = \sum_{j=4}^{\infty} k_{ej} , \qquad \text{(A.12}$$

where k_{ej} is given by (A.9), $f(E)$ is the Druyvesteyn distribution function and $\sigma_j(E)$ according to (A.11). The ratio of k_i, calculated by (3.11) using the macroscopic quantities of reduced total ionization coefficient and

Table A.2 Calculated $k_r\tau$ (10^{-23} m^3) as a function of k_{bj} and B.

k_{bj} (m^3s^{-1}) \ B (eV^{-1})	0.42	4.2
10^{-16}	4.0	5.9
10^{-17}	1.6	2.0
10^{-18}	0.32	0.35
10^{-19}	0.036	0.038

electron drift velocity, and the excitation rate k_e according to (A.12) is plotted in figure 3.7 as a function of E/N. It can be seen that the calculated ratio k_i/k_e shows a slower increase with increasing E/N than the measured data for k_i/k_e. The few previous results on k_i/k_e (Pah59, Dah62, Hor51) also indicate a strong dependence of this ratio on E/N. The calculated ratio k_i/k_e can only be changed into a steeper function of E/N if an electron energy distribution function is used which decreases much stronger for higher electron energies (above the first excitation energy of 16.7 eV) than the Druyvesteyn function. This is in agreement with the calculations made to explain the increase of $k_r\tau$ as a function of E/N.

REFERENCES

Afa75a Afanaseva, N.V. and Gruzdev, P.F., Opt.Spektrosk. 38 (1013) 1975.

Afa75b Afanaseva, N.V. and Gruzdev, P.F., Opt.Spektrosk. 38 (378) 1975.

Akr75 Akridge, G.R. *et al.*, J.Chem.Phys. 62 (4578) 1975.

Ari74 Arijs, E., Vacuum 24 (341) 1974.

Arm74 Armour, D.G., J.Phys.B. 7 (1213) 1974.

Arn39 Arnot, F.L. and M'Ewen, M.B., Proc.R.Soc. A171 (106) 1939.

Bea62 Beaty, E.C., Proc. 5th Int.Conf.Ion.Phen.Gases, Munich, 1 (183) 1961.

Bea68 Beaty, E.C. and Patterson, P.L., Phys.Rev. 170 (116) 1968.

Bec65 Becker, P.M. and Lampe, F.W., J.Chem.Phys. 42 (3857) 1965.

Bio52 Biondi, M.A., Phys.Rev. 88 (660) 1952.

Bol70 Bolden, R.C. *et al.*, J.Phys.B. 3 (61) 1970.

Bru60 Brubaker, W.M., Intern.Instr.Conf.Proc. 5th, Stockholm, Sweden, sept. 1960.

Cha63 Chanin, L.M. and Rork, G.D., Phys.Rev. 132 (2547) 1963.

Che68 Che Jen Chen, Phys.Rev. 177 (245) 1969.

Coh74 Cohen, J.S. and Schneider, B., J.Chem.Phys. 61 (3230) 1974.

Coh75 Cohen, J.S. and Schneider, B., Phys.Rev. A11 (884) 1975.

Coh78 Cohen, J.S. *et al.*, Phys.Rev. A17 (1343) 1978.

Con65 Connor, T.R. and Biondi, M.A., Phys.Rev. 140 (A778) 1965.

Dah62 Dahler, J.S. *et al.*, J.Chem.Phys. 36 (3332) 1962.

Daw74 Dawson, P.H., Int.J. of Mass Spectr. and Ion Physics, 14 (317) 1974.

Daw69 Dawson, P.H. and Whetten, N.R., "Mass Spectroscopy using R.F. Quadrupole Fields", Advances in electronics and electron physics, V27, Academic Press, N.Y., 1969. p.60.

Dem67 Demkov, Y.N. and Komarov, I.V., Sov.Phys. JETP 23 (189) 1966.

Dic72 Dickinson, A.S. *et al.*, J.Phys.B. 5 (355) 1972.

Die62 Diels, K. and Jaeckel, R., "Leybold Vacuum-Taschenbuch", Springer Verlag, Berlin, 1962, p.15.

Dix57 Dixon, J.R. and Grant, F.A., Phys.Rev. 107 (118) 1957.

Dor25 Dorgelo, H.B., Z.Phys. 34 (766) 1925.

Fit73 Fitzwilson, R.L. and Chanin, L.M., J.Appl.Phys 44 (5337) 1973.

Fre66 Freudenthal, J., "Ion transports and atomic diffusion in discharges in gas mixtures", thesis, Utrecht, 1966.

Gat77 Gatland, I.R. *et al.*, J.Chem.Phys. 68 (2775) 1978.

Goe78 Goedheer, W., "Models for a steady state in a gas blanket", thesis, Utrecht, 1978.

Gra51 Grant, F.A., Phys.Rev. 84 (844) 1951.

Gra53 Grant, F.A. and Krumbein, A.D., Phys.Rev. 90 (59) 1953.

Gri74 Gritsyna, V.V. *et al.*, Opt.Commun. 10 (320) 1974.

Hac66 Hackam, R., Br.J.Appl.Phys. 17 (197) 1966.

Hel77a Helm, H. and Elford, M.T., J.Phys.B. 10 (983) 1977.

Hel77b Helm, H. and Elford, M.T., ICPIG XIII, Berlin, 1977, p.63.

Hin70 Hintzpeter, G. von, J.Appl.Phys. 41, (1707) 1970.

Hir54 Hirschfelder, J.O. *et al.*, "Molecular theory of gases and liquids", J. Wiley and sons, N.Y., 1954.

Hir78 Hirsch, M.N. and Oskam, H.J., "Gaseous electronics" VI, electrical discharges (133) 1978.

Hol64 Hölscher, J.G.A., "The influence of positive space charge on the position and the movement of Holst and Oosterhuis light layers", thesis, Eindhoven, 1964.

Hol73 Hölscher, J.G.A., Ned.Tijdschr.v.Nat. 9 (128) 1973.

Hol77 Hölscher, J.G.A., private communication.

Hoo69 Hoog, F.J. de, "Aanslag en ionisatie van edelgassen in Townsend ontladingen", thesis, Eindhoven, 1969.

Hor51a Hornbeck, J.A., Phys.Rev. 83 (374) 1951.

Hor51b Hornbeck, J.A., Phys.Rev. 84 (615) 1951.

Hor51c Hornbeck, J.A., Phys.Rev. 84 (1072) 1951.

Hor51d Hornbeck, J.A. and Molnar, J.P., Phys,Rev. 84 (621) 1951.

Huf66 Huffman, R.E. and Katayama, D.H., J.Chem.Phys. 45 (138) 1966.

Hug70 Hughes, M.H., J.Phys.B. 3 (1544) 1970.

Ill75 Illenberger, E. and Niehaus, A., Z.Phys. B20 (33) 1975.

Kau60 Kaul, W. von and Fuchs, R., Z.Naturforsch. 15a (326) 1960.

Kir69 Kirilenko, V.M., Zh.Tekh.Fiz. 39 (738) 1969.

Kit78 Kitamori, K. *et al.*, J.Phys.D. 11 (283) 1978.

Kru37 Kruithof, A.A. and Penning, F.M., Physica, 4 (430) 1937.

Laa74 Laarschot, F.A.A.E. and de Hoog, F.J., Phys.Lett. 50A (11) 1974.

Lab68 Laborie, P. *et al.*, "Electronic cross sections, macroscopic coefficients, hydrogen and rare gases", Dunod, Paris, 1968.

Lei75 Leichner, P.K. *et al.*, Phys.Rev. A12 (2501) 1975.

Loe61 Loeb, L.B., "Basic processes of gaseous electronics", Univ. of Calif. Press (707) 1961.

Mah65 Mahan, B.H., J.Chem.Phys. 43 (3080) 1965.
Mar71 Märk, T.D. and Oskam, H.J., Z.Phys. 247 (84) 1971.
Mas58 Mason, E.A. and Vanderslice, J.T., J.Chem.Phys. 29 (361) 1958.
Mas58b Mason, E.A. and Schamp, H.W., Ann.Phys. 4 (233) 1958.
McD72 McDaniel, E.W. and Mason, E.A., "The mobility and diffusion of ions in gases", N.Y., 1972.
Mei25 Meisner, K.W., Annln der Phys. 76 (124) 1925.
Met72 Metaxas, A.C. and Cozens, J.R., J.Phys. D5 (1077) 1972.
Mil75 Milloy, H.B. and Elford, M.T., Int.J. of Mass Spectr. and Phys. 18 (21) 1975.
Mol51 Molnar, J.P., Phys.Rev. 83 (945) 1951.
Mon71 Montfort, L.H. van, "Stroomversterking en doorslag van Townsend ontladingen in neon en neon-argon mengsels", Thesis, Eindhoven, 1971.
Mor75 Morrison, W.F. *et al.*, J.Chem.Phys. 63 (2238) 1975.
Mul70 Mulliken, R.S., J.Chem.Phys. 52 (5170) 1970.
Mun63 Munson, M.S.B. *et al.*, J.Phys.Chem. 67 (1542) 1963.
Nil65a Niles, F.E. and Robertson, W.W., J.Chem.Phys. 42 (3277) 1965.
Nil65b Niles. F.E. and Robertson, W.W., J.Chem.Phys. 43 (1076) 1965.
Oma72 O'Malley, T.F. *et al.*, J.Phys. B5 (2126) 1972.
Ori73 Orient, O.J., Chem.Phys.Lett. 23 (579) 1973.
Pah58 Pahl, M. von and Weimer, U., Z.Naturforsch. 13a (745) 1958.
Pah59 Pahl, M. von, Z.Naturforsch. 14a (239) 1959.
Pah63 Pahl, M. von, Z.Naturforsch. 18a (1276) 1963.
Pal69 Palkina, L.A. *et al.*, Sov.Phys. JETP 29 (187) 1969.
Par71 Parkes, D.A., Trans. Faraday Soc. 67 (711) 1971.
Phe53 Phelps, A.V. and Molnar, J.P., Phys.Rev. 89 (1202) 1953.
Phe59 Phelps, A.V., Phys.Rev. 114 (1011) 1959.
Rap65 Rapp,D. and Englander-Golden, P., J.Chem.Phys. 43 (1464) 1965.
Rob72 Robben, F., Phys.Rev. A5 (1516) 1972.
Sau66 Sauter, G.F. *et al.*, Physica 32 (1966) 1921.
Sch74 Schneider, B. and Cohen, J.S., J.Chem.Phys. 61 (3240) 1974.
Sch70 Schmeltekopf, A.L. and Fehsenfeld, F.C., J.Chem.Phys. 53 (3173) 1970.
Sch75 Schmeltekopf, A.L., Int.J. Mass Spectr. & Ion Phys. 16 (151) 1975.
Sha70 Sharpton, F.A. *et al.*, Phys.Rev. A2 (1305) 1970.
Smi67 Smirnov, B.M., Sov.Phys.Usp. 10 (313) 1967.
Smi68 Smith, D. and Cromey, P.R., J.Phys.B. 1 (638) 1968.
Smi73 Smith, D. *et al.*, J.Phys.B. 7 (170) 1973.

Smi78 Smits, R.M.M., "Investigations on the positive column of a medium pressure neon discharge", thesis, Eindhoven, 1977.

Ste79 Steenhuysen, L.W.G., "Investigations on afterglows of neon gas discharges", thesis, Eindhoven, 1979.

Tom71 Tombers, R.B. *et al.*, J.Appl.Phys. 42 (4855) 1971.

Tux36 Tüxen, O., Z.Phys. 103 (463) 1936.

Tyn38 Tyndall, A.M., "The mobility of positive ions in gases", Cambridge, 1938.

Vie75a Viehland, L.A. and Mason, E.A., Ann.Phys. 91 (499) 1975.

Vie75b Viehland, L.A. *et al.*, Atomic data and mol. data tables, 6 (495) 19

Vie76 Viehland, L.A. *et al.*, Chem. Phys. 17 (433) 1976.

Vit72 Vitols, A.P. and Oskam, H.J., Phys.Rev. A5 (2618) 1972.

Wan51 Wannier, G.H., Phys.Rev. 83 (281) 1951.

Wei58 Weimer, U., Z.Naturforsch. 13a (278) 1958.

Weiz58 Weizel, W., "Lehrbuch der theoretische Physik", Springer Verlag, Berlin, 1958.

Wel72 Wellenstein, H.F. and Robertson, W.W., J.Chem.Phys. 56 (1072) 1972.

Wes75 West, W.P. *et al.*, J.Chem.Phys. 63 (1237) 1975.

SUMMARY

This thesis deals with elementary processes and transport phenomena of ionized and excited species studied in a Townsend discharge in neon using mass spectrometry. In particular elementary processes leading up to the formation and destruction of neon molecular ions and the processes governing the decay of metastable neon atoms have been investigated. The mobilities of positive ions in neon, measured in the present work, are examples of transport phenomena.

The experiments have been carried out with a Townsend discharge tube coupled to a quadrupole mass filter. Ions have been extracted from the discharge by means of a small orifice in one of the parallel electrodes. In this way the particle flux of a specific positive ion species at the cathode has been measured as a function of discharge parameters. To provide for the pure neon necessary in this field of gas discharge experiments, ultra-high vacuum techniques as well as cataphoretic cleaning of the gas have been used.

Because of its very low electric current density the Townsend discharge has certain properties which have been used advantageously in the present experiments. A homogeneous electric field without space charge distortion and a Debye length much larger than the geometrical dimension of the discharge tube provide for sound ion sampling, as has been investigated thoroughly. For the same reason mobility measurements can be carried out with the present experimental set-up. The absence of cumulative effects like dissociative recombination, stepwise excitation and ionization, eliminates a large number of possible reactions which normally obscure the analysis of experimental data. A well defined temperature is present in all experiments. When the discharge runs in a non-selfsustaining mode, discharge parameters like gas density, reduced electric field strength and electrode distance, can be varied independently.

The reactions for the processes leading to the formation of molecular neon ions, *viz.* associative ionization (A.I.) at low gas densities and termolecular association (T.A.) at higher gas densities, have been studied as functions of the reduced electric field strength E/N, and hence as functions of the mean ion energy. Measurements show the product of the reaction rate for A.I. and the unproductive lifetime of the highly excited

reactant to increase slightly from 0.6×10^{-23} m^3 at an E/N of 45 Td to about 2×10^{-23} m^3 at an E/N of 245 Td. From model calculations it appeared that this increase could only be explained by assuming the high energy tail of the electron energy distribution to decrease more rapidly at increasing energy than that of a Druyvesteyn distribution function. This is in agreemer with the measured ratio of the ionization rate and the rate for excitation to highly excited states, which show an increase by more than two orders of magnitude in the same range of E/N. Data on the termolecular association rate have been obtained over a range of mean ion energy wider than done in previous experiments. The present value for the reaction rate of 0.47×10^{-43} m^{6}s^{-1} for E/N smaller than 30 Td, is in good agreement with experimental data in literature. We measured a decrease in the T.A. rate, down to about 0.15×10^{-43} m^{6}s^{-1} at an E/N of 200 Td, at increasing E/N. The dissociation of a Ne_2^+-ion in a collision with a ground state parent atom was found to be an important loss process at high E/N. The dependence of the reaction rate for this process on the mean ion energy has been measured. The value of the dissociation energy calculated from these data shows a reasonable agreement with scattering values found in literature.

The decay frequency of Ne($^3P_2$)-atoms has been determined at 77 K and 295 K as a function of gas density from time sampling analysis of a N_2^+-ion impurity in the afterglow of a Townsend discharge in neon. The rate of formation of N_2^+-ions via a Penning reaction is proportional to the metastabl density. For the $^3P_2$-atoms we determined the diffusion coefficient, the excitation rate to the near resonant state and the excimer formation rate. Good agreement exists with experimental results in literature. We showed that the determined value of the excimer formation rate for $^3P_2$-atoms depend strongly on the value for the excimer formation rate of $^3P_1$-atoms.

From time sampling spectra of ions in the afterglow of a Townsend discharge, mobilities of positive ions in neon have been determined as a function of the reduced electric field strength at 77 K and 295 K. The use of a Townsend discharge enable us to make measurements at higher E/N than is the case in other drift tube experiments. From mobility data the interaction potential as a function of intermolecular distance between a N_2^+-ion and a neon atom is evaluated.

Elementaire processen en transportverschijnselen van geïoniseerde en aangeslagen atomen zijn bestudeerd in een Townsendontlading in neon d.m.v. massaspectrometrie. Met name processen die aanleiding geven tot de vorming en vernietiging van moleculaire neonionen en processen die het verval van metastabiele neonatomen bepalen zijn onderzocht. Ook de beweegbaarheden van positieve ionen in neon zijn bepaald.

Om deze verschijnselen te onderzoeken is een vierpool-massafilter gekoppeld aan een Townsendontladingsbuis. Via een klein gat in een van de evenwijdige elektrodes kan de ontlading bemonsterd worden. De fluxen van bepaalde positieve ionen aan de kathode kunnen zo gemeten worden als functies van ontladingsparameters. Ultra-hoogvacuüm technieken als ook cataforese van het gas zijn toegepast on voldoende zuiver neon, noodzakelijk voor gasontladingsonderzoek, te verkrijgen.

Door de kleine elektrische stroomdichtheid heeft de Townsendontlading vele gunstige eigenschappen waar in onze experimenten gebruik van gemaakt is. Een homogeen elektrisch veld en een Debyelengte die veel groter is dan de afmeting van de ontladingsbuis zorgen voor een juiste bemonstering van de ontlading van ionen, zoals uitvoerig onderzocht werd. Deze eigenschappen maken het tevens mogelijk om met dezelfde opstelling beweegbaarheden van positieve ionen in gassen te meten. Doordat cumulatieve processen zoals dissociatieve recombinatie, stapsgewijze aanslag en -ionisatie te verwaarlozen zijn, kan een groot aantal mogelijke reacties, die een analyse van experimentele gegevens vertroebelen, uitgesloten worden. De temperatuur van het gas in de ontladingsbuis is gelijk aan de omgevingstemperatuur. In een onzelfstandige ontlading kunnen de gasdichtheid, de gereduceerde elektrische veldsterkte en de elektrodenafstand, onafhankelijk van elkaar gevarieerd worden.

Twee reacties die moleculaire neonionen geven, associatieve ionisatie (A.I.) bij een kleine gasdichtheid en termoleculaire associatie (T.A.) bij een hoge gasdichtheid, zijn bestudeerd voor verschillende groottes van de met de gasdruk gereduceerde elektrische veldsterkte E/N en zo bij verschillende waarden van de gemiddelde ionenergie. Het produkt van de reactiesnelheid voor A.I. en de niet-produktieve levensduur van de hoogaangeslagen reactiepartner neemt toe van 0.6×10^{-23} m^3 bij een E/N van 45 Td naar

2×10^{-23} m^3 bij een E/N van 245 Td. Uit modelberekeningen blijkt dat deze stijging slechts verklaard kan worden door te veronderstellen dat de staart van de elektronenenergieverdeling rond de ionisatiepotentiaal sterker afneemt bij toenemende energie dan in het geval van een Druyvesteyn-verdelingsfunctie. De gemeten toename van meer dan twee orden van grootte in hetzelfde E/N-interval van het quotiënt van de ionisatiesnelheid en de snelheid voor aanslag naar niveaus vlak onder het ionisatieniveau is hiermee in overeenstemming.

De reactiesnelheid voor T.A., door ons bepaald bij waarden van de gemiddelde ionenergie groter dan in experimenten bekend in de literatuur, neemt af van 0.47×10^{-43} $m^6 s^{-1}$ bij E/N kleiner dan 30 Td tot 0.15×10^{-43} $m^6 s^{-1}$ bij een E/N van ongeveer 200 Td. De eerstgenoemde waarde is in goede overeenstemming met resultaten gevonden in de literatuur. De dissociatie van een Ne_2^+-ion bij een botsing met een neonatoom blijkt een belangrijk verliesproces te zijn bij grote waarden van E/N. De dissociatiesnelheid is gemeten als functie van de gemiddelde ionenergie. Met een eenvoudig model is uit deze metingen de dissociatie-energie van het moleculaire ion bepaald en in overeenstemming gebleken met literatuurwaarden.

De vervalfrequentie van $Ne(^3P_2)$-atomen in neon is gemeten bij 77 K en 295 K als funktie van de gasdichtheid door tijdsafhankelijke bemonsteringen van N_2^+-verontreinigingen in de nagloei van een Townsendontlading te analyseren. De per tijds- en volume-eenheid gevormde hoeveelheid N_2^+-ionen d.m.v. een Penningreactie is evenredig met de dichtheid van de metastabielen. De diffusiecoëfficiënt, de reactiesnelheid voor aanslag naar het dichtbij gelegen resonante niveau en de reactiesnelheid voor excimeervorming van het $^3P_2$-atoom zijn bepaald en blijken in goede overeenstemming te zijn met resultaten uit de literatuur. De gevonden waarde voor de reactiesnelheid voor excimeervorming van een $^3P_2$-atoom blijkt sterk afhankelijk van de waarde van de reactiesnelheid voor excimeervorming van een $^3P_1$-atoom.

Uit tijdsafhankelijke bemonsteringen van ionen in de nagloei van een Townsendontlading zijn de beweegbaarheden van positieve ionen in neon bepaald bij 77 K en 295 K als functie van de gereduceerde elektrische veldsterkte. Het gebruik van de Townsendontlading stelt ons in staat metingen uit te voeren bij hogere waarden van E/N dan in andere driftbuisexperimenten het geval is. Uit de gemeten beweegbaarheden is de wisselwerkingspotentiaal tussen een N_2^+-ion en een neonatoom bepaald als funktie van de kernafstand.

Aangeland bij een van de laatste pagina's van dit proefschrift zal het de lezer van het voorafgaande duidelijk zijn dat het beschreven onderzoek geen kluizenaarswerk geweest kan zijn. Een kort woord van dank aan degenen die hebben bijgedragen tot de totstandkoming van dit proefschrift is dan ook op zijn plaats.

De idee om elementaire processen te bestuderen in Townsendontladingen met behulp van massaspectrometrie is door Frits de Hoog opgedaan in de U.S. en door hem omgezet in concrete plannen. Zijn pittige begeleiding, inventiviteit en soms wilde ideeën gedurende mijn onderzoek zijn onmisbaar geweest.

De kundigheid en het technisch inzicht van Frans van de Laarschot hebben tot het grootste gedeelte van de bestaande opstelling en tot de eerste experimentele resultaten geleid. De resultaten van zijn afstudeerwerk hebben zo aangetoond dat de bovengenoemde idee daadwerkelijk te verwezenlijken is.

Het onderzoek naar de vernietiging van Ne_2^+-ionen is door Paul van der Kraan uitgevoerd en resulteerde in de nauwkeurige bepaling van de tot dan toe onbekende dissociatiesnelheid van dit moleculaire ion.

Dankbaar gebruik heb ik gemaakt van de "koude" Townsendontlading, de ontladingsbuis en het massafilter die afgekoeld kunnen worden tot 42 K, ontworpen en gebouwd door Wietse Veenstra en Jos Eijsermans om gebruikt te worden voor het onderzoek van Hans Hölscher naar He_{13}^+.

Jan Buijs, Cees Corsten, Frans Ramakers, René Vetjens, Rob Buijs en Loek Gaykema hebben als stagiairs belangrijke stukken onderzoek voor hun rekening genomen.

Zonder de bereidwillige hulp van Jos Holten, die de moeilijk te vervaardigen kwartsglazen anode maakte, van Giel Hoddenbagh en van Ries van de Sande, die voor de altijd aanwezige assistentie zorgden, en van de afdelingswerkplaats zou dit promotie-onderzoek niet mogelijk geweest zijn.

Verder dank ik Lambert Bisschops die met veel enthousiasme en creativiteit de tekeningen voor dit proefschrift maakte.

Het keurige typewerk en de professionele verzorging van de lay-out door Rian Teurlings hebben ervoor gezorgd dat dit onderzoek in woord en beeld gepresenteerd kan worden.

PERSOONLIJKE GEGEVENS VAN DE SCHRIJVER

18 februari 1951	Geboren te Eindhoven.
Juli 1968	Diploma HBS-B, St.-Joriscollege te Eindhoven.
September 1974	Diploma natuurkundig ingenieur, Technische Hogeschool Eindhoven.
Oktober 1974 - oktober 1978 Januari 1979 - mei 1979	Wetenschappelijk medewerker in de onderwerpgroep Atoomfysica van de vakgroep Deeltjesfysica van de Technische Hogeschool Eindhoven.

STELLINGEN

1. Door de lage elektrische stroomdichtheid heeft de onzelfstandige Townsendontlading eigenschappen die haar in vergelijking met andere gasontladingen zeer geschikt maken voor het bestuderen van elementaire processen, welke niet in bundelexperimenten onderzocht kunnen worden.

   Dit proefschrift.

2. In het botsings-stralingsmodel van Katsonis voor het ArI-systeem zijn enkele aanvechtbare veronderstellingen verwerkt die de resultaten van dit model veel minder betrouwbaar maken dan het grote aantal in rekening gebrachte energieniveaus doet vermoeden.

   Katsonis,K., proefschrift Orsay 1976.
   Mullen,J.J.A.M. van der, et al., Proc.XIII ICPIG Berlijn 1977, p 323.

3. De door Loeb berekende waarde voor de kritische druk rond welke een drukafhankelijkheid in de primaire ionisatiecoëfficiënt van edelgassen zou moeten optreden op grond van het Hornbeck-Molnar proces, is te groot. Door het in aanmerking nemen van de-excitatie van de aangeslagen atomen door botsingen met atomen in de grondtoestand wordt deze kritische druk verlaagd en is er geen aanleiding meer om te spreken van een paradox.

   Loeb,L.B., "Basic processes of gaseous electronics", Univ. of California Press, Berkeley 1961, p 703.

4. Bij de interpretatie van experimenten in een glimontlading waarin een snelle toename van het verstuiven van een metalen kathode als functie van de stroom optreedt, wordt ten onrechte geen rekening gehouden met de bijdrage tot deze verstuiving van door ladingswisseling tot stand gekomen metaalionen.

   Orlinov,V., et al., Int.J.Electronics 36(431)1974.
   Hoog,F.J. de, et al., J.Appl.Phys. 48(3701)1977.

5. Verwarring over de voor- en nadelen van krachttraining in diverse takken van sport kan vermeden worden door de verschillende vormen van krachttraining exact te definiëren.

   Kuipers,H., De Schaatskroniek 4(1978), 5(1979), 7(1979).

6. Het wekt verwondering dat twee overkoepelende bergsport-verenigingen in een land zonder hooggebergte niet in staat blijken afgravingen van het Limburgse heuvellandschap tegen te houden.

7. "De verzotheid om onderscheidingen te vinden" als definitie van wetenschap blijkt uit talloze stellingen bij proefschriften.

Hesse,H., "Narziss en Goldmund", De Arbeiderspers 1970, p 39.

8. Het moment op een tussenwervelschijf uitgeoefend tijdens het openen van een tochtdeur op de T.H.E. ligt bij een niet-herniapatiënt reeds gevaarlijk dicht bij de deformatiegrens.

Panjabi,M.M., et al., J.Biomechanics 9(185)1976.

9. In Tokamaks met hoge dichtheid kan de waargenomen toename van de energielevensduur τ_E met de elektronendichtheid n_e verklaard worden door voor het binnengebied van de ontlading neo-klassieke warmtegeleiding te veronderstellen.

Schüller,F.C., Schram,D.C., Proc.8th Eur. Conf. on Contr. Fusion and Plasma Phys., Prague 1(8)1977.

Eindhoven, 4 september 1979 J.W.H. Dielis